Universität Trier

Bie, Weiwei

Dem Fachbereich VI
(Raum- und Umweltwissenschaften)
der Universität Trier
zur Erlangung des akademischen Grades
Doktor der Naturwissenschaften (Dr. rer. nat.)
eingereichte Dissertation

Studies on surface resistance in a hydrological model with the evapotranspiration estimated by Penman-Monteith equation and remote sensing techniques in Nahe catchment forest area

Betreuender:
Univ.-Prof. Dr. Markus C. Casper
Berichterstattende:
Prof. Dr. Thomas Udelhoven
Prof. Dr. Michael Vohland

August 2015

I would like to dedicate this thesis to my beloved parents and husband. Thanks for always being there for me.

Declaration

I hereby declare that except where specific reference is made to the work of others, the contents of this dissertation are original and have not been submitted in whole or in part for consideration for any other degree or qualification in this, or any other university. This dissertation is my own work and contains nothing which is the outcome of work done in collaboration with others, except as specified in the text and Acknowledgements.

Bie, Weiwei
August 2015

Acknowledgements

Foremost, I would like to express my special appreciation and thanks to my supervisor Prof. Dr. Markus C. Casper, during my PhD studies, you are always gentle and patient, give me good advices in research, share your experiences, and encourage me to move forward. There is an old saying in my country that "one day as a teacher, a life as a father". I am so pleasure to have you as one of my most respected teachers in my research career.

The work of this thesis integrated data sets and methods in both hydrological model and remote sensing. I would like to thank Prof. Dr. Michael Vohland, you impart me core knowledges of remote sensing and teach me main techniques in data processing. I would like to also thank Prof. Dr. Thomas Udelhoven, you give me good suggestions in remote sensing. I am grateful to Oliver Schmidt and my colleague Philipp Reiter, you offer me so much help in my research works. I wish to express my sincere thanks to Dr. Oliver Gronz, Dr. Hugo Hellbrand, Dr. Thomas Iserloh, Dr. Rita Ley and Dr. Stefan Wirtz, for giving me good suggestions on the revision of this thesis. I would also like to thank Gayaneor Grigoryan, Sabrina Plegnière and all the staffs in the Physical Geography Department of University Trier as well as Alina Schmidt from University Leipzig, for your companion, help and contributions.

A special thanks to my family. Words can not express how grateful I am to my mother-in law, father-in-law, my mother, and father for always being there for me. Your love and support are always my driving force. Dear mom and dad, in your minds, I am always the best little girl in the World! I would also like to thank my beloved husband, Dr. Yu Wang. Thank the fate let us meet 13 years ago. You are always my strong backing and super hero. My home locates wherever you are.

Finally, the deepest miss to Prof. Zhiwei Yu, I wish you all the way best...

Abstract

Evapotranspiration (ET) is one of the most important variables in hydrological studies. In the ET process, energy exchange and water transfer are involved. ET consists of transpiration and evaporation. The amount of plants transpiration dominates in ET. Especially in the forest regions, the ratio of transpiration to ET is in general 80-90 %. Meteorological variables, vegetation properties, precipitation and soil moisture are critical influence factors for ET generation.

The study area is located in the forest area of Nahe catchment (Rhineland-Palatinate, Germany). The Nahe catchment is highly wooded. About 54.6 % of this area is covered by forest, with deciduous forest and coniferous forest are two primary types. A hydrological model, WaSiM-ETH, was employed for a long-term simulation from 1971-2003 in the Nahe catchment. In WaSiM-ETH, the potential evapotranspiration (ETP) was firstly calculated by the Penman-Monteith equation, and subsequently reduced according to the soil water content to obtain the actual evapotranspiration (ETA). The Penman-Monteith equation has been widely used and recommended for ETP estimation. The difficulties in applying this equation are the high demand of ground-measured meteorological data and the determination of surface resistance.

A method combined remote sensing images with ground-measured meteorological data was also used to retrieve the ETA. This method is based on the surface properties such as surface albedo, fractional vegetation cover (FVC) and land surface temperature (LST) to obtain the latent heat flux (LE, corresponding to ETA) through the surface energy balance equation. LST is a critical variable for surface energy components estimation. It was retrieved from the TM/ETM+ thermal infrared (TIR) band. Due to the high-quality and cloudy-free requirements for TM/ETM+ data selection as well as the overlapping cycle of TM/ETM+ sensor is 16 days, images on only five dates are available during 1971-2003 (model ran) – May 15, 2000, July 05, 2001, July 19, August 04 and September 21 in 2003. It is found that the climate conditions of 2000, 2001 and 2003 are wet, medium wet and dry, respectively. Therefore, the remote sensing-retrieved observations are noncontinuous in a limited number over time but contain multiple climate conditions.

Aerodynamic resistance and surface resistance are two most important parameters in the Penman-Monteith equation. However, for forest area, the aerodynamic resistance is calculated by a function of wind speed in the model. Since transpiration and evaporation are separately calculated by the Penman-Monteith equation in the model, the surface resistance was divided into canopy surface resistance r_{sc} and soil surface resistance r_{se}. r_{sc} is related to the plants transpiration and r_{se} is related to the bare soil evaporation. The interception evaporation was not taken into account due to its negligible contribution to ET rate under a dry-canopy (no rainfall) condition.

Based on the remote sensing-retrieved observations, r_{sc} and r_{se} were calibrated in the WaSiM-ETH model for both forest types: for deciduous forest, $r_{sc} = 150\ \mathrm{s\,m^{-1}}$, $r_{se} = 250\ \mathrm{s\,m^{-1}}$; for coniferous forest, $r_{sc} = 300\ \mathrm{s\,m^{-1}}$, $r_{se} = 650\ \mathrm{s\,m^{-1}}$. We also carried out sensitivity analysis on r_{sc} and r_{se}. The appropriate value ranges of r_{sc} and r_{se} were determined as (annual maximum): for deciduous forest, [100,225] $\mathrm{s\,m^{-1}}$ for r_{sc} and [50,450] $\mathrm{s\,m^{-1}}$ for r_{se}; for coniferous forest, [225,375] $\mathrm{s\,m^{-1}}$ for r_{sc} and [350,1200] $\mathrm{s\,m^{-1}}$ for r_{se}.

Due to the features of the observations that are in a limited number but contain multiple climate conditions, the statistical indices for model performance evaluation are required to be sensitive to extreme values. In this study, boxplots were found to well exhibit the model performance at both spatial and temporal scale. Nush-Sutcliffe efficiency (NSE), RMSE-observations standard deviation ratio (RSR), percent bias (PBIAS), mean bias error (MBE), mean variance of error distribution (S_d^2), index of agreement (d), root mean square error (RMSE) were found as appropriate statistical indices to provide additional evaluation information to the boxplots. The model performance can be judged as satisfactory if $NSE > 0.5, RSR \leq 0.7, PBIAS < \pm 12, MBE < \pm 0.45, S_d^2 < 1.11, d > 0.79, RMSE < 9,97$.

r_{sc} played a more important role than r_{se} in ETP and ETA estimation by the Penman-Monteith equation, which is attributed to the fact that transpiration dominates in ET. The ETP estimation was found the most correlated to the relative humidity (RH), followed by air temperature (T), relative sunshine duration (SSD) and wind speed (WS). Under wet or medium wet climate conditions, ETA estimation was found the most correlated to T, followed by RH, SSD and WS. Under a water-stress condition, there were very small correlations between ETA and each meteorological variable.

Zusammenfassung

Die Evapotranspiration (ET) ist eine der wichtigsten Variablen in hydrologischen Studien. Beim Prozess der Evapotranspiration finden Energieaustausch und Wasserfluss statt. Die ET setzt sich aus Transpiration und Evaporation zusammen. ET wird durch den Anteil der Pflanzentranspiration dominiert. Insbesondere in Waldregionen ist der Anteil der Transpiration an der ET 80-90 %. Meteorologische Variablen, Vegetationseigenschaften, Niederschlag und Bodenfeuchte sind kritische Einflussgrößen für Ableitung der ET.

Das Untersuchungsgebiet ist das Waldgebiet des Nahe-Einzugsgebietes (Rheinland-Pfalz, Deutschland). Das Nahe-Einzugsgebiet weist einen hohen Waldanteil auf: Ungefähr 54,6 % der Fläche sind waldbedeckt, mit Laub- und Nadelwald als die beiden dominierenden Typen. Im hydrologischen Modell WaSiM-ETH wird die potenzielle Evapotranspiration (ETP) über die Penman-Monteith-Formel errechnet. Danach wird dieser Wert über den Bodenwassergehalt auf die aktuelle Evapotranspiration (ETA) reduziert. Die Penman-Monteith-Formel wird weithin eingesetzt und empfohlen für die Schätzung der ETP. Die Schwierigkeiten bei der Anwendung dieser Formel liegen in ihrem hohen Bedarf an meteorologischen Eingangsdaten und an der Notwendigkeit den Oberflächenwiderstand (surface resistance) zu bestimmen.

In dieser Studie wurde eine weitere Methode zu Schätzung der ETA eingesetzt. Dazu wurden Fernerkundungsdaten mit meteorologischen Messwerten kombiniert. Diese Methode basiert auf Oberflächeneigenschaften wie Oberflächenalbedo, Anteil Pflanzenbewuchs (FVC) und der Oberflächentemperatur (LST). Aus diesen Informationen wird der latente Wärmestrom (LE, entspricht ETA) abgeleitet. Die Oberflächentemperatur ist dabei die kritische Variable für die Schätzung einzelnen Komponenten der Oberflächenenergiebilanz. LST wurde aus dem Thermalkanal von TM/ETM+ abgeleitet. Es wurden nur sehr gute, wolkenfreie Datensätze verwendet, was die verfügbaren Datensätze auf fünf Termine einschränkt. Innerhalb der Periode 1971-2003 (Modelllauf) wurden Werte für den 15.5.2000, den 5.7.2001, den 19.7.2003, den 4.8.2003 und den 21.9.2003 abgeleitet. Die klimatischen Bedingungen waren für die Termine in 2000, 2001 and 2003 nass, feucht und trocken. Das bedeutet, dass die Fernerkundungsdaten zwar nur für wenige Termine vorliegen aber ganz unterschiedliche Feuchtebedingungen abdecken.

Der aerodynamische Widerstand und der Oberflächenwiderstand sind die beiden wichtigsten Parameter der Penman-Monteith-Gleichung. Im Wald wird der aerodynamische Widerstand durch eine Funktion der Windgeschwindigkeit ermittelt. Da Transpiration und Evaporation separat gerechnet werden, wird der Oberflächenwiderstand in den Bestandeswiderstand r_{sc} und den Bodenwiderstand r_{se} aufgeteilt. r_{sc} bezieht sich auf die Transpiration r_{se} auf die Verdunstung der unbewachsenen Bodenoberfläche. Die Interzeptionsverdunstung wurde nicht berücksichtigt, da sie unter trockenen Bedingungen (kein Niederschlag) vernachlässigt werden kann.

Auf der Basis der Fernerkundungsschätzungen wurden r_{sc} und r_{se} im Modell WaSiM-ETH kalibriert. Für Laubwald ist $r_{sc} = 150\ \mathrm{s\,m^{-1}}$, $r_{se} = 250\ \mathrm{s\,m^{-1}}$; für Nadelwald ist $r_{sc} = 300\ \mathrm{s\,m^{-1}}$, $r_{se} = 650\ \mathrm{s\,m^{-1}}$. Außerdem wurde eine Sensitivitätsanalyse für r_{sc} und r_{se} durchgeführt mit folgenden Werte-Intervallen: Laubwald [110,225] $\mathrm{s\,m^{-1}}$ für r_{sc}, [50,450] $\mathrm{s\,m^{-1}}$ für r_{se}; für Nadelwerte [225,375] $\mathrm{s\,m^{-1}}$ für r_{sc} und [350,1200] $\mathrm{s\,m^{-1}}$ für r_{se}.

Wegen der Tatsache, dass nur wenige Beobachtungsdaten mit verschiedenen klimatischen Bedingungen vorliegen sind statistische Indices notwendig to sensitiv auf Extremwerte sind. Mit Hilfe von Boxplots konnte die Modellgüte sowohl auf der zeitlichen als auch auf der räumlichen Skale gut dargestellt werden. Es wurden Nash-Sutcliffe Efficiency (NSE), RMSE-observations standard deviation ratio (RSR), Prozentuale Abweichung (PBIAS), mittlerer Bias-Fehler (MBE), mittlere Varianz der Fehler (S_d^2), index of agreement (d) und RMSE (root mean square error) als geeignete Kennwerte angesehen um die Modellgüte zu evaluieren. Ein Modell wurde als akzeptabel bewertet, wenn $NSE > 0.5, RSR \leq 0.7, PBIAS < \pm 12, MBE < \pm 0.45, S_d^2 < 1.11, d > 0.79, RMSE < 9,97$.

r_{sc} spielt eine wichtigere Rolle als r_{se} bei Abschätzung von ETP und ETA mittels der Penman-Monteith-Gleichung, was dadurch erklärt werden kann, dass die Transpiration ET dominiert. The Schätzung von ETP ist am stärksten korreliert mit der relativen Feuchte (RH), gefolgt von der Lufttemperatur (T), der relativen Sonnenscheindauer (SSD) und der Windgeschwindigkeit (WS). Unter nassen oder feuchten Bedingungen ist die Schätzung von ETA am stärksten mit der Temperatur korreliert, gefolgt von RH, SSD und WS. Unter Bedingungen mit Wasserstress existieren nur noch geringe Korrelationen zwischen ETA und den einzelnen meteorologischen Variablen.

Table of contents

List of figures

List of tables

Nomenclature

Roman Symbols

Δ	Slope of saturated vapor pressure curve at temperature T_a.
γ	Psychrometric constant.
E_a	An empirical representation of the latent heat flux density.
e_a	Actual vapor pressure.
e_s	Vapor pressure of saturated air.
ET_o	Reference evapotranspiration.
G	Soil heat flux.
H	Sensible heat flux.
r_a	Bulk aerodynamic resistance.
R_g	Global radiation.
R_n	Net radiation.
r_{sc}	Canopy surface resistance.
r_{se}	Soil surface resistance.
r_{si}	Interception surface resistance.
r_s	Bulk surface resistance.
T_a	Air temperature, abbreviated as T.
u	Wind speed, abbreviated as WS.

EI Interception evaporation.

EIP Potential interception evaporation.

ET Evapotranspiration

ETA Actual evapotranspiration.

ETP Potential evapotranspiration.

FVC Fractional vegetation cover, denote as f_r.

LAI Leaf area index.

LE Latent heat flux, corresponding to ETA.

LST Land surface temperature.

SI Interception storage.

TIR Thermal infrared.

TP Potential transpiration.

TR Actual transpiration.

Chapter 1

Introduction

1.1 Evapotranspiration

Evapotranspiration (ET) is an invisible process, through which the liquid water on the Earth (e.g. the plants' inner water, the soil containing water, the surface water storage and the flows such as lakes, rivers and oceans, and the water on the interception surfaces after rainfall) is transferred from a variety of surfaces to the atmosphere as water vapor. In the ET process, energy transfer and water cycling are involved. ET consists of two simultaneous processes – transpiration and evaporation. The transpiration transports the water within a plant through its roots, stems, branches and finally from its leaf stomata to the atmosphere. It is a both physical and biological process and is highly related to the photosynthesis. The evaporation occurs on almost all kinds of surfaces, such as the soil, the water bodies and other interception mediums, from which the liquid water evaporates to the atmosphere. The amount of transpiration dominates in ET. The partitioning of transpiration and evaporation in ET has been reported in a number of studies: in full canopy regions, e.g. forest, the transpiration contributes 80-90 % of ET (Kurpius et al., 2003; Szilagyi, 2000; Wilson et al., 2001); in irrigated crop regions, the ratio range is 85-90 % (Granger, 2000; Hunsaker et al., 2005; Kite and Droogers, 2000; Williams et al., 2004); in dry crop regions, it is 70-75 % (Persaud and Khosla, 1999); and in arid and semiarid sparse vegetated regions, the ratios reported in publications are still more than half of the total ET amount, in a range of 70-90 % (Ferretti et al., 2003; Williams et al., 2004; Yepez et al., 2003).

ET is one of the most important components in hydrological studies. It is the second largest quantity in the hydrological water balance, while the precipitation is the first largest (Dyck, 1985). On average, an amount of 60 % precipitation on the earth evaporates; in arid and semi-arid dominated regions, this amount raises to 85 % while it is down to 15 % in snow and ice permanently covered regions (Gash and Shuttleworth, 2007). The estimation of ET

has been widely used in agricultural irrigation scheduling. The amount of water loss in the ET process is defined as the crop water requirement (Allen et al., 1998). In a cropped field, the irrigation water requirement is equal to the difference between the effective precipitation and the water loss in ET. In the ET process, about $2/3$ of the total absorbed extraterrestrial radiant energy is transferred as the latent heat flux to support the vaporizing. In general, ET is not only a critical component in the land surface water cycling or energy exchange, but also the principle way to return water and energy from the land surface to the atmosphere (Gash and Shuttleworth, 2007).

Monitoring ET in a large scale also provides information on how the climate and the hydrological cycle impact the natural and agricultural ecosystem (Kustas and Norman, 1996). Huntington (2006) asserted that the climate warming in the future would induce an intensification of the global water cycle, thereby promote ET generation. There is an old idea that the surface vegetation affects the climate (Shukla and Mintz, 1982). Shukla and Mintz (1982) found that the global precipitation, the air temperature and motions were very dependent on the vegetation generated ET. The ET amount in a forested catchment is always higher than in a grassed catchment (Zhang et al., 2001). Re- and deforestation have an impact on the ET generation and thereby affect the water yield and the groundwater recharge in terms of the hydrological budget – reforestation rises ET rate and consequently reduces the annual or even long-time runoff, whereas deforest decreases the ET rate and consequently increases the runoff (Zhang et al., 2001). It is also found that the local weather can be affected by the ET amount, and the effect is embodied in air temperature, humidity and cloud formation (Rabin et al., 1990; Segal and Arritt, 1992) .

In the ET studies, there are three widely used sub concepts should be distinguished. They are potential evapotranspiration (ETP, Thornthwaite (1948)) , reference evapotranspiration (ET_o, Allen et al. (1998)) , and actual evapotranspiration (ETA, Dyck (1985)).

1.1.1 Potential evapotranspiration

The term ETP is coined by Thornthwaite (1948) to distinguish from ETA as: "There is a distinction, then, between the amount of water that actually transpires and evaporates and that which would transpire and evaporate if it were available. When water supply increases, as in a desert irrigation project, evapotranspiration rises to a maximum that depends only on the climate." Hence, ETP represents the maximum water loss to the atmosphere under a given weather condition, and is commonly used for ETA estimation in the rainfall-runoff models. Penman (1948) proposed an aerodynamic and energy-balance combined approach to estimate evaporation from the open water on the basis of the meteorological variables, and respectively calculated the ETP from the bare soil, the wet soil and the grass surfaces as a

fraction of the open water evaporation. The Penman equation has been considered as the prototype of a standard method for ETP estimation. In the equation, the energy supply to the surface and the atmospheric parameters are held as constant when the surface becomes saturated. The Penman equation has been widely accepted since the ETP can be conveniently calculated through it with the meteorological variables (Thornthwaite, 1948). It is written as (Penman, 1948):

$$ETP = \frac{H \cdot \Delta + \gamma \cdot E_a}{\Delta + \gamma} \tag{1.1}$$

with

$$E_a = 0.35(0.5 + u/100)(e_s - e_a) \tag{1.2}$$

where H is the sensible heat flux; Δ is the slope of the saturated vapor pressure curve at temperature T_a; γ is the psychrometric constant; E_a is an empirical representation of the latent heat flux density; u is the wind speed ; e_s is the vapor pressure of saturated air and e_a is the actual vapor pressure.

However, the Penman equation is not suitable for tall crops, e.g. the forest, whose aerodynamic and surface resistances are much different from the grassland (Calder, 1977). The aerodynamic resistance r_a is used to express the aerodynamic restrain while the heat and the water vapor transferring. The surface resistance r_s is related to the transpiring from plants and the evaporation from surfaces. The development of the Penman equation containing parameters r_a and r_s have been subsequently introduced in a series of publications (Covey, 1959; Penman and Long, 1961; Slatyer et al., 1961; Tanner and Pelton, 1960; Van Bavel, 1966). Based on these studies, Monteith et al. (1965) proposed an ultimately modified approach termed as the Penman-Monteith equation, which has been to date widely used and recommended for ETP estimation (Allen et al., 1989, 1998; Droogers and Allen, 2002). The high demand of ground-measured data such as solar radiation, air temperature, air humidity and wind speed is an usage restriction of this method. Thus, the Penman-Monteith equation could not be applied in lacking-data regions. Moreover, the determination of r_s is also very difficult. The ETP is a climatic parameter estimated from the meteorological variables and is independent of the crop characteristics and the soil water conditions (Allen et al., 1998).

1.1.2 Reference evapotranspiration

The reference evapotranspiration (or the reference crop evapotranspiration, ET_o) has been commonly used for the crop water requirement determination and consequently for the irrigation planning and the agriculture water management (Droogers and Allen, 2002). In many publications, the definition of ET_o is confused with ETP (e.g. Gong et al. (2006)).

Indeed, there is a difference – the definition of ET_o is more narrow than ETP. The ET_o is defined as the ETP rate from a reference crop surface, with the crop are well-grown and well-watered. Like ETP, the ET_o depends only on the climatic factors, with no regard to the impact from the crops or the soil water.

To obtain the crop water requirement, a two-step method referred to as "$K_c.ET_o$" approach is proposed by Doorenbos and Pruitt (1977) in the FAO (Food and Agriculture Organization of the United Nations) -24 report. In the approach, the first step is to calculate the ET_o, which is defined in the report as "the rate of evapotranspiration from an extensive surface of 8 to 15 cm tall, green grass cover of uniform height, actively growing, completely shading the ground and not short of water". The crop water requirement is then estimated by transferring ET_o with a crop coefficient K_c, which depends on the crop characteristics and the site conditions. This approach has been accepted as an international standard method for the crop water requirement estimation (Smith et al., 1998).

In the FAO-24 report, four methods were recommended for the ET_o estimation – the Blaney-Criddle method (Blaney, 1952), the Radiation method, the modified Penman method, and the Pan Evaporation method, while the modified Penman (hereafter referred to as FAO Penman) method was found to generate the best result with minimal errors (Doorenbos and Pruitt, 1977). However, it is found that the FAO Penman equation frequently overestimates the ET_o rate, and the other three methods show variable adherence to the reference-crop evapotranspiration standard of grass (Allen et al., 1989; Batchelor, 1984; Jensen et al., 1990). A modified Penman-Monteith approach referred to as FAO Penman-Monteith equation is subsequently developed and recommended as the sole standard method for the ET_o estimation (Allen et al., 1998; Droogers and Allen, 2002; Smith et al., 1998). In the standard FAO Penman-Monteith equation, the reference surface is defined as: "A hypothetical reference crop with an assumed crop height of 0.12 m, a fixed surface resistance of 70 $\mathrm{s\,m^{-1}}$ and an albedo of 0.23" (Allen et al., 1998).

The standard FAO Penman-Monteith equation is written as:

$$ET_o = \frac{0.408\Delta(R_n - G) + \gamma(900/(T_a + 273))u(e_s - e_a)}{\Delta + \gamma(1 + 0.34u)} \tag{1.3}$$

where R_n is the net radiation at the crop surface in $\mathrm{MJ\,m^{-2}\,day^{-1}}$; G is the soil heat flux density in $\mathrm{MJ\,m^{-2}\,day^{-1}}$; T_a is the air temperature at 2 m height in $^{\mathrm{o}}\mathrm{C}$; u is the wind speed at 2 m height in $\mathrm{m\,s^{-1}}$; e_s is the vapor pressure of saturated air in kPa; e_a is the actual vapor pressure in kPa; Δ is the slope of the vapor pressure curve in $\mathrm{kPa\,^{o}C^{-1}}$; γ is the psychrometric constant in $\mathrm{kPa\,^{o}C^{-1}}$.

In the Table 1.1, typical values of ET_o for different agroclimate are listed. The general ET_o is in an approximate range from 1 to 9 mm day^{-1}.

Regions		Mean daily temperature (^{o}C)		
		Cool $\sim$ 10 ^{o}C	Moderate 20 ^{o}C	Hot $>$ 30 ^{o}C
Tropics and subtropics	humid and sub-humid	2-3	3-5	5-7
	arid and semi-arid	2-4	4-6	6-8
Temperate region	humid and sub-humid	1-2	2-4	4-7
	arid and semi-arid	1-3	4-7	6-9

Table 1.1 Average ET_o (mm day^{-1}) for different agroclimate regions (Allen et al., 1998).

1.1.3 Actual evapotranspiration

The term ETA is defined by Dyck (1985) as: "a largely empirical function of plant specific potential evapotranspiration and soil water content SM or soil matric potential ψm and threshold value above which actual and potential evapotranspiration are equal". ETA is also termed as the crop evapotranspiration under non-standard conditions ($ET_{c\,adj}$) , distinguished from ET_o in a reference grass surface (Allen et al., 1998). In the early time, lysimeters, eddy flux instrumentation and Bowen-ratio instrumentation were directly used for ETA measurement. However, the high cost of instruments, the requirement of constant attendance for skilled operators, the basis of unverified assumptions and the point-value measure results all point out that a direct measure is an inappropriate means for ETA estimation (Morton, 1983). A common application of ETA is the crop water requirement determination, which is generally obtained by ET_o multiplying the crop coefficient K_c. The parameter K_c is the integrated effects of crop height, albedo, canopy resistance and evaporation from soil. It is thereby determined by crop types, crop growth stages, soil evaporation and climate conditions (Allen et al., 1998). However, this means has drawbacks because the K_c is difficult to determine. In order to physically calculate the ETA, Dyck (1985) introduced four steps: (1) to calculate the ET_o on a short green grass surface, assuming the water supply is adequate; (2) to calculate the site-related ET_o, taking the surface properties such as slope, aspect and surface albedo into account; (3) in terms of (2), to calculate the ETP with particular vegetation type with sufficient water supply; (4) to calculate the ETA according to the soil moisture by reducing ETP obtained in (3). To date, in most hydrological models, these steps are simplified into two – to obtain the ETP; then reduce it according to the actual soil water content to get ETA (e.g. WaSiM-ETH model Schulla and Jasper (2007)).

Therefore, meteorological variables, crop features and soil water conditions are important factors affecting ETA estimation.

In last decades, remote sensing techniques have also been frequently used for ETA estimation (Bastiaanssen et al., 1998a,b; Carlson et al., 1995; Hatfield et al., 1983; Jiang and Islam, 1999; Kustas and Norman, 1996; Soer, 1980). The advantages of remote sensing images such as economic, efficient, and large-area available alleviate the high demand for ground-measured data and make remote sensing techniques popular in hydrological studies. In sparse-data catchments, the remote sensing-retrieved variables can provide additional information. The remote sensing-based data are always superior in spatial accuracy with contrast to the ground measurements – the spatial accuracy of the former depends on the remote sensing images whereas for the latter, it depends on the locations and numbers of available climate stations. The land surface temperature (LST) retrieved from the thermal infrared (TIR) bands in the remote sensing images provides information on ETA and the soil water conditions. Therefore, it has been widely used for ETA amount and soil moisture condition estimation (Carlson et al., 1981; Gurney and Camillo, 1984; Seguin and Itier, 1983). To estimate ETA (corresponding to the latent heat flux (LE) in the energy balance equation) , the LST is commonly used to firstly retrieve the sensible heat flux (H) through an empirical method (Carlson et al., 1995; Jackson et al., 1977; Seguin and Itier, 1983). However, LST is difficult to obtain due to the high-heterogeneity of land surface, the unknown emissivity and atmospheric conditions (Jin, 2004). Using remote sensing TIR data is the the only means for a large-scale LST retrieving. The LST-based methods eliminate the difficulty of surface resistance determination in ET estimation with conventional methods (Brown, 1974).

There is a misconception that a larger ETP rate necessarily indicated a larger ETA rate. However, Bouchet (1963) found that as a moist surface dried, the ETP increased whereas the ETA decreased. He consequently proposed a concept termed as "complementary relationship", which describes the correlation between ETA, ETP and the potential evaporation under a saturate-surface condition that when ETA equals ETP (ETP_s). The complementary relationship assumes that as the surface dries, the decrease amount of ETA is equal to the increase amount of ETP; and this amount is twice of ETP_s. Based on the relationship, some evaporation models have been developed (Brutsaert and Stricker, 1979; Morton, 1983). In these models, the Penman equation is used to estimate the ETP rate.

1.2 Factors affecting evapotranspiration

According to these sub ET concepts, it is obviously that meteorological data, crop characteristics and soil water content are very important factors that affecting the ET estimation.

Zhang et al. (2001) concludes that ET is very dependent on rainfall interception, net radiation, advection, turbulent transport, leaf area and plant available water capacity, whose relative importances are related to the crop, soil and climate.

1.2.1 Meteorological variables

In the Penman-Monteith equation, solar radiation, air temperature, air humidity and wind speed are the basic meteorological variables for ET estimation. The sunshine radiation supplies energy for water cycling and heat exchanging. Thus more effective incident solar radiation to the land surface, namely more absorbed net radiation (R_n) may partition more energy supporting the ET process – in general, about $2/3$ of the total absorbed radiant energy is partitioned for ET generation (Gash and Shuttleworth, 2007). The vapor pressure deficit – the difference between the saturated air vapor pressure and the actual air vapor pressure ($e_s - e_a$) encourages the ET generation. The bigger the term ($e_s - e_a$) is, the rapidly the ET generates. An increase of air temperature raises the capacity of air to hold the water vapor (e_s) – approximately equals to 5 or 6 % per ^{o}C, to enlarge the vapor pressure deficit and consequently increase the ET amount. High wind speed also accelerates the ET process.

The relative importance of each variable has been reported in a number of publications (Bakhtiari et al., 2012; Beven, 1979; Gleick, 1986; Gong et al., 2006; Goyal, 2004; McCuen, 1974; Piper, 1989; Revelle and Waggoner, 1983; Samani, 2000; Saxton, 1975). McCuen (1974) found that temperature and humidity were the most sensitive variables to the Penman equation, whereas wind speed was the least. Saxton (1975) derived sensitive equations from a modified Penman equation and found that the ETP was the most sensitive to the net radiation – radiation change in each unit would result in 50-90 % change in ETP during midyear. Beven (1979) found that, in both hourly and monthly time steps, the relative importance of net radiation for the Penman-Monteith ETA estimation was very high in the grassland but became very small in the forest regions. In the earliest studies, ET was formulated as a function of temperature (Gleick, 1986; Revelle and Waggoner, 1983), indicating that the air temperature was considered as the most important factor. Piper (1989) examined the sensitivity of the Penman evaporation to the uncertainty in measured input variables under a wide range of climate conditions, and found that ET_o was most sensitive to the errors in the measurement of air temperature, as well as the errors in sunshine duration, wind speed and wet bulb temperature had small and more or less the same relative impact on ET_o. Samani (2000) used the minimal and maximal temperature through a modified equation to estimate the solar radiation and subsequently the ET_o rate. He concluded that solar radiation and air temperature were the most important factors, since the major energy used for ET is from solar radiation, and the air temperature is highly correlated with the solar radiation. Goyal (2004)

concluded that the sensitivity of climatic factors to ET estimated by the Penman-Monteith approach were in an order as: air temperature > solar radiation > wind speed > air humidity. Gong et al. (2006) studied the Penman-Monteith ET_o in the Changjiang basin, and found that the relative humidity was the most sensitive factor, followed by shortwave radiation, air temperature and wind speed in orderly. Bakhtiari et al. (2012) stated that ET_o estimated by the FAO Penman-Monteith equation was the most sensitive to net radiation; and in arid and semiarid cool regions, the sensitivity of each meteorological variable was higher than that in arid warm regions. Thus, the meteorological variables are very important factors affecting the ET estimation, and their relative importances vary in different cases.

1.2.2 Vegetation properties

Plants on the Earth's surfaces such as grasses, agricultural crops, bushes and forests are generally referred to as vegetation. Vegetation is helpful in preventing the desertification process, conserving the soil and water and consequently reducing the runoff. The surface vegetation not only plays a significant role in biogeochemical cycle, water cycle, and energy exchange, but also affects the climate. All these can be attributed to the effect of the ET generated by vegetation. Based on 39 studies on how forest cover changes impact the water yield, Hibbert (1965) found that re- and deforestation led to the de- and increase of water yield, respectively. Based on a review of the experiences of 94 catchments, Bosch and Hewlett (1982) updated Hibbert's conclusion that a reduction in forest cover decreased the ET amount and consequently increased the water yield. In the forested catchments, ET is mainly generated by the plants, and its magnitude is much higher than that in the grassland. Zhang et al. (2001) concluded that management and rehabilitation mainly changed the vegetation surfaces and affected the water balance of catchments. This can be explained by the direct impact from vegetation on ET, which subsequently affects the climate, water balance and discharge. In the ET process, the regional climate in forest area is very dependent on the vegetation. Apart from the vegetation density, the plant characteristics such as the surface albdeo, the normalized difference vegetation index (NDVI), the fractional vegetation cover (FVC), the canopy surface temperature and resistance are also important factors. In the Penman-Monteith equation, the aerodynamic resistance and the surface resistance are critical parameters for ET estimation; especially in forest regions, the ETA is found to be much more sensitive to canopy resistance than aerodynamic resistance (Beven, 1979; Calder, 1977). In general, the vegetation properties are critical influence factors for ET estimation since the transpiration directly generated by vegetation dominates in the total ET rates in almost all kinds of land use types (Glenn et al., 2007; Kurpius et al., 2003; Szilagyi, 2000; Wilson et al., 2001).

1.2.3 Precipitation and soil moisture

The soil moisture is a critical factor that influences ETA estimation – since in many physical equations or models for ETA estimation, the amount of ETA is decided by reducing ETP according to the actual soil moisture in the root zone (e.g. WaSiM-ETH model). Well-watered plants open their stomata for the transpired water passing. In this process, the temperature of plants' leaves are cooling and the surrounding air are subsequently warming. However, in case that the soil moisture in the root zone is not sufficient, the stomata close to preserve the inner water, and consequently decrease the ET rate. The soil moisture is commonly simulated with the precipitation measurements due to their strong association with each other (Koster et al., 2004). Thus, the impact of soil moisture on ETA can be actually returned to the correlation between precipitation and ET.

Precipitation and ET are two reverse processes caused by different reasons – the former transfers the water from atmosphere to the land surface and the latter transfers them back as water vapor to the atmosphere. Precipitation and ET are in turns the first and second largest components in magnitude in the water budget (Dyck, 1985). Pike (1964) proposed an equation based on the water balance, in which the annual ET in Malawi was obtained as the residual between annual rainfall and the sum of runoff, seepage passed the gauging stations, as well as the change in groundwater storage. In a water balance equation in volume per surface area over time that proposed by Eagleson (1978), the precipitation is transformed into ETA, surface storage, subsurface storage, direct flow, base flow and stream flow (discharge). The precipitation directly and significantly affects the hydrological budget and the antecedent soil moisture conditions, and it also plays a significant role in runoff magnitude (Loague and Freeze, 1985). A rational equation for the calculation of the annual ET in watershed in a Mediterranean-type climate was proposed by Turner (1991), in which, annual ET is obtained by a function of annual precipitation and a fractional vegetation cover in the watershed (shrubs and trees). Zhang et al. (2001) studied a result from 250 forested catchments and pointed out the good relationship between average ET and precipitation in a long time period. A study in Beijing mountain area also reported that precipitation had an seasonal impact on vegetation coverage (Jing et al., 2011). High accuracy precipitation data is necessary for ETA estimation. However, the accuracy of precipitation data measured and computed from climate station networks is always not sufficient due to its high spatial-temporal variability (Dyck, 1985).

To tell whether a climate is moist or dry, not only the amount of precipitation should be known, but also the precipitation is greater or less than the ETA should be taken into account (Thornthwaite, 1948).

1.3 Material and techniques

1.3.1 Study area

The study area is the Nahe catchment locating in the state of Rhineland-Palatinate, in the southwest of Germany (Figure 1.1). River Nahe is about 120 km in length, rising from the bound of Saarland and joining into River Rhine in Bingen. The drainage basin of River Nahe is in total 4065 km^2. This area is famous for grape cultivation and quality wine production due to its moderate climate. The elevation of the entire Nahe catchment is on an average of 353 m. In Figure 1.2a, the distribution of River Nahe and its tributaries is pointed out by the elevation values range in 101-200 m. The northwest region of Nahe catchment is mountainous, whose elevation ranges from 300 to 817 m. The Nahe catchment is highly wooded. About 54.6 % areas of Nahe catchments is covered with forest (Figure 1.2b). Deciduous forest and coniferous forest are two primary forest types here. The proportion of deciduous and coniferous forest to the entire region are 59.1 % and 40.9 %, respectively.

The Nahe catchment has long been known as flood prone area. The residents settled along River Nahe and its tributaries have suffered a lot from flood damages. In the recent huge flood events in 1993 and 1995, the damage cost was over 100 million Deutsche Mark for the entire region.

1.3.2 Hydrological model

This study is based on the former works of the KlimLand-Project (Casper et al., 2013). In the study, a hydrological model – WaSiM-ETH (Water Flow and Balance Simulation Model, firstly developed in ETH, Zurich) was applied for a long-term simulation from year 1971 to 2003 in the Nahe catchment. WaSiM-ETH is a distributed, deterministic, mainly physical-based hydrological model. It has been widely used in Europe and frequently reported in publications (Cullmann et al., 2006; Gurtz et al., 2000; Jasper, 2005; Jasper et al., 2002; Klok et al., 2001; Verbunt et al., 2003). In WaSiM-ETH, several sub modules take part in water balance simulation above and under the land surfaces. In this study, three steps were performed in the model to obtain ETA. The first step is to estimate ETP by the Penman-Monteith equation (Monteith et al., 1965) on the basis of the ground-measured meteorological variables. The second step is to simulate the soil water content in vertical direction via Richards equation (Richards, 1931). Based on the previous steps, ETA was obtained by reducing ETP according to the actual soil water content in a daily time step.

The ground-measured meteorological variables such as relative sunshine duration (SSD, dimensionless), air temperature (T, in ^{o}C), relative humidity (RH, dimensionless) and wind

Fig. 1.1 Location of the Nahe catchment.

speed (WS, in $\mathrm{m\,s^{-1}}$) are basic input data for ETP estimation. These data were selected from 19 climate stations over the entire region of Rhineland-Palatinate (Figure 1.3a). The SSD is the ratio of the actual sunshine duration hours to the possible maximum sunshine duration hours. It ranges from 0 to 1 and have to exceed 0.1, since the value of SSD less than 0.1 indicates that only diffuse radiation exist, which is incorrect (Schulla and Jasper, 2007). The RH is the ratio of the actual vapor pressure to the saturated vapor pressure, which indicates the saturation degree of the air. When T is high and RH is low, water evaporates rapidly, whereas when T is low and RH is high, water evaporates slowly. Moreover, the regional air temperature and humidity are also found to be affected by ET (Rabin et al., 1990; Segal and Arritt, 1992).

The precipitation is an important input data for snow accumulation and melting, interception evaporation and soil water content estimation. Due to the high spatial and temporal

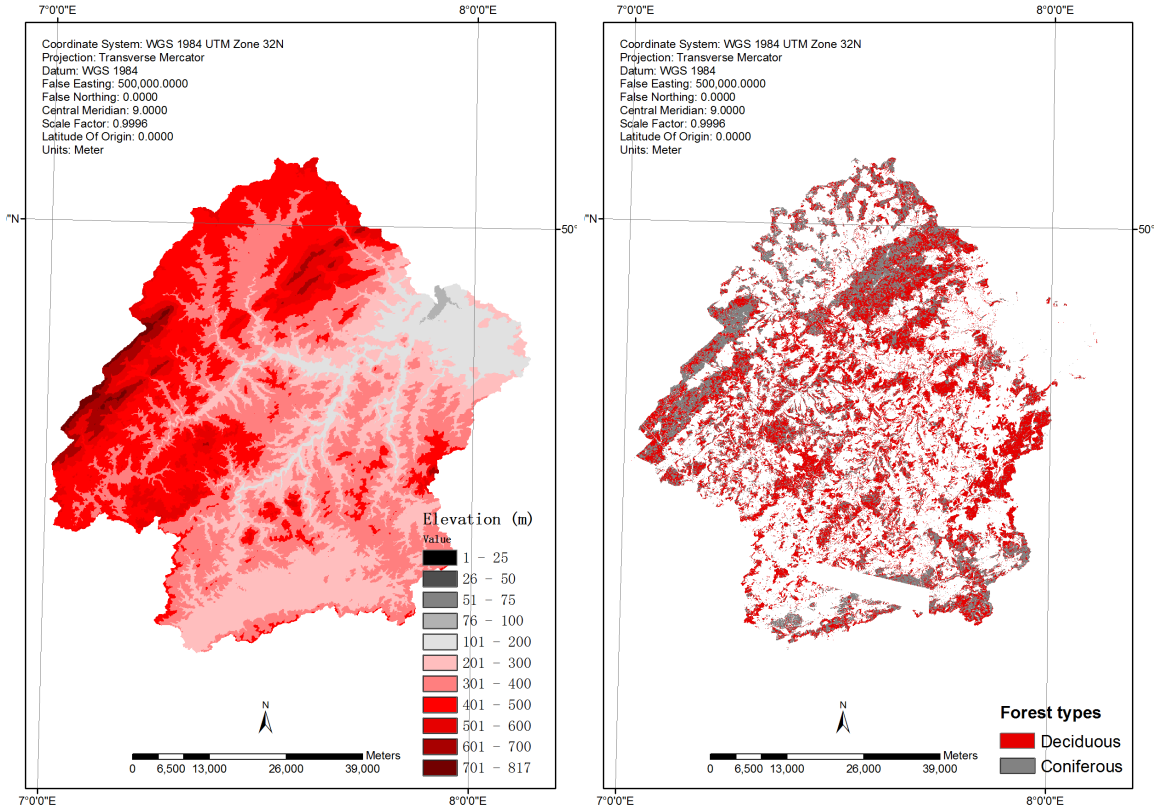

(a) Elevation (m) (b) Forest distribution

Fig. 1.2 Elevation and forest distribution of the Nahe catchment.

variability of precipitation data, a dense mesh of gauging stations are required for data measurement and computation. The precipitation station networks are shown in Figure 1.3b.

1.3.3 Remote sensing

Landsat

Remote sensing techniques were also employed for ETA retrieving. The basic input data are remote sensing images combining with the same meteorological ground measurements used in the WaSiM-ETH model. The remote sensing-based ETA are considered as ideal observation data corresponding to the ETA simulated by WaSiM-ETH. The remote sensing images from Landsat Thematic Mapper (TM) and Enhanced Thematic Mapper plus (ETM+) were selected in the time period 1971-2003 (model run). Due to the high-quality and cloudy-free requirements for the data selection, images on only five separate dates are available – May 15, 2000, July 05, 2001, and July 19, August 04, and September 21, in 2003 (Table 1.2). It is known that the summer in 2003 was extremely warm and dry in Germany.

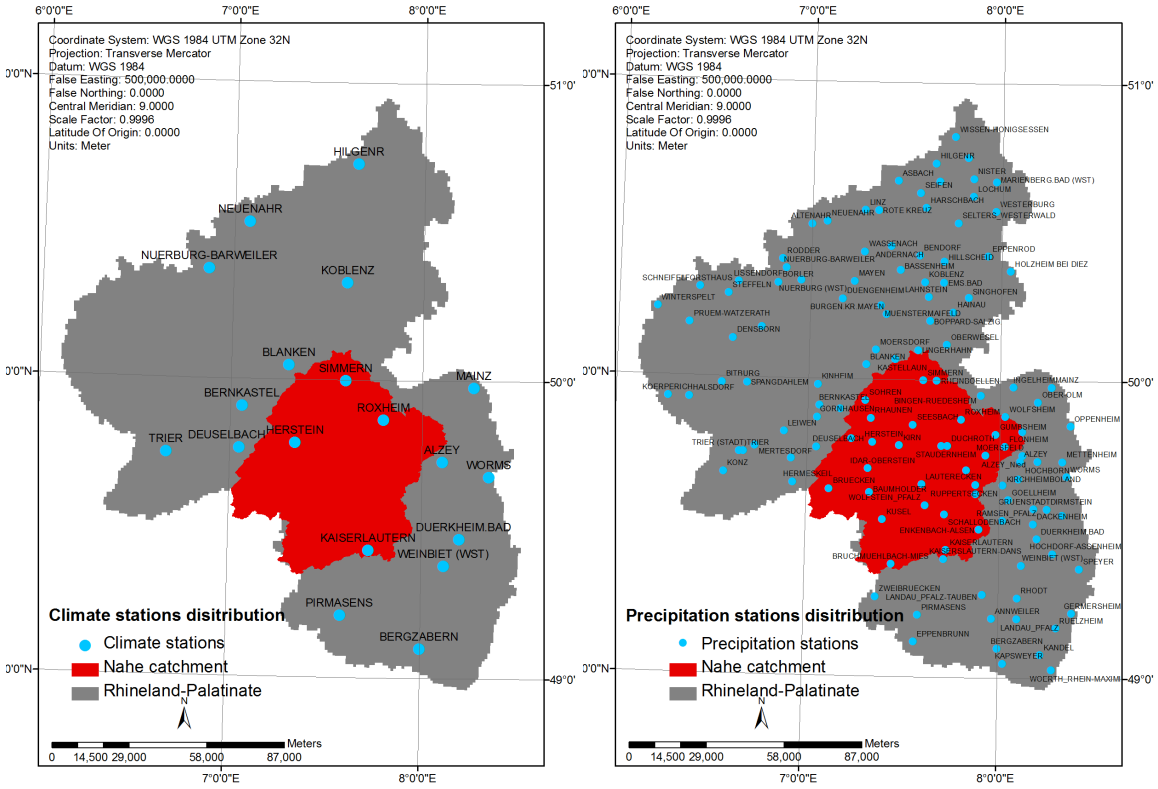

(a) Climate stations (b) Precipitation stations

Fig. 1.3 Available climate and precipitation stations in Rhineland-Palatinate, Germany.

The TM sensor was carried on Landsat 4 and 5 from July 1982 to May 2012, with an overlapping cycle of 16 days. TM images consist of 7 bands, with bands 1-5 and 7 are in a spatial resolution at 30 m as well as the resolution of thermal band 6 is collected at 120 m but resampled to 30 m (NASA, 2015e; USGS, 2015). The ETM+ sensor was carried on Landsat 7 since July 1999. However, a scan line corrector failure has occurred to the data since May 30, 2003. The rescan cycle of the ETM+ sensor is also 16 days. The ETM+ images consist of 8 spectral bands, with band 6 is also the thermal band and band 8 is the panchromatic band. The spatial resolution is 30 m for band 1-7 (band 6 is selected as 60 m and resampled to 30 m) as well as it is 15 m for band 8 (Irish, 2000; NASA, 2015a). In this study, the reflected bands 1-5 and 7 of TM/ETM+ were used for a series of surface properties computation: surface albedo, normalized difference vegetation index (NDVI), fractional vegetation cover (FVC) and land surface emissivity (LSE). The thermal infrared (TIR) band 6 was used for the land surface temperature (LST) retrieval. The finally retrieved daily ETA on five separate dates were applied as observations for model performance comparison and evaluation, which corresponded to the simulated ETA by the WaSiM-ETH model.

Spacecraft	Sensor	Date	Path_Row	Temporary
Landsat7	ETM+	2000-05-15	196_025	daily
Landsat7	ETM+	2000-05-15	196_026	daily
Landsat7	ETM+	2001-07-05	196_025	daily
Landsat7	ETM+	2001-07-05	196_026	daily
Landsat5	TM	2003-07-19	196_025	daily
Landsat5	TM	2003-07-19	196_026	daily
Landsat5	TM	2003-08-04	196_025	daily
Landsat5	TM	2003-08-04	196_026	daily
Landsat5	TM	2003-09-21	196_025	daily
Landsat5	TM	2003-09-21	196_026	daily

Table 1.2 Selected Landsat images on 5 sample dates during the period 1971-2003 (model runs).

MODIS product

In this study, Moderate Resolution Imaging Spectroradiometer (MODIS) products - MOD 03, MOD 05 and MOD 09 on five sample dates were also selected (Figure 1.3). MOD 09 was used for the atmospheric correction of the Landsat images with an empirical method. MOD 05 was used for the surface water vapor retrieving, which is an important input data for LST determination (NASA, 2015c). MOD 03 is the basic geolocation data for the level 2 MODIS products (e.g. MOD 09) processing (NASA, 2015b). The MODIS instrument is designed for land, ocean and atmosphere monitoring. It was carried on the Earth Observing System (EOS) Terra and Aqua satellites that respectively launched in 1999 and 2002. The MODIS image combined the characteristics of both AVHRR (Advanced Very High Resolution Radiometer) and TM data. Thus, its radiometric and geometric quality is very high. There are many standard MODIS products for a variety of uses.

MOD 03

MOD 03 is the MODIS Geolocation product, which contains information on geodetic coordinates, ground elevation, solar and satellite zenith and azimuth angle. It is an auxiliary data set for the further processing of MODIS Level 2 products (NASA, 2015b).

MOD 05

The MODIS Precipitable Water product (MOD 05) is used for water vapor estimation. It consists of vertical column water-vapor amounts in cm and is in a spatial resolution at 1 km (NASA, 2015c).

MOD 09

The MODIS Surface-Reflectance Product (MOD 09, (Vermote et al., 2011)) is computed from the MODIS Level 1B land bands 1, 2, 3, 4, 5, 6, and 7 (centered at 648 nm, 858 nm, 470 nm, 555 nm, 1240 nm, 1640 nm, and 2130 nm, respectively). The product is an estimate of the surface spectral reflectance for each band as it would have been measured at ground level if there were no atmospheric scattering or absorption (NASA, 2015d; Vermote et al., 2011).

Products	Date	Level	Resolution (m)	temporary
MOD 03	2000-05-15	1B	1000	daily
MOD 05	2000-05-15	2	1000	daily
MOD 09	2000-05-15	2	500/1000	daily
MOD 03	2001-07-05	1B	1000	daily
MOD 05	2001-07-05	2	1000	daily
MOD 09	2001-07-05	2	500/1000	daily
MOD 03	2003-07-19	1B	1000	daily
MOD 05	2003-07-19	2	1000	daily
MOD 09	2003-07-19	2	500/1000	daily
MOD 03	2003-08-04	1B	1000	daily
MOD 05	2003-08-04	2	1000	daily
MOD 09	2003-08-045	2	500/1000	daily
MOD 03	2003-09-21	1B	1000	daily
MOD 05	2003-09-21	2	1000	daily
MOD 09	2003-09-21	2	500/1000	daily

Table 1.3 Selected MODIS products on 5 sample dates.

1.4 Climate conditions

Since ET is very dependent on the climate conditions, it is necessary to understand the variances of the basic meteorological variables firstly in the study area. In Figure 1.4 (deciduous forest) and Figure 1.5 (coniferous forest), the ground-measured meteorological variables such as precipitation (P, in mm), air temperature (T, in ^{o}C), relative humidity (RH, dimensionless), relative sunshine duration (SSD, dimensionless) and wind speed (WS, in $\mathrm{m\,s^{-1}}$) from May 01, 2000 to September 30, 2003 (the long-time period included the five sample dates) in a daily time step are shown. It is noted that on the five sample dates, there was no rainfall. The other meteorological variables such as T, RH, SSD and WS on these sample dates in both forests are also shown in Figure 1.7.

In Figure 1.4a, it is shown that in deciduous forest there were abundant rainfall in 2000, especially in July and September, whose maximal daily rainfall respectively approximated to 25 and 30 mm per day. In contrast, on most days in 2003, there were little rainfall. It was very dry on the days before May as well as in July and August in 2003, whereas about half a month before September 21, 2003, a precipitation over 20 mm occurred. In contrast to the "wet" year 2000 as well as the "dry" year 2003, the temperate precipitation amounts in 2001 and 2002 are thereby rated as "medium". With respect to the five sample dates, it was extremely wet on May, 2000, which closely followed a huge precipitation over 20 mm; on July 19, and August 04 in 2003, it seems to be very dry due to the rarely rainfall; on September 21, 2003, it is hard to rate, since the impact of the huge rainfall that occurred half a month before was unknown; on July 05, 2001, it is also considered as medium wet with compare to the other dates. In the coniferous forest (Figure 1.5a), the precipitation conditions were more or less the same as in the deciduous forest. However, since to judge a climate is wet or dry should not only on the basis of the precipitation amount (Thornthwaite, 1948), these ratings such as wet, medium wet, and dry should be further verified.

In general, the T rises in the summer time and always reaches to the top values of the whole year in July or August. In Figure 1.4b and 1.5b, the variances of T over time in both forest types followed this seasonal variation rule. It is noted that in the August of 2003, the T values were much higher than those days at the same time in the previous years. Moreover, on August 04, 2003, the T was also the top of all five sample dates (over 26 ^{o}C, Figure 1.7a). On May 05, 2000 and September 21, 2003, the T were relatively lower than the other three dates in summer.

In Figure 1.4c and 1.5c, the RH increased in winter time and decreased in the summer, which was opposite to the seasonal variance of T. The RH were very high in 2000, whereas in 2003, the RH were obviously lower than the other three years. It is noted that on July 19, August 04, and September 21 in 2003, the RH were lower than their corresponding periods' mean values in 2000-2002. Especially in July and August in 2003, the RH were extremely low that were consistent with the known climate condition that the summer of 2003 in Germany was extremely warm and dry. In terms of the P and RH measurements, the wet climate in 2000, medium wet climate in 2001, and dry climate in 2003 summer are confirmed. With regard to the five sample dates (Figure 1.7b), the relatively low RH on August 04, 2003 accompanying with the highest T would lead to a rapid ET generation on that day, whereas on May 15, 2000, the opposite simultaneous low T and relatively high RH would result in slow ET generating. Therefore in terms of the measurements of P, T and RH, the five sample dates are confirmed to contain multiple climate conditions such as wet, medium wet and dry.

In Figure 1.4d and 1.5d, apparently abundant SSD were shown in 2003 with compare to in 2000 (the SSD in 2000 were the minimum in 2000-2003). In general, relatively high SSD were shown in the summer, whereas in the winter, the SSD value were the annual minimum. On the three sample dates in 2003 (Figure 1.7c), the SSD amount were much higher than at the other two dates (around 0.9 v.s. not more than 0.8), which might lead to more energy supplements to the water cycle and energy exchange. It is noted that on July 05, 2001, the SSD was extremely low with compare to the general cases in summer. In Figure 1.4e and 1.5e, a seasonal rule for the WS is also shown: the values of WS were high in winter time and became relatively low in summer time. The wind speed of all five dates were not more than 2.5 $\mathrm{m\,s^{-1}}$.

In Figure 1.6, the differences of each meteorological variable between deciduous and coniferous forest are shown. The negative value indicates that the variable amount in the deciduous forest was higher than in the coniferous forest. In general, the T, RH, and WS data respectively exhibited apparent differences between two forest types in daily scale during the whole time period. With regard to the five sample dates (Figure 1.7), it is noted that, for both forest types, there were also significant differences respectively in T and RH values between forests, whereas the SSD and WS were almost the same on each date. In terms of the fact that T in deciduous forest were generally higher than in coniferous forest, we infer that more ET generated in deciduous forest than in coniferous forest, since high air temperature encourages ET generation. With regard to the RH (Figure 1.6c), in the plants growing season of deciduous forest (May to August), the RH in the deciduous forest were obviously lower than in the coniferous forest. This fact also support the inference that – during growing season, the deciduous forest generated more ET than the coniferous forest, while in non-growing season, it was opposite. Likewise, the higher WS values in the deciduous forest (in Figure 1.6e) speeded the ET process and encouraged the ET generating in a higher level with compare to in the coniferous forest. On the other hand, the local air temperature, air humidity and cloud formation are also affected by the ET amount (Rabin et al., 1990; Segal and Arritt, 1992). It also makes sense, that in the deciduous forest with more regional ET rates in a long-time period, the regional T increased due to more heat transferred to the atmosphere; the RH decreased since the rising T increased the water vapor capacity of the saturated air; the WS became rapid since the intensification of the water cycling promoted the air motion. Therefore, those differences of T, RH and WS between two forest types are assumed as not only the causes of the difference in amount of generated ET rates in two forest types but also the results from the feedback of the generated ET rates in a long-term period.

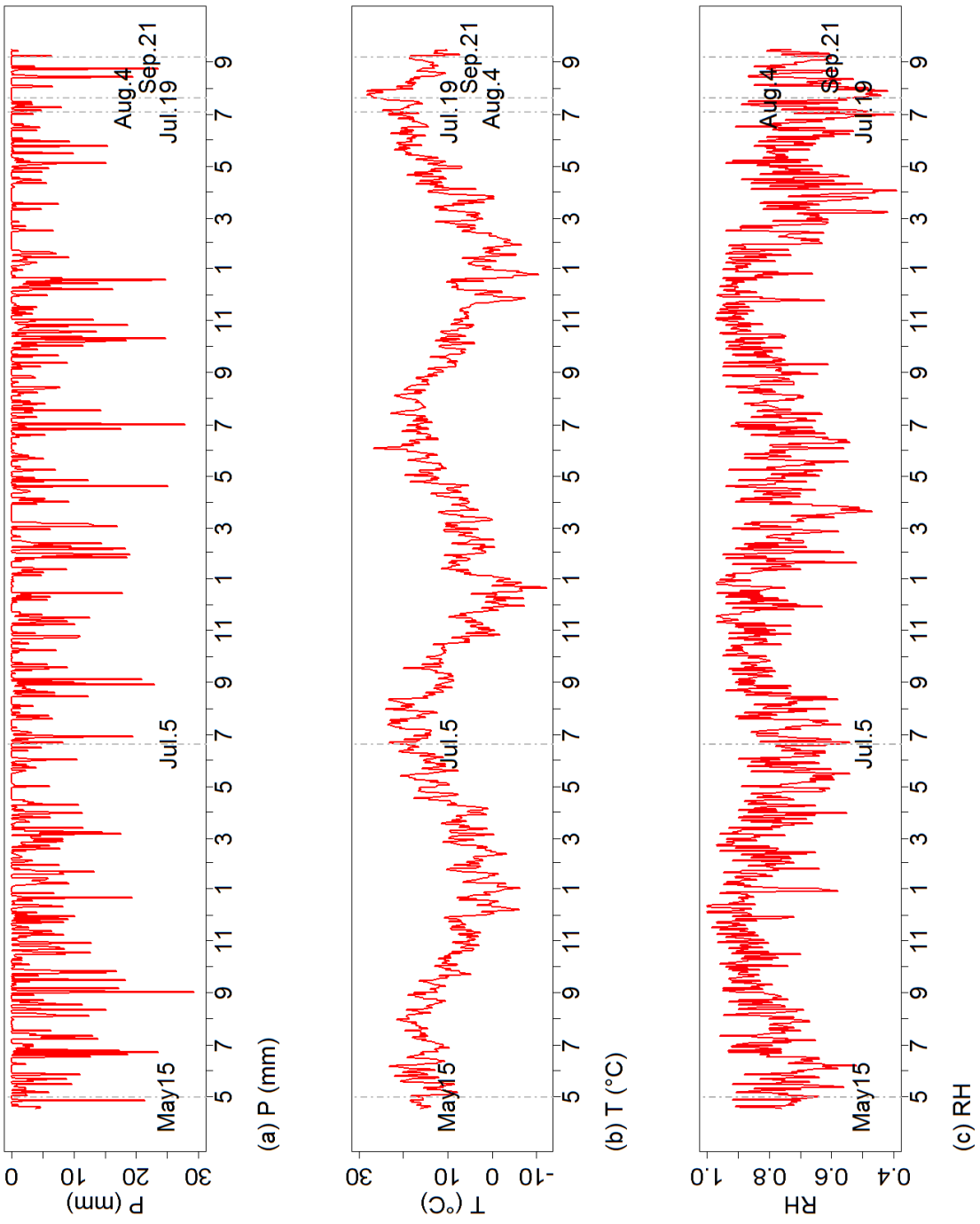
P (mm)
0
10
20
30
May15
Jul.5
Jul.19
Aug.4
Sep.21
(a) P (mm)
T (°C)
-10
0
10
30
May15
Jul.5
Jul.19
Aug.4
Sep.21
(b) T (°C)
RH
0.4
0.6
0.8
1.0
May15
Jul.5
Jul.19
Aug.4
Sep.21
(c) RH

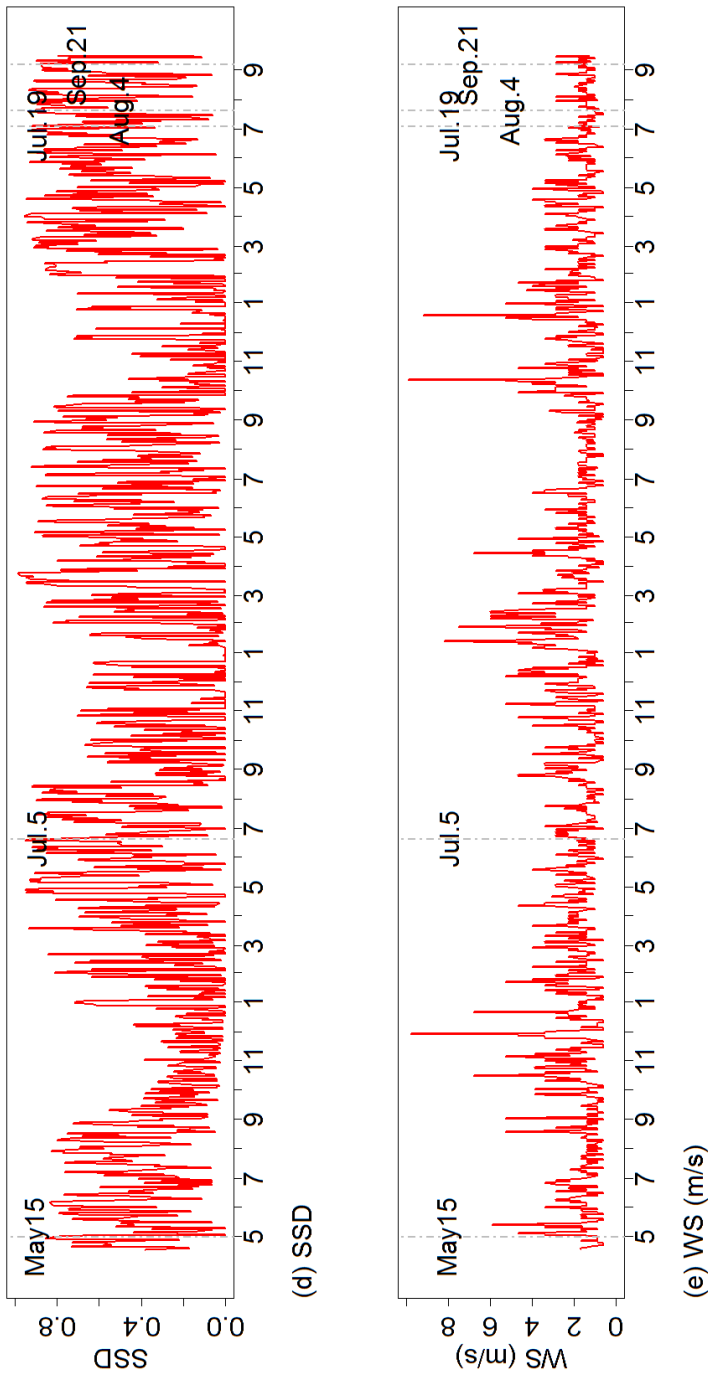

Fig. 1.4 Daily meteorological variables (a) P, (b) T, (c) RH, (d) SSD, (e) WS from May 01, 2000 to September 30, 2003 in deciduous forest of the Nahe catchment.

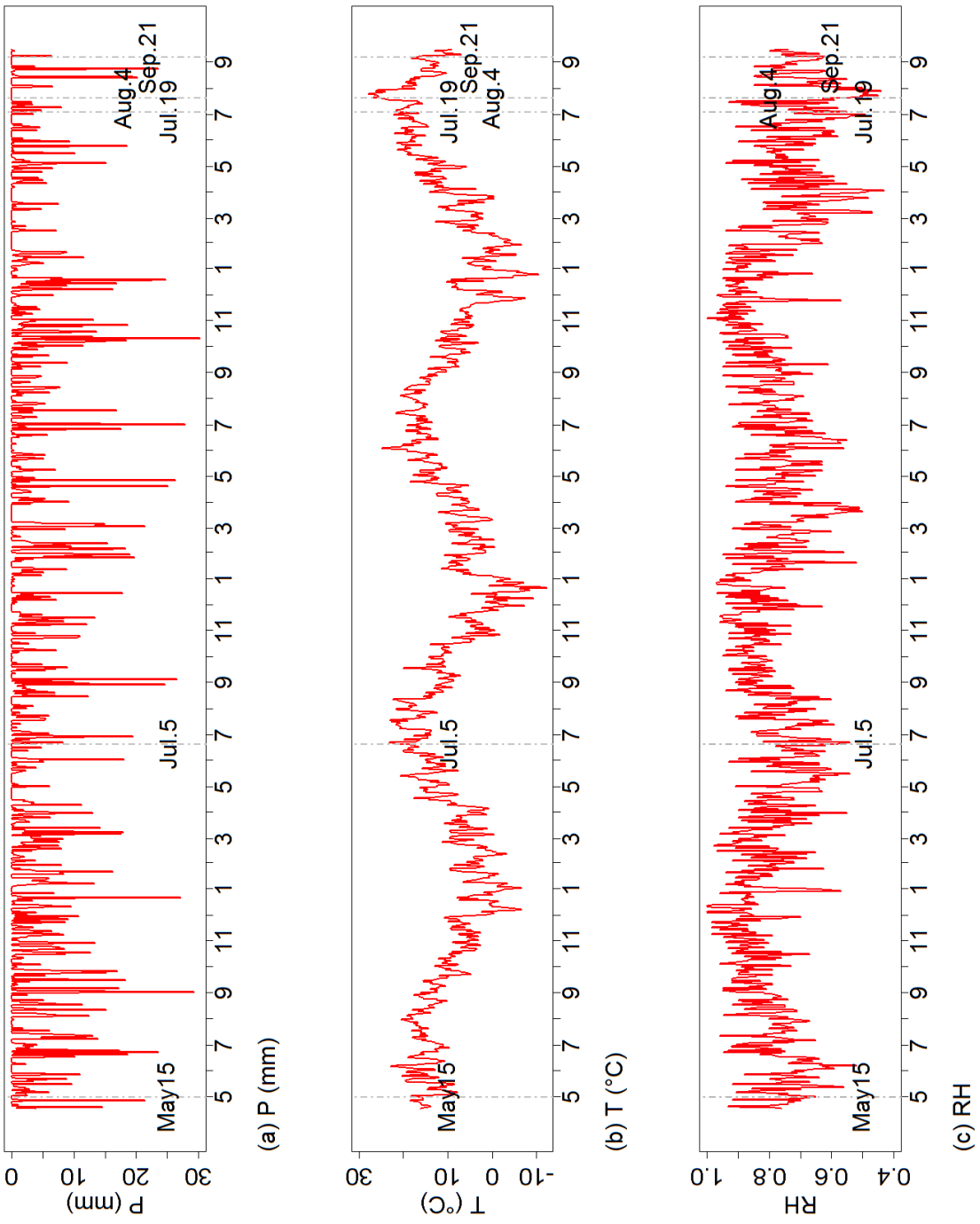
P (mm)
0
10
20
30
May15
Jul.5
Jul.19
Aug.4
Sep.21
(a) P (mm)
T (°C)
-10
0
10
30
May15
Jul.5
Jul.19
Sep.21
Aug.4
(b) T (°C)
RH
0.4
0.6
0.8
1.0
May15
Jul.5
Aug.4
Sep.21
(c) RH

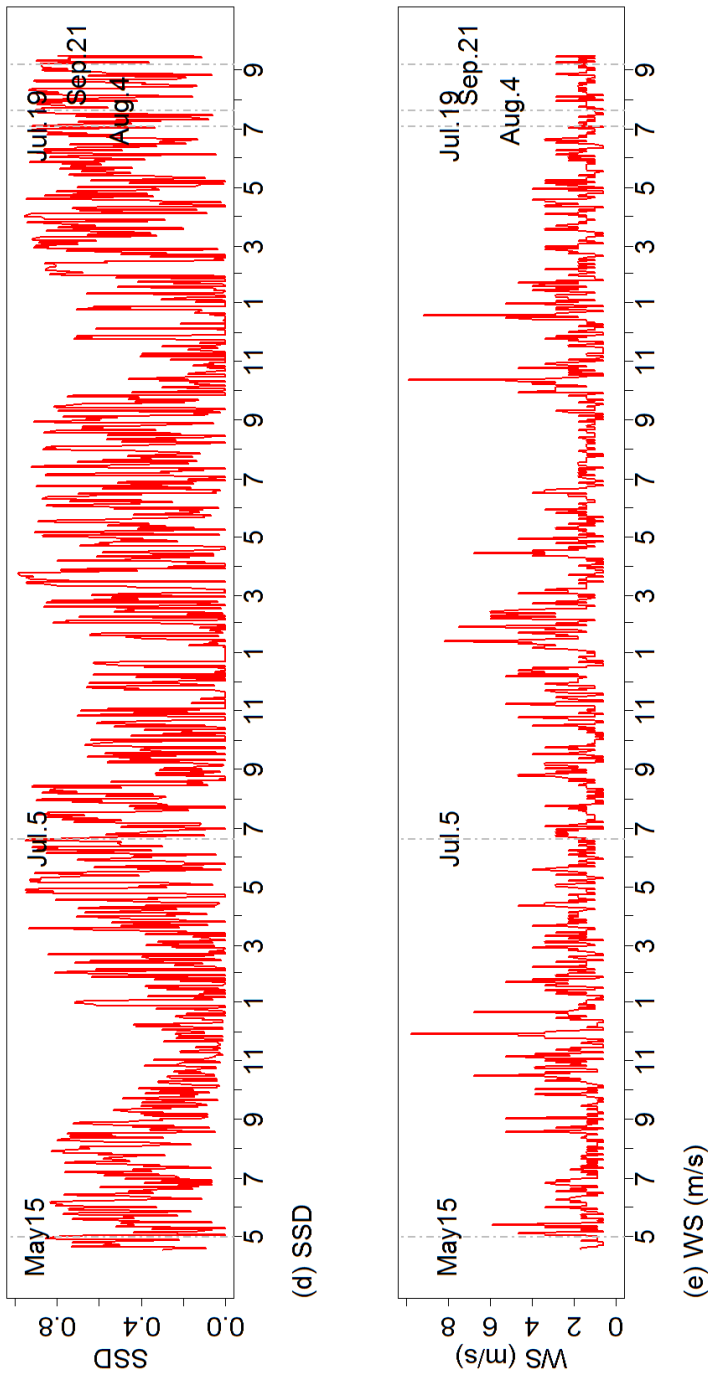

Fig. 1.5 Daily meteorological variables (a) P, (b) T, (c) RH, (d) SSD, (e) WS from May 01, 2000 to September 30, 2003 in coniferous forest of the Nahe catchment.

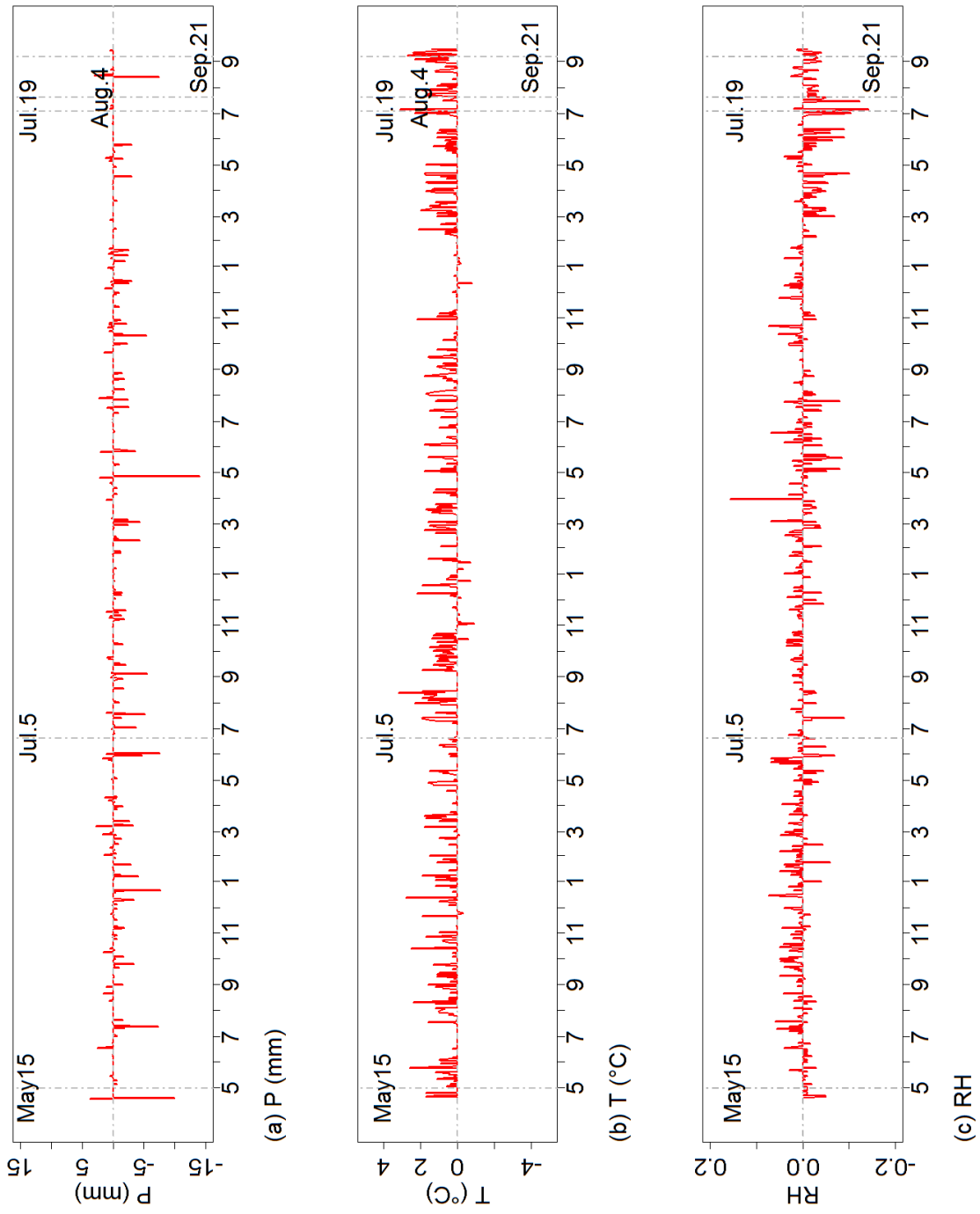
May15
Jul.5
Jul.19
Aug.4
Sep.21
P (mm)
-15
-5
5
15
(a) P (mm)
T (°C)
-4
0
2
4
(b) T (°C)
RH
-0.2
0.0
0.2
(c) RH

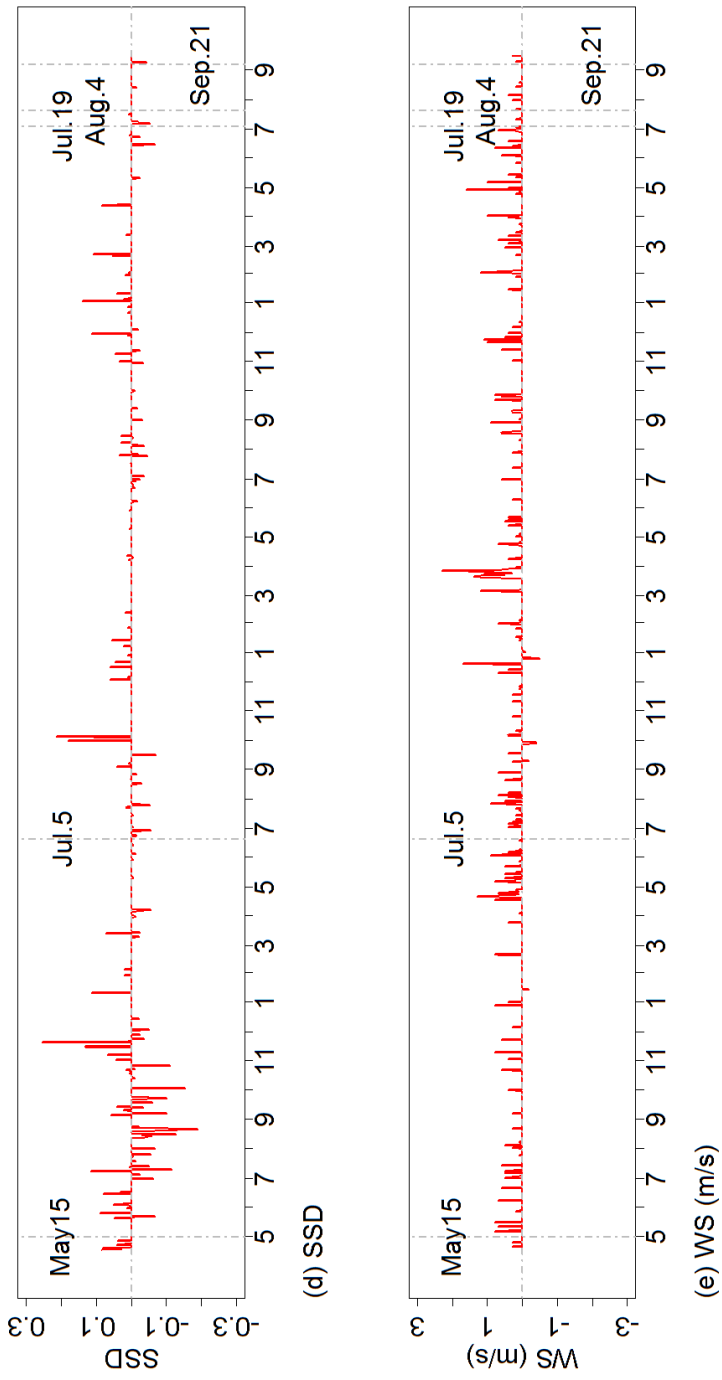

Fig. 1.6 Difference of daily meteorological variables (a) P, (b) T, (c) RH, (d) SSD, (e) WS from May 01, 2000 to September 30, 2003 between deciduous and coniferous forest in the Nahe catchment.

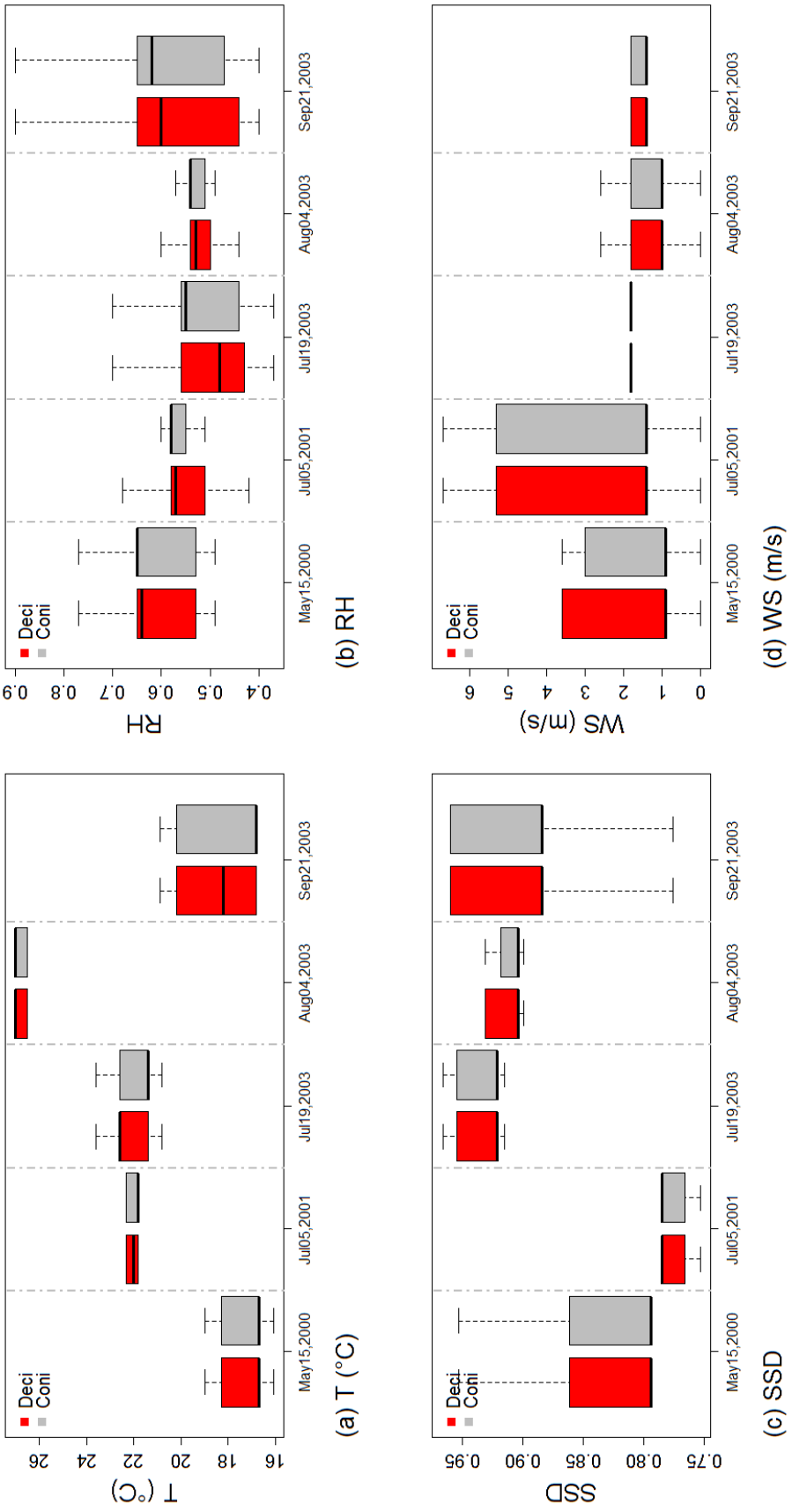

Fig. 1.7 Daily meteorological variables (a) T, (b) RH, (c) SSD, (d) WS on five sample dates in deciduous and coniferous forest of the Nahe catchment.

1.5 Framework of this thesis

In Chapter 2, main techniques of the ETA simulation in the WaSiM-ETH model were presented. The WaSiM-ETH is a mature hydrological model in Europe that has been widely used and reported in publications. It consists of several sub modules. In this chapter, the model structure, the main function of each module, the important formulas for ETP, soil water content and ETA calculation, and the critical parameters setting in the WaSiM-ETH model were introduced. In the final part, the model outputs were discussed for a further understanding of the model features.

In Chapter 3, the remote sensing-based techniques for ETA estimation were presented. Since it is found that different ET rates are generated by different methods, remote sensing-based method is required as similar to the method used in the WaSiM-ETH as possible. In this chapter, the basic principle, data processing flow, methods of critical variables retrieving such as surface properties and surface energy components were introduced in detail. The important surface properties included: surface albedo, normalized different vegetation index (NDVI), fractional vegetation cover (FVC), surface emissivity and land surface temperature (LST). The important surface energy components included: net radiation (R_n), sensible heat flux (H), soil heat flux (G) and latent heat flux (LE). The outputted data of these variables on five sample dates were discussed in the final part.

In Chapter 4, a manual model calibration was conducted in the WaSiM-ETH. The calibrated parameter was surface resistance, which was further divided into the canopy surface resistance r_{sc} and the soil surface resistance r_{se} since in WaSiM-ETH, transpiration and evaporation are separately calculated. A review of commonly used model performance evaluation indices were also shown. The simulated and observed data sets for comparison were the ETA simulated by the WaSiM-ETH with different surface resistances and the ETA retrieved by Landsat TM/ETM+ images on five sample dates. Both graphical and statistical techniques were employed for the model performance evaluation at spatial-temporal scale. Due to the high spatial-resolution of observations, model performance evaluation in spatial scale was also studied. The appropriate techniques were recommended.

In Chapter 5, sensitivity analysis of surface resistance were conducted on the canopy surface resistance r_{sc} and the soil surface resistance r_{se} to study their relative importance in both forest types. The appropriate value ranges of r_{sc} and r_{se} for each forest type were respectively determined. The previously recommended statistical indices for model performance evaluation in Chapter 4 were verified, and their general value range for a satisfactory model performance judgement were also determined. The relative and absolute responses of ETP and ETA respectively to the perturbations of r_{sc} and r_{se} were studied.

Chapter 6 is the summary of this whole thesis. The main works has been done, the techniques comparison between the WaSiM-ETH model and remote sensing methods for ETA estimation, the features of the simulated and observed data in this study, the meteorological impact and the ET feedback, the features of the WaSiM-ETH model, the critical surface properties in ETA estimation, and the model performance evaluation techniques were all summarized in this chapter.

1.6 Main idea and objective

The main idea of this thesis is using remote sensing retrieved ETA as observations for the model performance evaluation and parameter calibration, in order to make the WaSiM-ETH model more physical and the model simulated ETA more realistic. The weakness of the remote sensing based observations is apparent – they are available in a limited number (only five samples) as well as are noncontinuous in the time series (on May 15, 2000, July 05, 2001, July 19, August 04 and September 21 in 2003). However, the ground-measured meteorological variables show that in 2000, there were abundant precipitation and relatively high air humidity, whereas in the summer of 2003, there were rare precipitation, extremely high air temperature and low air humidity. In contrast to 2000 (wet) and 2003 (dry), the relatively temperate climate condition in 2001 is thereby considered as medium wet. In terms of the extremely warm and dry condition in the summer of 2003, we assume that there are relatively low ETA rates generated at that time in contrast to the previous years during the same time. On the basis of the precipitation, the air temperature and relative humidity measurements, the observations on five sample dates were confirmed to represent multiple climate conditions – wet (on May 15, 2000), medium wet (on July 05, 2001), and dry (on July 19 and August 04 in 2003). Moreover, an extremely low ETA rate on August 04, 2003 is inferred due to the extremely dry weather on that day and is considered as an extreme event in the observations. Another advantage of the observations is the high-resolution in the spatial scale. The remote sensing based observations are superior in spatial resolution to the simulated ETA rates by the WaSiM-ETH model since the former were retrieved from TM/ETM+ images, whose spatial resolution is 30 $\times$ 30 m for the reflective bands as well as respectively 120 $\times$ 120 m and 60 $\times$ 60 m for the thermal band; for the latter, the spatial resolution is very dependent on the density of the climate station networks (Courault et al., 2005).

Due to the the features of the observations that: (1) with low temporal resolution but high spatial resolution, (2) be representative for multiple climate conditions such as wet, medium wet and dry, the main objectives of this study are: (1) to investigate the response of ET under

these different climate conditions; (2) to find the critical influence factors for ET estimation; (3) to find the important parameters for ET estimation in the WaSiM-ETH model; (4) to find appropriate techniques for the model performance evaluation with the remote sensing-based observations; (5) to calibrate the important parameters for ET estimation in the WaSiM-ETH model.

1.7 Summary

In this chapter, three commonly used conceptions of ET were introduced – ETP, ET_o and ETA. The term ETP is the maximal ET rate estimated under the given meteorological variables. The term ET_o is the ETP according to the reference vegetation surfaces. The term ETA is the actual ET rate according to the actual soil water content. For the ET estimation, meteorological variables, vegetation properties, precipitation and soil moisture are all critical influence factors. The study area is the Nahe catchment in the southwest of Germany, which is mainly covered by deciduous and coniferous forest. The WaSiM-ETH model was used for ETA simulation in a daily time step. The running period of the WaSiM-ETH model is 1971-2003. In the aims of comparing and evaluating the model performance, the remote sensing TM/ETM+ images were also employed for ETA estimation. The meteorological variables from May 01, 2000 to September 30, 2003 in a daily time step showed that: the climate in 2000 was wet due to abundant rainfall and humid air; it was dry in the summer of 2003, since during that period, there were rare precipitation, warm air temperature and low air humidity. The remote sensing-based observations on five sample dates were thereby considered as to be representative for multiple climate conditions – wet, medium wet and dry. It is noted that there were significant differences respectively in T, RH and WS between two forest types. These differences were assumed as not only the causes of the inference that – the generated ET in the deciduous forest were in general more than in the coniferous forest due to their different vegetation properties, but also the results from the feedback of the generated ET in a long-time period. The main objectives of this thesis are to evaluate the model performance of the WaSiM-ETH model in ETA simulation and to calibrate important parameters in ETA calculation.

Chapter 2

A hydrological model WaSiM-ETH

2.1 Introduction

The evapotranspiration (ET) estimation in the hydrological models is typically on the basis of meteorological variables, surface energy budget and algorithms that related to the aerodynamic characteristics of the vegetation (Allen et al., 2011). In this chapter, we introduced the main techniques concerning the simulation of actual evapotranspiration (ETA) by a hydrological model – WaSiM-ETH. The WaSiM-ETH (abbreviation of "Water Flow and Balance Simulation Model", firstly developed between 1994 and 1996 at the ETH Zurich in Switzerland) is a distributed, deterministic, mainly physical and grid-based hydrological model (Schulla and Jasper, 2007). The WaSiM-ETH model has been widely used in Europe and frequently reported in publications (e.g. Elfert and Bormann (2010); Gurtz et al. (2000); Middelkoop et al. (2001)). In general, a successful hydrological model should be suitable for a range of different types of hydrological systems. The pre-alpine and alpine catchments are challenge for the application of a hydrological model due to their highly variable soil and vegetation types as well as meteorological variables at the spatial-temporal scale (Gurtz et al., 2000). However, the WaSiM-ETH model has been successfully applied in pre-alpine and alpine catchments (Gurtz et al., 2000; Jasper, 2005; Jasper et al., 2002; Klok et al., 2001; Verbunt et al., 2003). The WaSiM-ETH model also performed well in middle-mountain (e.g. Middelkoop et al. (2001)) and lowland catchments (e.g. Elfert and Bormann (2010)). Gurtz et al. (2000) compared two spatially distributed simulation model – WaSiM-ETH and PREVAH (Viviroli et al., 2007), and found WaSiM-ETH was more physically based and performed better in the simulation of flood events. Klok et al. (2001) applied the WaSiM-ETH model in a heavily glaciated Alpine river basin and found it performed well in discharge simulation. Based on the test of WaSiM-ETH for its suitability in flow simulation and flood forecasting, Cullmann et al. (2006) concluded that calibration is necessary for WaSiM-ETH

in case the spatial or temporal resolution changes, since the model is very sensitive to the resolution variation. In high mountain areas, Rößler and Löffler (2010) suggested to improve the soil moisture modelling ability of WaSiM-ETH, since its simulated soil moisture variability across different altitudes and land cover types was only in moderate accuracy. The land use is a sensitive variable for the WaSiM-ETH model, and the final land use is more sensitive than the scenario difference (Elfert and Bormann, 2010). Singh et al. (2012) concluded that using critical events replacing whole time series for the model calibration was suitable for WaSiM-ETH. In general, WaSiM-ETH is a mature water balance simulation model, which has been successfully applied in various areas under different climatic conditions.

WaSiM-ETH is a modular system, which is driven by the meteorological data sets. To simulate daily ETA in the Nahe catchment, several sub modules of the WaSiM-ETH model were employed. The modules that took part in provided functions such as radiation and temperature correlation, ET estimation, snow accumulation and melt calculation, interception evaporation estimation, soil moisture simulation, groundwater simulation. Simply, three steps are important in WaSiM-ETH for ETA estimation – (1) to obtain ETP based on the basic meteorological inputs; (2) to calculate the actual soil moisture (SM) in the unsaturated zone based on the precipitation measurements; (3) to obtain ETA by reducing the ETP according to the actual SM.

For ETP estimation, five categories have been divided from the existing main methods (Xu and Singh, 2002): (1) water budget (e.g. Guitjens (1982)). The water budget methods are also termed as storage methods, in which the ET is obtained as the residual of water budgets (calculated by the sum of storage, precipitation and inflow minus outflow). (2) mass-transfer (e.g. Harbeck (1962)). The mass-transfer methods are based on the Dalton's law, which states that the evaporation from the open water surface is proportional to the vapor pressure difference between the water surface and the surrounding air as well as the wind speed affects this proportionally. The simplicity in the model form and the reasonable accuracy are advantages for the mass-transfer methods. (3) combination (e.g. Monteith et al. (1965); Penman (1948)). The prototype of the combination methods is the Penman equation (Penman, 1948), which combines both aerodynamic-based (mass-transfer) and energy balance-based techniques. The Penman equation has been improved in numbers of publications (Covey, 1959; Penman and Long, 1961; Slatyer et al., 1961; Tanner and Pelton, 1960; Van Bavel, 1966). The Penman-Monteith equation (Monteith et al., 1965) is the most recommended and widely used one, in which the aerodynamic resistance and the surface resistance are two very important parameters. The usage restriction of the Penman-Monteith equation that can not be applied in data-sparse catchments is due to its high demand of meteorological variables. (4) radiation (e.g. Priestley and Taylor (1972)). The general form

of the radiation-based methods are linearly related the ETP rate to the net radiation with a temperature- and altitude-dependent factor as well as a humidity- and wind speed-dependent coefficient. However, Abtew (1996) used a simple equation for ET estimation when only radiation data is available. The radiation methods are found to show good results in humid areas but overestimate in arid areas (Allen et al., 1998). (5) temperature-based (e.g. Blaney (1952); Thornthwaite (1948)). The temperature-based methods require only temperature as input data.

2.2 Model structure

The model structure of WaSiM-ETH is shown in Figure 2.1. The WaSiM-ETH model consists of several sub modules. The model carries out step by step to simulate the water flow and balance on the earth. In this study, the input data are: (1) the meteorological data sets collected from 19 available climate stations in the entire Rhineland-Palatinate region (climate station network is shown in Figure 1.3a), such as the relative sunshine duration (SSD, dimensionless), the air temperature (T, in ^{o}C), the relative humidity (RH, dimensionless) and the wind speed (WS, in $\mathrm{m\,s^{-1}}$), which are basic inputs for ETP estimation; (2) the precipitation measurements collected from precipitation stations in the entire Rhineland-Palatinate region (station network is shown in Figure 1.3b), which is important for the estimation of interception ET after rainfall, snow melt and soil water content; (3) the land surface property data sets, such as land use, soil types, digital elevation model (DEM), land surface exposure, field capacity and river networks, which are also important auxiliary data to set up the entire projection in the WaSiM-ETH model. The model run step by step to simulate a series of hydrological variables. These variables that related to ETA in orderly are: the potential transpiration and evaporation, the evaporation from snow, the evaporation from interception surfaces after rainfall, the soil moisture in unsaturated zone and the ETA. The complete simulation process was executed by WaSiM-ETH from year 1971 to 2003 in a daily time step. The output daily ETA are the grid data sets in a resolution of 20 $\times$ 20 m.

2.2.1 Radiation correction module

The radiation correction module is used to estimate the effective shortwave radiation to each grid cell, with considering the topographic impact. In this study, we processed the radiation correction with shadow as well as the temperature correction by the model. The radiation

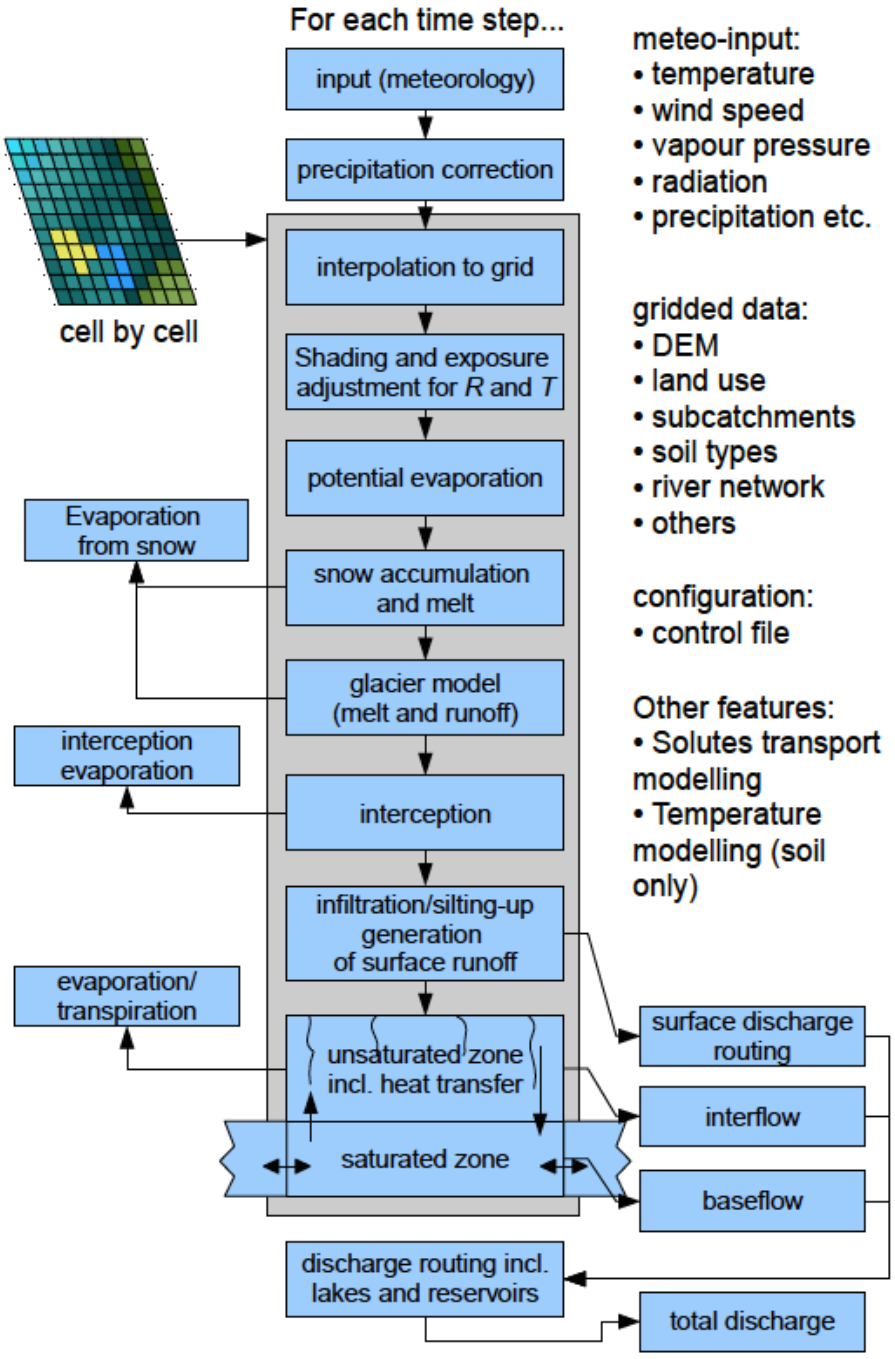

Fig. 2.1 Model structure of the WaSiM-ETH model (Schulla and Jasper, 2007).

correction equation is written as (Schulla and Jasper, 2007):

$$RG_{eff} = RG \cdot (1 + (1 - cr_0) \cdot SSD \cdot \left[\frac{cos\hat{\Theta}}{cosZ} - 1 \right]) \tag{2.1}$$

where RG_{eff} and RG are respectively the after corrected effective global radiation and original interpolated global radiation in $\mathrm{Wh\,m^{-2}}$; SSD is the original interpolated relative sunshine duration (dimensionless); cr_0 is the empirical factor for shortwave radiation diffusion; $\hat{\Theta}$ is the incident angel between the sun-to-surface direction and the normal incident direction to the surface; Z is the zenith angel between the direction to the sun and the zenith direction. When a cell is in the shadow of other cells or the cell is not in the sun, the correlation factor should be 0.

The same terms in Equation 2.1 are used for temperature correction. The equation is written as (Schulla and Jasper, 2007):

$$T_{corr} = \begin{cases} T_{obs} - c_t \cdot SSD \cdot 1.609 & cos\hat{\Theta} \cdot (cosZ)^{-1} < 0.2 \\ T_{obs} + c_t \cdot SSD \cdot ln\dfrac{cos\hat{\Theta}}{cosZ} & 0.2 \leq cos\hat{\Theta} \cdot (cosZ)^{-1} \leq 5 \\ T_{obs} + c_t \cdot SSD \cdot 1.609 & \cos\hat{\Theta} \cdot (cosZ)^{-1} > 5 \end{cases} \tag{2.2}$$

where T_{corr} and T_{obs} are the after-corrected air temperature and observed original air temperature, respectively; c_t is a empirical factor. It is noted that the radiation correlation factor is valid only under cloudless conditions. When it is full cloudy, the temperature correction will not process. In general, c_t is smaller than 5 K.

2.2.2 Evapotranspiration module

The ET module calculates the ETP rates, including the potential transpiration from plants, the evaporation from bare soil and the evaporation from interception surfaces after rainfall. Each type of the evaporation is separately calculated using the same method but different parameters. On no-rainfall days (dry-canopy), the interception evaporation was not taken into account and only the transpiration from plants and the evaporation from bare soil were calculated. There are four different methods available in this module: (1) Penman-Monteith, (2) Hamon (Federer and Lash, 1978), (3) Wendling (Wendling, 1975), (4) Haude (Haude, 1955). The application of the Penman-Monteith method requires the most detailed ground-measured meteorological variables, such as solar radiation, air temperature, air humidity and wind speed, therefore this method can not be used in a data-lacking region. The other three methods are only available for the estimation in a time step not less than one day. The

Hamon method used only temperature data; the Wendling method used solar radiation and air temperature as input data; the Haude method is an empirical method and only requires the water vapor saturation data. Since the Penman-Monteith equation is the most widely used and recommended method for ETP estimation (Allen et al., 1989, 1998; Droogers and Allen, 2002), in this study, we chose it for ETP estimation in the forest area of the Nahe catchment. The detailed algorithm is introduced in Section 2.3.

2.2.3 Snow module

The snow module is used to estimate the accumulated snow and snow melt. In this module, the precipitation is corrected with the wind speed and threshold temperature into two forms – the liquid precipitation (rain) and the solid precipitation (snow). The accumulated snow is obtained in terms of the precipitation amount, according to the air temperature (Equation 2.3). When the air temperature is in the range of the rain-snow transition temperature, both types of the precipitation exist. The formula is written as (Schulla and Jasper, 2007):

$$p_{snow} = \frac{T_{R/S} + T_{trans} - T_a}{2 \cdot T_{trans}} \quad for \quad (T_{R/S} - T_{trans}) < T_a < (T_{R/S} + T_{trans}) \tag{2.3}$$

where p_{snow} is the fraction of snow on the total precipitation; T_a is the air temperature in ^{o}C; $T_{R/S}$ is the transition temperature in ^{o}C, at which 50 % of precipitation are solid (snow); T_{trans} is the transition temperature in ^{o}C, at which 50 % of snow are liquid (rain).

There are a variety of methods for snow melt computation: temperature index approach, temperature-wind-index approach, Anderson combination method and Braun combination method. In this study, the temperature-wind-index approach is used, which is formulated as (Schulla and Jasper, 2007):

$$M = (c_1 + c_2 \cdot u) \cdot (T_a - T_{0,m}) \cdot \frac{\Delta t}{24} \quad for \quad T_a > T_{0,m} \tag{2.4}$$

where M is the melt rate; C_1 is the temperature-dependent melt factor in $\mathrm{mm\,{}^{o}C^{-1}\,d^{-1}}$; C_2 is the wind-depended melt factor in $\mathrm{mm\,({}^{o}C\,m\,s^{-1}\,d)^{-1}}$; u is wind speed in $\mathrm{m\,s^{-1}}$; T_a is the air temperature in ^{o}C; $T_{0,m}$ is the temperature of stating melt in ^{o}C; Δt is the time step. If $T \leq T_{0,m}$, $M = 0$.

2.2.4 Interception module

The interception module is used to calculate the ETP from the interception surfaces after rainfall. The interception evaporation is obtained in terms of the interception storage. Since

the interception module runs followed the snow module, both the water from the snow melt and the rainfall are taken into account for the components of the interception storage. In equation 2.5, it shows that the leaf area index, the fractional vegetation cover and the land use type are important factors for effective storage capacity determination.

$$SI_{max} = f_r \cdot LAI \cdot h_{SI} \tag{2.5}$$

where SI_{max} is the maximal interception storage capacity in mm; f_r is the degree of the vegetation cover; LAI is the leaf area index and h_{SI} is the maximal height of water at leaf surfaces in mm.

Based on the interception storage SI , the interception evaporation is estimated as (Schulla and Jasper, 2007):

$$EI = \begin{cases} EIP \quad \text{and} \quad TR = 0 & \text{for} \quad SI \leq EIP \leq TP \\ EIP \quad \text{and} \quad TR = TP - EI & \text{for} \quad SI \leq TP \leq EIP \\ EIP \quad \text{and} \quad TR = TP - EI & \text{for} \quad TP \leq SI \leq EIP \\ SI \quad \text{and} \quad TR = TP - SI & \text{for} \quad SI \geq EIP \geq TP \\ SI \quad \text{and} \quad TR = TP - SI & \text{for} \quad SI \geq TP \geq EIP \\ SI \quad \text{and} \quad TR = 0 & \text{for} \quad TP \geq SI \geq EIP \end{cases} \tag{2.6}$$

where EI is the interception evaporation in mm; EIP is the potential interception evaporation in mm; TR is the actual transpiration in mm; TP is the potential transpiration in mm.

2.2.5 Unsaturated zone module

The unsaturated zone module is one of the soil model versions in WaSiM-ETH. Since in the unsaturated zone vertical flow is much more important than lateral flow, the Richards equation was employed in this module to simulate fluxes inner soil vertically in one-dimension. The unsaturated zone was divided into numerous layers. Soil water content is obtained by simulating the fluxes in the soil between each two neighbour layers. This module is very important for ETA estimation, since the ETA amount highly depends on the available soil water content.

2.2.6 Groundwater flow module

The groundwater flow module simulates multilayer aquifers for groundwater. For each layer, the aquifer is horizontally two-dimension grid data. Leakage factors are the links between

layers. Groundwater is connected to the surface water through unsaturated zone model. The surface water falls into ground water through leakage approach while groundwater rises to the surface generating the surface flow. Both processes are simulated in unsaturated zone model.

2.3 Important formulas for ETA estimation

2.3.1 Penman-Monteith equation

The Penman-Monteith equation (Monteith et al., 1965) is the most widely used and recommended approach for ETP estimation. Its prototype is the Penman equation (Penman, 1948), in which both aerodynamic-based and energy balance-based approaches were firstly combined to estimate the evaporation from the surfaces such as open water, bare soil and turf. On the basis of the aerodynamic theory, the ET is calculated as the turbulent transport of vapor. On the basis of the surface energy theory, the ET is calculated as the latent heat flux through the surface energy balance equation. Combining these two theories in ET estimation eliminates the difficulties in calculating the surface temperature, and employs the basic meteorological variables into ET estimation - the historical ET is therefore available (Penman, 1948). In the Penman-Monteith equation, two parameters are very important – the bulk aerodynamic resistance r_a and the bulk surface resistance r_s . The evaporation surface in the Penman-Monteith equation is described as a single big leaf. The r_a is related to the heat and water vapor transfer from the evaporation surfaces to the air above the canopy. The r_s describes the resist ability while plant transpiring and bare soil evaporating. In this study, the bulk surface resistance is further divided into two terms – the canopy surface resistance r_{sc} and the soil surface resistance r_{sc} , respectively corresponding to the transpiration and the evaporation. The Penman-Monteith equation is formulated as (Monteith et al., 1965):

$$\lambda E = \frac{3.6\frac{\Delta}{\gamma_p}(R_n - G) + \frac{\rho c_p}{\gamma_p r_a}(e_s - e)t_i}{\frac{\Delta}{\gamma_p} + 1 + r_s/r_a} \tag{2.7}$$

where λ is the latent vaporization heat, $\lambda = (2500.8 - 2.372T)$ $\mathrm{KJ\,Kg^{-1}}$, with T is the temperature in ^{o}C; E is the latent heat flux in $\mathrm{mm\,m^{-2}} \equiv \mathrm{Kg\,m^{-2}}$; Δ is the tangent to the saturated vapor pressure curve in $\mathrm{hP_a\,K^{-1}}$; R_n is the net radiation in $\mathrm{Wh\,m^{-2}}$ and $G = 0.1 \cdot R_n$ is the soil heat flux in $\mathrm{Wh\,m^{-2}}$, the factor 3.6 is used to convert both fluxes from $\mathrm{Wh\,m^{-2}}$ to $\mathrm{KJ\,m^{-2}}$; ρ is the density of dry air, $\rho = p/(R_L T)$, at 0 ^{o}C and 101325 $\mathrm{hP_a}$, $\rho = 1.29$ $\mathrm{Kg\,m^{-3}}$; c_p is the specific heat capacity of the dry air at constant pressure, $c_p = 1.005$ $\mathrm{KJ\,Kg^{-1}\,K^{-1}}$;

e_s is the saturation vapor pressure at temperature T, in hP_a; e is the observed actual vapor pressure in hP_a; t_i is the number of seconds within a time step; γ_p is the psychrometric constant in $hP_a\,K^{-1}$; r_a and r_s are respectively the bulk-aerodynamic resistance and the bulk-surface resistance in $s\,m^{-1}$.

The slope of the saturated vapor pressure curve Δ in $hP_a\,K^{-1}$ is calculated as (Tetens, 1930):

$$e_s = 06.1078 \cdot e^{\frac{17.27 \cdot T}{237.3+T}} \tag{2.8}$$

$$\Delta = \frac{\partial e_s}{\partial T} = \frac{25029}{(273.3+T)^2} \cdot e^{\frac{17.27 \cdot T}{237.3+T}} \tag{2.9}$$

where T is the air temperature in ^oC.

The psychrometric constant γ_p in $hP_a\,K^{-1}$ is calculated as (Schulla and Jasper, 2007):

$$\gamma_p = \frac{c_p \cdot p}{0.622 \cdot \lambda} \tag{2.10}$$

with

$$p \approx 1013 \cdot e^{-\frac{h_M}{7991+29.33 \cdot T_v}} \tag{2.11}$$

where p is the air pressure at level h_M in hPa; 0.622 is the ratio of the molecular weights of water vapor to dry air; h_M is the altitude in m; T_v is the mean virtual temperature of the air column in ^oC.

The net radiation R_n is the difference between shortwave radiation and longwave radiation. To calculate R_n, the global radiation R_g (shortwave incident and outgoing radiation from the land surface) is very important. The input relative sunshine duration SSD is used for R_g estimation. The formulas are (Schulla and Jasper, 2007):

$$R_n = (1-\alpha)R_g - R_l \tag{2.12}$$

with

$$\begin{aligned} R_g &= I_{norm}(cr_0 + cr_1 \cdot SSD + cr_2 \cdot SSD^2 + cr_3 \cdot SSD^3) \\ &= I_{norm}(0.23 + 1.77 \cdot SSD + (-2.28) \cdot SSD^2 + 1.28 \cdot SSD^3) \end{aligned} \tag{2.13}$$

$$\begin{aligned} R_L &= \Delta t \cdot \sigma T^4 \cdot (0.48 - 0.065\sqrt{e}) \cdot (cr_0 + (1-cr_0) \cdot SSD) \\ &= \Delta t \cdot 5.67 \cdot 10^{-8} T^4 \cdot (0.48 - 0.065\sqrt{e}) \cdot (0.23 + 0.77 \cdot SSD) \end{aligned} \tag{2.14}$$

where R_n and R_g are in $\mathrm{Wh\,m^{-2}}$; α is the shortwave surface albedo (dimensionless); R_l is the longwave radiation (outgoing less incident to the surface) in $\mathrm{Wh\,m^{-2}}$; I_{norm} is the theoretical clear sky radiation in $\mathrm{Wh\,m^{-2}}$; SSD is the relative sunshine duration (dimensionless); $cr_0 \dot{c}r_3$ are the empirical constants; Δt is the time step converted from power to energy in h; σ is the Boltzmann-constant, $\sigma = 5.68 \times 10^{-8}\ \mathrm{W\,m^{-2}\,K^4}$; T is the air temperature in K; e is the actual vapor pressure in mbar.

2.3.2 Richards equation

The soil model in WaSiM-ETH is based on the Richards equation (Richards, 1931), which is used for the fluxes simulation in the unsaturated soil zone. As the vertical flow is considered as much more important than the lateral flow, the soil is divided into several layers in one-dimension in the vertical direction. The continuity equation for soil model is written as (Schulla and Jasper, 2007):

$$\frac{\partial \Theta}{\partial t} = \frac{\partial q}{\partial z} = \frac{\partial}{\partial z}(-k(\Theta)\frac{\partial \Psi(\Theta)}{\partial z}) \tag{2.15}$$

where Θ is the soil water content in $\mathrm{m^3\,m^{-3}}$; t is the time in s; k is the hydraulic conductivity in $\mathrm{m\,s^{-1}}$; Ψ is the hydraulic head of the suction ψ plus geodetic latitude h in m; q is the specific flux in $\mathrm{m\,s^{-1}}$; z is the vertical height in m.

And the discrete Richards equation is formulated as (Schulla and Jasper, 2007):

$$\frac{\Delta \Theta}{\Delta t} = \frac{\Delta q}{\Delta z} = q_{in} - q_{out} \tag{2.16}$$

with

$$q = k_{eff} \cdot \frac{h_h(\Theta_u) - h_h(\Theta_l)}{0.5 \cdot (d_u + d_l)} \tag{2.17}$$

$$\frac{1}{k_{eff}} = \frac{d_u}{d_u + d_l} \cdot \frac{1}{k(\Theta_u)} + \frac{d_u}{d_u + d_l} \cdot \frac{1}{k(\Theta_l)} \tag{2.18}$$

where q_{in} is the inflow into soil layer in $\mathrm{m\,s^{-1}}$; q_{out} is the outflow from soil layers in $\mathrm{m\,s^{-1}}$, including both interflow and artificial drainage; q indicates the flux between two neighboring layers in $\mathrm{m\,s^{-1}}$; u denotes the upper layer and l denotes the lower one; k_{eff} is the effective hydraulic conductivity in $\mathrm{m\,s^{-1}}$; h_h is the hydraulic head in m that depended on the water content and is given as the sum of suction $\Psi(\Theta)$ and geodetic altitude h; d is the thickness of the layer in m.

The hydraulic parameter is formulated as (Van Genuchten, 1980):

$$\psi(\Theta) = \frac{1}{\alpha}[(\frac{\Theta - \Theta_r}{\Theta_s - \Theta_r})^{-1/m} - 1]^{1/n} \tag{2.19}$$

$$\frac{k(\Theta)}{k_s} = [\frac{\Theta - \Theta_r}{\Theta_s - \Theta_r}]^{1/2}[1 - 1 - (\frac{\Theta - \Theta_r}{\Theta_s - \Theta_r})^{-1/m^{m}}]^2 \tag{2.20}$$

$$k_{s,z} = k_s \cdot k_{rec}^z \tag{2.21}$$

where ψ is the suction; Θ, Θ_r and Θ_s are respectively the actual, residual and saturated water content (dimensionless); α, n and m are empirical parameters; k_s, $k_{s,z}$ are respectively the saturated hydrological conductivity within the depth z m and at soil surface in $\mathrm{m\,s^{-1}}$; k_{rec} is the recession constant.

Based on the Equation 2.19, the actual soil water content Θ is calculated by the actual soil suction $\psi(\Theta)$ (Schulla and Jasper, 2007):

$$\Theta = \Theta_r + (\Theta_s - \Theta_r)(\frac{1}{1 + (\psi(\Theta)\alpha)^n})^m \tag{2.22}$$

2.3.3 Actual evapotranspiration estimation

According to the actual soil moisture, the ETA was then obtained based on the ETP. All soil water conditions are considered (Schulla and Jasper, 2007):

$$ETA_i = \begin{cases} 0 & \Theta(\psi) < \Theta_{wp} \\ ETP_i \cdot \dfrac{(\Theta_{(\psi_i)} - \Theta_{wp})}{(\Theta_{\psi_g} - \Theta_{wp})} & \Theta_{wp} \le \Theta(\psi) \le \Theta_{\psi_g} \\ ETP_i & \Theta_{\psi_g} < \Theta(\psi) \le \eta \cdot \Theta_{sat} \\ ETP_i \cdot \dfrac{(\Theta_{sat} - \Theta_{(\psi_i)})}{(\Theta_{sat} - \eta \cdot \Theta_{sat})} & \eta \cdot \Theta_{sat} < \Theta(\psi) \le \Theta_{sat} \end{cases} \tag{2.23}$$

where i is the index of soil layer; $\Theta(\psi)$ is the actual relative soil water content at suction ψ (dimensionless), with ψ is the actual suction (capillary pressure, in m); Θ_{wp} is the soil water content at permanent wilting point ($\psi = 1.5$ MPa ≈ 150 m); Θ_{ψ_g} is the soil water content at a given suction ψ_g, with ψ_g indicates the beginning point of dry soils; Θ_{sat} is the saturated soil water content; η is the maximum relative soil water content under no anaerobe bacterial conditions (still with Oxygen in soil), $\eta \approx 0.9 \ldots 0.95$.

In Equation 2.23, four types of soil water conditions are considered – very dry soils ($\Theta(\psi) < \Theta_{wp}$), dry soils ($\Theta_{wp} \le \Theta(\psi) \le \Theta_{\psi_g}$), well-watered soils ($\Theta_{\psi_g} < \Theta(\psi) \le \eta \cdot \Theta_{sat}$)

and too wet soils ($\eta \cdot \Theta_{sat} < \Theta(\psi) \leq \Theta_{sat}$). Three parameters are given in the WaSiM-ETH control file: *TReduWet* indicates the relative soil water content at the beginning of the Oxygen stress, *LimitReduWet* is the relative reduction factor of real transpiration for water-saturated soils, *HReduDry* is the hydraulic head for beginning dryness stress in m. Those parameters vary for different crop types. Therefore the reduction of ETP depends on both the soil water content and crop types. In deciduous and coniferous forest, the default setting values of those three parameters are totally the same (in Table 2.1).

Forest types	TReduWet	LimitReduWet	HReduDry
Deciduous	0.95	0.5	3.0
Coniferous	0.95	0.5	3.0

Table 2.1 Soil water condition parameters.

2.4 Important parameters setting

2.4.1 Bulk-aerodynamic resistance

The aerodynamic resistance and the surface resistance are two important parameters, to which the ET estimation by the Penman-Monteith approach are very sensitive. Beven (1979) studied the ETA estimated by the Penman-Monteith equation in a broadly temperate region and found it was very dependent on the values of the aerodynamic and surface resistance than other inputs in grassland surface. The aerodynamic resistance is estimated in WaSiM-ETH by the following formula (Schulla and Jasper, 2007):

$$r_a = \frac{4.72 \cdot (ln\frac{z}{z_0})^2}{1+0.54u} \tag{2.24}$$

where z is the sampling elevation above ground in m; z_0 is the aerodynamic roughness length in m. Different land use types leads to different z_0. $z_0 \approx 0.1 \cdot$ (crop height-shift height), with the (crop height-shift height) is the effective height; u is the wind speed in $\mathrm{m\,s^{-1}}$. While $z_0 >$ 2 m, r_a is calculated as (Schulla and Jasper, 2007):

$$r_a = 25/(1+0.54u) \tag{2.25}$$

In this study, the general aerodynamic roughness length of deciduous and coniferous forest are both more than 2 m (Table 2.2). Therefore in the Nahe catchments forest regions, r_a for both forest types depend only on the wind speed u. More rapid wind speed leads to

smaller aerodynamic resistance and thereby results in an increase of the heat and water vapor transfer.

Forest types	z_0 (m)
Deciduous	3.93
Coniferous	3.69

Table 2.2 Aerodynamic roughness length z_0 (m) for deciduous and coniferous forest in the Nahe catchment.

2.4.2 Bulk-surface resistance

The bulk-surface resistance describes the resistance for (1) vegetation transpiration, (2) bare soil evaporation, and (3) evaporation from the interception surfaces under wet surface conditions. In the WaSiM-ETH model, these three processes of evaporation are calculated respectively by the Penman-Monteith equation. Therefore the bulk-surface resistance is divided into three terms: the canopy surface resistance r_{sc}, the soil surface resistance r_{se} and the interception surface resistance r_{si}. The canopy surface resistance r_{sc} is found to play a leading role in affecting the magnitudes of ETA estimated by the Penman-Monteith equation in forest regions (Beven, 1979). Values of the canopy resistance show diurnal and seasonal variations. A rule of the diurnal value variation of a significant canopy resistance (more than 10 $\mathrm{m\,s^{-1}}$) was found by Van Bavel (1967): the initial value of canopy resistance after sunrise was low and it rose up to about 20 times after midday and then decreased. In WaSiM-ETH, the surface resistance is calculated separately according to different cases (Schulla and Jasper, 2007):

For daytime:

$$r_s = \begin{cases} \dfrac{1}{\dfrac{(1-A)}{r_{sc}}} & \text{for plant transpiration} \\ 2500 & \text{for plant transpiration when LAI or FVC =0} \\ 0 & \text{for open water evaporation} \\ r_{si} & \text{for evaporation from interception surfaces} \\ r_{se} & \text{for bare soil evaporation} \end{cases} \tag{2.26}$$

where r_s is the minimal surface resistance in $\mathrm{s\,m^{-1}}$; r_{sc} is the minimal surface resistance of crop with sufficient water supply in $\mathrm{s\,m^{-1}}$; 1-A is the evaporation effective vegetation

coverage with $A = f^{LAI \cdot FVC}$, $f \approx 0.6 \sim 0.7$, LAIis the leaf area index and FVC is the fractional vegetation cover; r_{se} is the surface resistance for bare soil whose commonly rough range is [150,250] in $\mathrm{s\,m^{-1}}$; r_{si} is the surface resistance for interception whose commonly rough range is [20,100] in $\mathrm{s\,m^{-1}}$.

For night time:

$$r_s = \begin{cases} \dfrac{1}{\dfrac{(LAI \cdot FVC)}{2500}} & \text{for plant transpiration} \\ 2500 & \text{for plant transpiration when LAI or FVC =0} \\ 0 & \text{for open water evaporation} \\ r_{si} & \text{for evaporation from interception surfaces} \\ r_{se} & \text{for bare soil evaporation} \end{cases} \tag{2.27}$$

It is obvious that the surface resistance for plant transpiration at night differs from the value at the daytime, while in other cases the corresponding surface resistances keep the same for both day and night values. Take an example by assuming $f = 0.7, LAI = 6, FVC = 0.9, r_{sc} = 240$ for plant transpiration, the minimal surface resistance $r_s \approx 280.94\ \mathrm{s\,m^{-1}}$ at the daytime as well as at night r_s increases to $462.92\ \mathrm{s\,m^{-1}}$. And this agrees with the diurnal variation of surface resistance – it diminishes to low value after sunset (Van Bavel, 1967).

In Table 2.3, the default parameters setting of surface resistance in WaSiM-ETH for each month are listed. The initial values for the deciduous forest are worked out from the KlimLand-Project (Casper et al., 2013), as well as the initial values for coniferous forest are based on the Forestclim-Project (Plegnière and Casper, 2011). For both forest types, in November to February, the value of canopy surface resistance r_{sc} reaches its maximal whereas in May to September, it reduces to its annual minimal. The soil surface resistance r_{se} and the interception surface resistance r_{si} remain constant for an entire year.

		Jan	Feb	Apr	Mar	May	Jun	Jul	Aug	Sep	Oct	Nov	Dec
Deci	r_{sc}	150	150	142	112	98	98	98	98	98	128	150	150
	r_{se}	250	250	250	250	250	250	250	250	250	250	250	250
	r_{si}	0.5	0.5	0.5	0.5	0.5	0.5	0.5	0.5	0.5	0.5	0.5	0.5
Coni	r_{sc}	240	240	225	195	165	165	165	165	165	225	240	240
	r_{se}	300	300	300	300	300	300	300	300	300	300	300	300
	r_{si}	0.5	0.5	0.5	0.5	0.5	0.5	0.5	0.5	0.5	0.5	0.5	0.5

Table 2.3 Surface resistance ($\mathrm{s\,m^{-1}}$) for deciduous and coniferous forest in WaSiM.

2.4.3 Other property parameters

In Table 2.4, default parameter settings such as surface albedo, LAI (leaf area index) and FVC (fractional vegetation cover) are listed. In deciduous forest, the surface albedo is always higher than that of coniferous forest. With regard to the LAI and FVC, the seasonal variability in deciduous forest is higher than in coniferous forest, since summer is the grown season for deciduous plants and the deciduous plants drop their leaves in autumn.

		Jan	Feb	Apr	Mar	May	Jun	Jul	Aug	Sep	Oct	Nov	Dec
Deci	*albedo*	0.2	0.2	0.2	0.2	0.2	0.2	0.2	0.2	0.2	0.2	0.2	0.2
	LAI	1	1	1	1	3	5	5	5	5	5	3	1
	FVC	0.25	0.25	0.25	0.25	0.55	0.85	0.85	0.85	0.85	0.85	0.55	0.25
Coni	*albedo*	0.1	0.1	0.1	0.1	0.1	0.1	0.1	0.1	0.1	0.1	0.1	0.1
	LAI	6	6	6	6.3	6.3	6.7	6.7	6.7	6.3	6.3	6	6
	FVC	0.9	0.9	0.9	0.9	0.95	0.95	0.95	0.95	0.95	0.9	0.9	0.9

Table 2.4 Albedo, LAI and FVC for deciduous and coniferous forest in WaSiM.

2.5 Results and discussion

Figure 2.2 and 2.3 show the regional median values of outputs simulated by the WaSiM-ETH model, such as daily ETP (mm), daily ETA (mm), decline between daily ETP and ETA (deETP, in mm) as well as daily relative soil moisture (SM, dimensionless) in the root zone. These outputs are on five sample dates (May 15, 2000, July 05, 2001, and July 19, August 04, September 21, in 2003), in deciduous and coniferous forest of the Nahe catchment. For each forest type, the outputs are simulated with 12 different representative surface resistance combinations. Each surface resistance combination includes two sub parameters – the surface canopy resistance r_{sc} and the soil surface resistance r_{se}. The former describes the resistance of the plants' canopy in transpiring process as well as the latter is the resistance for bare soil evaporation. Although r_{sc} and r_{se} are parameters for ETP calculation and thereby affect the estimation of ETP and subsequently the amount of ETA, in the WaSiM-ETH model, their perturbations also influence the SM simulation (Figure 2.2d and 2.3d). This can be attributed to the model conception of WaSiM-ETH, in which the simulations of ETA and SM are associated with each other and follow the water balance principle – an in- or decrease of ETA will lead to opposite responses in SM in a long-time period. It is obviously that for each surface resistance combination, their corresponding ETP, deETP and SM for both forest types respectively exhibit consistent change trend on five sample dates but in different

amounts (Figure 2.2 and 2.3). Thus, the impacts of surface resistance on ETP, deETP and SM are mainly in magnitude, whereas their fluctuations over time are assumed to reflect the climatic changes.

The ETP generation is only dependent on the meteorological variables such as T, RH, SSD and WS as well as is with no regard to the precipitation. Based on the meteorological variables, we previously inferred in Chapter 1 that in the summer of 2003, high T and low RH values might lead to higher ETP rates, especially on August 04, whose T values were extremely high might lead to extremely high ETP rates; on May 15, 2000, the relatively low T and high RH might result in smaller ETP rates. In Figure 2.2a and 2.3a, the order of ETP rates on five dates for both forest types are approximately: $ETP_{Aug04,2003} > ETP_{Jul19,2003} > ETP_{Jul05,2001} > ETP_{May15,2000}, ETP_{Sep21,2003}$. This order is consistent with the previous inference.

The moisture degree of a climate is suggested by Thornthwaite (1948) to be judged on the basis of the amounts of both precipitation and ETA rather than only on precipitation – if the amount of precipitation is more than ETA, the climate is wet; conversely, it is dry. On the basis of the precipitation and relative humidity measurements, we draw a conclusion in Chapter 1 that the observations on five sample dates are representative for multiple climate conditions – wet (on May 15, 2000), medium wet (on July 05, 2001) and dry (on July 19 and August 04 in 2003). Boulet et al. (2007) introduced a stress factor to indicate the crop water stress in the soil, which was defined as a function of the ratio between ETA and ETP rates. In order to confirm the climate conditions, we studied the decline amounts between daily ETP and ETA (deETP, Figure 2.2c and 2.3c) as well as the soil moisture (SM, Figure 2.2d and 2.3d). For both forest types, deETP on five dates are sorted as: $deETP_{Aug04,2003} > deETP_{Jul19,2003} > deETP_{Jul05,2001} > deETP_{Sep21,2003} > deETP_{May15,2000}$. It is shown that on August 04, 2003, the ETP rates was the top of all as well as the decline amount on that day was also the largest. Since: (1) ETP is the maximal evaporation rates for crops under given meteorological variables with sufficient water supply; (2) the decline of ETP to ETA is according to the actual SM, the decline amount deETP is considered as an ideal indicator of water stress. In terms of the deETP, the moisture degree of the climate on five dates are sorted from wet to dry in order as – May 15, 2000 > July 05, 2001 > September 21, 2003 > July 19, 2003 > August 04, 2003, which is consistent with the previous conclusion. In terms of the SM, the climate conditions are also confirmed. Moreover, on May 15, 2000, the SM simulated with different surface resistance combinations uniformly approximated to 0.9, which indicates the almost saturated soil water content (wet) on that day.

The variations of ETA simulated from different surface resistance combinations on five dates are very complicated (Figure 2.2b and 2.3b). This appearance is attributed to the

combined effects that the impact of the surface resistance perturbation – mainly influences ETP in magnitude, the impact of the meteorological variables variances – reflected on the ETP fluctuations over time, and the impact of the actual soil moisture restriction – determined the reducing amount on the ETP rate.

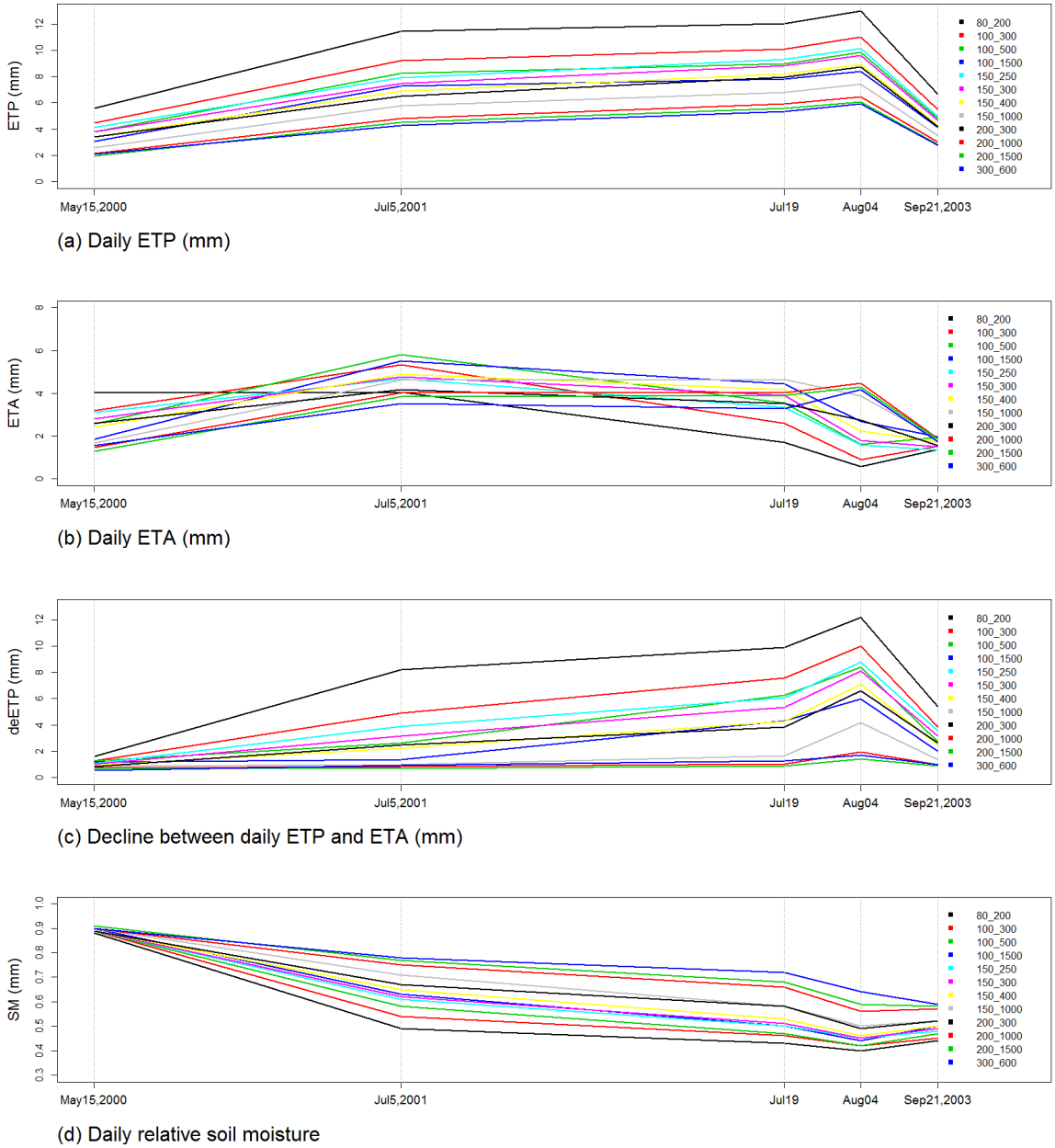

(a) Daily ETP (mm)

(b) Daily ETA (mm)

(c) Decline between daily ETP and ETA (mm)

(d) Daily relative soil moisture

Fig. 2.2 Model outputs (a) daily median ETP (mm), (b) daily median ETA (mm), (c) decline between daily median ETP and ETA (mm), (d) daily median relative soil moisture in root zone, of WaSiM-ETH on five sample dates in deciduous forest of the Nahe catchment.

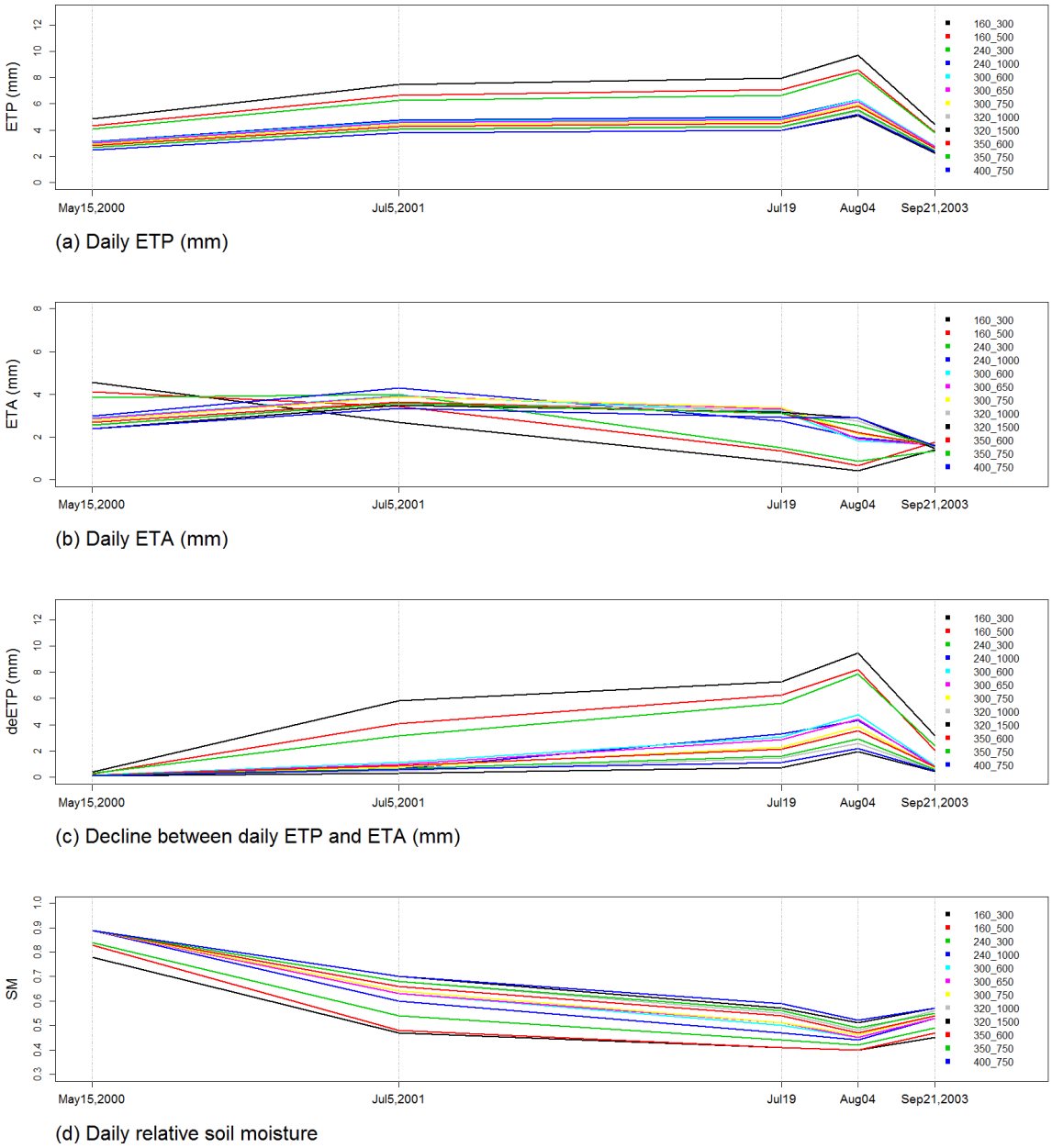

Fig. 2.3 Model outputs (a) daily median ETP (mm), (b) daily median ETA (mm), (c) decline between daily median ETP and ETA (mm), (d) daily median relative soil moisture in root zone, of WaSiM-ETH on five sample dates in coniferous forest of the Nahe catchment.

2.6 Summary and conclusion

In this chapter, we introduced the main techniques concerning ETA estimation in the WaSiM-ETH model. WaSiM-ETH is a mature hydrological model that has been successfully applied in different cases. It consists of several sub modules. In this study, seven sub modules were involved orderly: (1) the radiation correction module corrected the sunshine radiation to achieve effective radiation for each grid cell; (2) the ET module separately calculated the ETP from plants transpiration, soil surfaces evaporation and interception evaporation after rainfall; (3) the snow module calculated the snow accumulation and melting in terms of the precipitation and temperature measurements; (4) the interception module computed the interception storage, taking both the water from snow melt and rainfall into account; (5) the unsaturated zone module simulated the soil water content vertically in one-dimension in the soil; (6) the groundwater flow module simulated the multi-layer aquifers for groundwater. With regard to the ETA estimation, there were three main steps: (1) on the basis of the ground-measured meteorological variables such as SSD, T, RH and WS, to calculate the ETP by the Penman-Monteith equation; (2) using the precipitation measurements to simulate the soil water content in the unsaturated zone by the Richards equation; (3) to obtain ETA by reducing the ETP according to the actual soil water content.

In the Penman-Monteith equation, the bulk aerodynamic resistance r_a and the bulk surface resistance r_s are the most important parameters for ET estimation (Beven, 1979; Calder, 1977; Rana and Katerji, 1998). Since in WaSiM-ETH, the transpiration from plants, the evaporation from bare soil and the interception evaporation are separately calculated with the Penman-Monteith equation, r_s are thereby divided into the canopy surface resistance r_{sc}, the soil surface resistance r_{se} and the interception surfaces r_{si}. In this study, we focused our studies only on the parameters r_{sc} and r_{se}, as only the dry-canopy (no rainfall) condition was taken into account, as well as r_s plays a much more significant role than r_a in a forest region (Beven, 1979).

The simulation with different r_{sc} and r_{se} values were executed in WaSiM-ETH. For each forest type, 12 different representative combinations of r_{sc} and r_{se} were selected to explore the performances of their corresponding outputs on five sample dates. It was found that the changes in r_{sc} and r_{se} leaded to variances of ETP mainly in magnitude whereas the fluctuations over time were assumed to correspond to the impact of daily meteorological variables. The parameters r_{sc} and r_{se} also impacted deETP and SM in magnitude. In WaSiM-ETH, ETA and SM estimation are associated with each other in a long time series – decrease of ETA would lead to more water remaining in the soil whereas increase of ETA would reduce the soil moisture due to the water balance principle in the model.

Due to the suggestion that to judge the moisture degree of a climate by the amounts of both precipitation and ETA (Thornthwaite, 1948), the deETP is considered as a good indicator. For instance, the meteorological condition on August 04, 2003 was considered relatively dry due to the highest deETP value on five sample days whereas it was considered as wet on May 15, 2000 in terms of its lowest deETP value (Figure 2.2c and 2.3c). In terms of the deETP, the remote sensing-based observation on five sample days are verified to contain multiple meteorological conditions. However, on May 15, 2000, it was confirmed very wet due to the uniform model-simulated soil moisture values with different surface resistances, which all approximated to 0.9.

Chapter 3

Remote sensing

3.1 Introduction

Remote sensing data have been frequently used in hydrological studies since they are economic, efficient and large-scale available materials for the hydrological state variables or energy fluxes in the water cycle estimation. The conventional methods urgently require ground measurements, whereas the introduction of the remote sensing data alleviate or even eliminate this requirement. On the basis of the remote sensing data, additional information on meteorological variables, surface properties and crop features can be supplied in data-lacking basins, and these research data are available over a large landscape scale. With the developing of remote sensing instruments and techniques, the accuracy of remote sensing-based estimations is also increasing. In the last decades, several methods on the basis of remote sensing images combining with the ground measurements have been proposed and improved in evapotranspiration (ET) estimation. These methods have improved the accuracy of the meteorological measurements and the estimated ET (Wilson et al., 2003).

The remote sensing techniques for ET estimation have been divided into four categories (Courault et al., 2005): (1) empirical direct methods; (2) residual methods of the energy budget; (3) inference methods; (4) deterministic methods. The empirical direct methods are based on the simplified approach firstly proposed by Jackson et al. (1977), which linearly relates the daily sensible heat flux H to the instantaneous temperature difference between surface and air ($T_s - T_a$) at midday, assuming that the ratio of H to net radiation (R_n) is a constant and the soil heat flux (G) in a 24-hours period is negligible. In the approach, T_s is the land surface temperature (LST) retrieved by remote sensing data in ^oC and T_a is the air temperature that 150 cm above the soil in ^{o}C. ($T_s - T_a$) is also termed as the stress degree day (SDD). The simplified approach has been subsequently improved in a number of studies (Carlson and Buffum, 1989; Carlson et al., 1995; Lagouarde, 1991; Nieuwenhuis et al., 1985;

Seguin and Itier, 1983); a non-constant coefficient B and an additional exponential coefficient n are finally employed to retrieve H from the surface-air temperature difference at midday. In the empirical direct methods, the ground meteorological measurements and the Thermal Infra Red (TIR) remote sensing data are basic input data. The basic principle of the empirical direct methods is that to estimate ET (corresponding to the latent heat flux, LE) by assessing the surface energy balance through the surface properties such as surface albedo, fractional vegetation cover (FVC) and LST. The biggest difficulty in the empirical direct methods is the determination of LST. The residual methods of the energy budget estimate the ET as the residual of the energy balance equation. The other energy components are obtained by empirical and physical combined methods. The most representative approach is SEBAL (Surface Energy Balance Algorithm for Land) (Bastiaanssen et al., 1998a,b). In SEBAL model, remote sensing images are used to estimate R_n and G at a regional scale. The ground-measured meteorological data also play an important role in SEBAL. It is also suggested to obtain reasonable accurate results with SEBAL in midday, and the accuracy very depends on the density of the available climate stations in the study area (Courault et al., 2005). SEBAL is suggested not to work in cloudy days (Bastiaanssen et al., 1998a) and it is not suitable for all regions. However, the biggest difficulty in applying SEBAL is to detect the wet and dry pixels (Courault et al., 2005). In the wet pixels, H is considered as zero and T_s equals T_a whereas in the dry pixels, LE is assumed as zero since all energy transforms into H (Calcagno et al., 2007). The inference methods are actually the "$K_c.ET_o$" approach firstly proposed in the FAO-24 report (Doorenbos and Pruitt, 1977), in which the actual evapotranspiration ETA is calculated by the reference evapotranspiration (ET_o) multiplying the crop coefficient K_c. In the inference methods, ET_o is estimated by the ground measurements and k_c is calculated by the remote sensing data. It is difficult to determine k_c, since it is dependent on crop types, crop growth stages, soil evaporation rates and climate conditions (Allen et al., 1998). The vegetation indices such as the normalized difference vegetation index (NDVI) and the leaf area index (LAI) are critical parameters in k_c calculation due to the high correlations between them and k_c. Both NDVI and LAI are retrieved from the red and near red reflective bands of the remote sensing images. The deterministic methods are based on the complicated soil-vegetation-atmosphere transfer (SVAT) model. In these methods, the remote sensing data are employed as the auxiliary materials for the energy flux components estimation and the input data of SVAT model integration or calibration.

In this study, we used remote sensing images from the Landsat Thematic Mapper (TM) and Enhanced Thematic Mapper plus (ETM+) as basic input data for ETA estimation. The accuracy of the remote sensing-based outputs are very dependent on the precisions of the remote sensors, the spatial and temporal resolutions of the satellites and the impacts from the

atmosphere and clouds (Lagouarde and Brunet, 1993). It is important to make sure that LST retrieved from the remote sensing TIR data is under totally clear-sky conditions, since even very thin cloud covers will considerably affect the thermal band readings, lead to large errors in LST estimation and sensible heat flux calculation (Allen et al., 2002). Therefore, high quality and cloudy-free remote sensing images are required. The atmospheric correction is also necessary for data pre-processing to alleviate the atmospheric effect and improve the accuracy of the remote sensing images. The spatial resolution of TM and ETM+ images are very high: 30 $\times$ 30 m for the reflective bands, and respectively 120 $\times$ 120 m and 60 $\times$ 60 m for the thermal band. However, due to the overlapping cycle of the Landsat TM/ETM+ sensor for the entire earth is 16 days, high quality and cloudy-free images during the period 1971-2003 (the WaSiM-ETH model run) for the Nahe catchment are available on only five dates – May 15, 2000, July 05, 2001, and July 19, August 04, and September 21 in 2003.

The TM and ETM+ images have been widely used in environmental studies. TM sensor was carried on the Landsat 4 and 5 satellites during 1982-2012. The TM image consists of seven bands – band 1-5 and 7 are in the visible and near infrared (NIR) regions, and band 6 is in the thermal infrared (TIR) region. Band 1 (0.45-0.520 μm) is used for studies on coastal water; band 2 (0.52-0.6) is used for crops and vegetation stage identification; band 3 and 4 (0.63-0.69 μm and 0.76-0.9 μm), respectively red and NIR band, are commonly used for NDVI retrieving; band 5 and 7 (1.55-1.75 μm and 2.08-2.35 μm), both median infrared band, are used for studies on clouds, snow and ice; the thermal band 6 (10.4-12.5 μm) is used for land surface temperature determining (Sobrino et al., 2004). The ETM+ sensor has carried on Landsat 7 and launched since 1999. However, since May 30, 2003, a scan line corrector occurred to the data. The ETM+ image consists of eight bands, with an additional Panchromatic band 8. Like TM, the TIR band of ETM+ is also frequently used for LST retrieving. The spatial resolution of TIR band in TM and ETM+ (120 m and 60 m) are high enough to detect the thermal variations in space scale on the land surface. With contrast to the visible and NIR bands, the characteristics of the TIR radiation are: (1) the atmospheric scatting of TIR radiation is small due to its relatively long wavelength; (2) the radiation can be acquired both in daytime or nighttime since it is emitted rather than reflected. Based on the TIR band of TM/ETM+, three single-channel methods were proposed for LST retrieving: (1) the relative transfer equation; (2) the nomo-widow algorithm (Qin et al., 2001); (3) the Jiménez-Muñoz and Sobrino's single-channel method (Jiménez-Muñoz and Sobrino, 2003). The first method estimates LST using situ radiosounding data by the relative transfer equation. The mono-window algorithm employs the atmospheric water vapor and near-surface air temperature as input data. The single-channel method only requires the atmospheric water vapor content. Sobrino et al. (2004) compared them all and found that the single-channel

method performed best in LST retrieving. LST is strongly related to the ET rate, therefore TM and ETM+ TIR data are extensively used for large-scale surface ET estimation.

The purpose of this chapter is to estimate ETA with the remote sensing and ground-measured combined data, through an appropriate method that is as similar as possible to the techniques employed in WaSiM-ETH model, thereby to obtain ideal observation data corresponding to the model simulated ETA. In this chapter, we introduced the main techniques of daily ETA retrieving from TM/ETM+ images on five sample dates.

3.2 Method statement

In this study, the empirical direct method was used for ETA retrieving from remote sensing images. Figure 3.1 shows the main flow chart of data processing. The basic principle of this method is to estimate ETA as the latent heat flux through the surface energy balance equation with the surface properties. The input data are high-quality and cloudy-free TM and ETM+ images selected on five sample dates during the period that model run (1971-2003) – May 15, 2000, July 05, 2001, July 19, August 04 and September 21 in 2003. The MODIS (Moderate Resolution Imaging Spectroradiometer) products (MOD 09 and MOD 05) on the same dates were collected as auxiliary data. MOD 09 is the MODIS surface reflectance product, which estimates the surface spectral reflectance and used for the atmospheric correction of TM and ETM+ images. Bands 1–5 and 7 of both TM and ETM+ images are the reflectance bands. The spectral radiance of these bands with a spatial resolution of 30 m were used for a series of surface properties achieving: surface albedo, NDVI, FVC and land surface emissivity (LSE). The MODIS Precipitable Water product (MOD 05) was used for water vapor estimation. It consists of vertical column water-vapor amounts in cm and is in a spatial resolution at 1 km. The thermal band 6 with a resolution of 120 m for TM and 60 m for ETM+ combining with the water vapor estimates were used for LST retrieving.

The LST is a critical variable in surface energy assessment (Figure 3.2). It is an important input data for the sensible heat flux (H) calculation. In this study, we used a modification of the simplified method proposed by (Jackson et al., 1977). The H is linearly related to the instantaneous temperature difference between surface and air at midday – to retrieve daily integrated H based on the maximal LST and ground measured air temperature. LST is also an important input data for net radiation (R_n) estimation. The outgoing longwave radiation was calculated by the mean LST. After the soil heat flux (G) was calculated as an fractional of R_n, the ETA on five sample dates were finally obtained as latent heat flux by the surface energy equation. The retrieved data are with a grid resolution of 30×30 m.

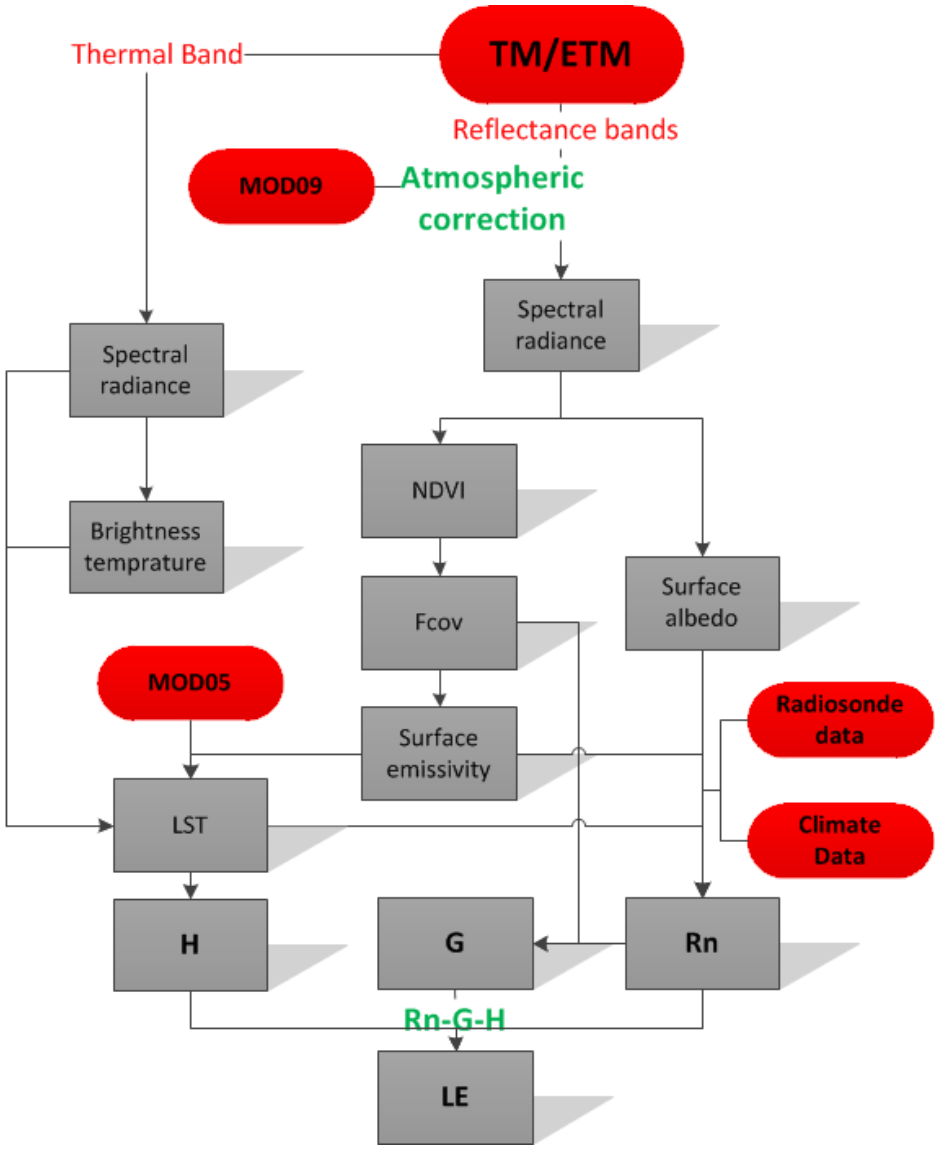

Fig. 3.1 Flow chart of data processing.

3.3 Atmospheric correction

Remote sensing images are commonly expressed in arbitrary units, e.g., digital number (DN). To obtain lasting quantitative values of remote sensing images, it is necessary to calibrate them into physical units such as reflectance (Teillet, 1986). The reflectance values of remote sensing images are generally affected by sensor characteristics, illumination geometry and atmospheric scattering and absorption (Smith and Milton, 1999). To remove the effect of the sensor, usually a known relationship between DN and sensor-recorded radiance is used. In this study, the DN values of Landsat TM/ETM+ images were converted to the at-sensor

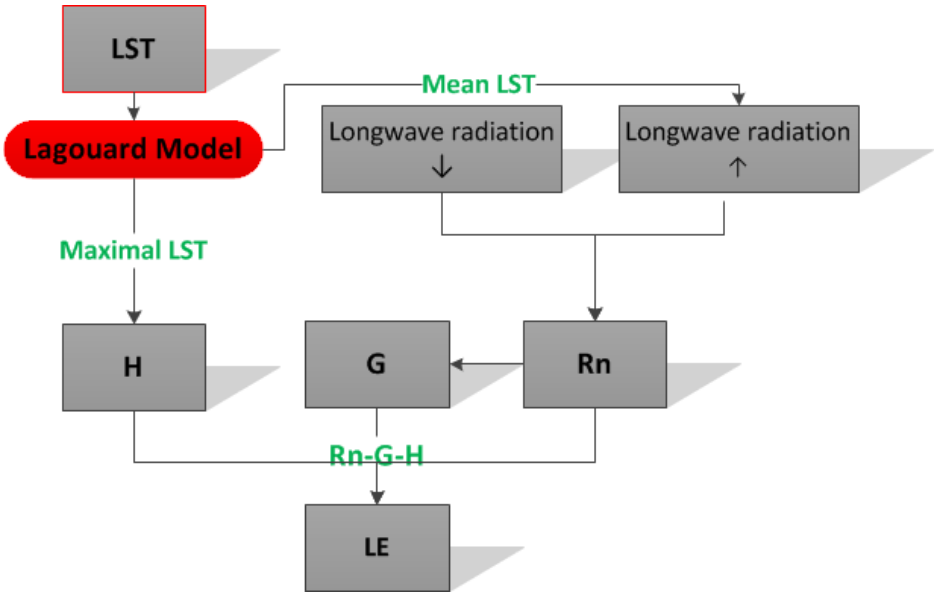

Fig. 3.2 LST for heat fluxes retrieving.

spectral radiance by the following equation (Chander et al., 2009):

$$L_\lambda = (\frac{LMAX_\lambda - LMIN_\lambda}{Q_{cal\,max} - Q_{cal\,min}})(Q_{cal} - Q_{cal\,min}) + LMIN_\lambda \tag{3.1}$$

where L_λ is the spectral at-sensor radiance at the sensor's aperture in $\mathrm{W\,m^{-2}\,sr^{-1}\,\mu m^{-1}}$; $LMAX_\lambda$ is the spectral at-sensor radiance that is scaled to $Q_{cal\,max}$; $LMIN_\lambda$ is the spectral at-sensor radiance that is scaled to $Q_{cal\,min}$; Q_{cal} is the quantized calibrated pixel value (DN); $Q_{cal\,max}$ is the maximum quantized calibrated pixel value corresponding to $LMAX_\lambda$ (DN); $Q_{cal\,min}$ is the minimum quantized calibrated pixel value corresponding to $LMIN_\lambda$ (DN).

The thermal band of Landsat TM/ETM+ was converted from at-sensor spectral radiance to effective at-sensor brightness temperature. The conversion formula is:

$$T_\lambda = \frac{K_2}{ln(\frac{K_1}{L_\lambda} + 1)} \tag{3.2}$$

where T_λ is the effective at-sensor brightness temperature in K; K_1 and K_2 are the calibration constants in K.

There are a number of methods to account for the influence of illumination and atmosphere on the sensor-recorded radiance, such as (Karpouzli and Malthus, 2003; Smith and Milton, 1999): (1) dark subtraction methods (e.g. Chavez (1996)). Dark subtraction methods remove the atmospheric effects from an image by subtracting the pixel value that repre-

Sensor	K_1	K_2
Landsat TM	607.76	1260.56
Landsat ETM+	666.09	1282.71

Table 3.1 Calibration constants for at-sensor radiance to effective brightness temperature.

sents the background; (2) normalization method (e.g. FLAASH). Normalization methods normalized the reflectance of an image to a spectrally flat target or an image average; (3) empirical line method. Empirical line method calibrated an image by forcing its spectral data to match an already corrected reference image. (4) radiative transfer methods. Radiative transfer models such as MODTRAN (Ferrier and Trahair, 1995), EXACT (Popp, 1995) and 6S (Vermote et al., 1997) are frequently used to simulate the interaction between radiation with the atmosphere and the surface. In this study, we used the empirical line method, which calibrated the Landsat TM/ETM+ images by forcing their spectral data to match the selected field reflectance spectra from MOD 09 images (already corrected). The empirical line method is a logistically simple means of atmospheric correction, and it generates acceptable surface reflectance of remote sensing images (Smith and Milton, 1999). The method is formulated as:

$$L_{\lambda corr} = a * L_{\lambda} + b \tag{3.3}$$

where $L_{\lambda corr}$ is the correlated spectral at-sensor radiance; a and b are the regression coefficients obtained from the linear regression function of the spectral data between the raw remote sensing images that need to be calibrated and filed images (reference).

The study area, Nahe catchment, was classified into more than 10 land used types, e.g. open water, deciduous forest, coniferous forest, grape field, bare soil, bushes, mountains, residential district, highway, industrial district. For each land used type, we selected 50 homogeneous targets on the Landsat TM/ETM+ image to collect the image spectra. These targets were also located to the MOD 09 images to select the corresponding reference field spectra. The linear regression function was subsequently found between two spectra data sets. The obtained regression coefficients were used for Landsat TM/ETM+ images calibration.

3.4 Surface properties

3.4.1 Surface albedo

The surface albedo is the ratio of the reflected solar radiation to the total incident solar radiation. The surface albedo determines the amount of effective incident solar radiation that

is absorbed by the land surface – an increasing surface albedo leads to the reducing of net radiation (R_n), thereby less energy will be supplied for the surface energy exchanging and the water circling between atmosphere and surface, and ET rates will consequently decrease. All these appearances are attributed to the significant albedo-climate coupling and feedback mechanism between the land surface and the atmosphere (Cess, 1978). Charney et al. (1977) studied the albedo change in arid to semi-arid regions and hypothesized that the increase of surface albedo also caused a net reduction of convective cloud and precipitation. Sud and Fennessy (1982) draw the same conclusion that increasing surface albedo in the subtropic regions leads to above atmosphere cooling, a reduction in the convective and subsequently the total precipitation. It is also found by Dirmeyer and Shukla (1994) that while albedo increases, the ET and H exhibit similar reduction due to the reduced R_n and result in convection and precipitation reduction in tropic Africa and Amazon basin. In general, the approximated range of albedo for forest is 0.05-0.2, while it is 0.1-0.25 for grassland and cropland (Weast, 1969). Surface albedo can be effectively and globally monitored through remote sensing multi-spectral sensors. The atmospheric conditions and surface properties are critical factors affecting surface albedo determination (Liang, 2001). In this study, the shortwave surface albedo is calculated with the high-resolution TM/ETM+ narrowband radiance. The formula was proposed by Liang (2001) as:

$$\alpha_{short} = 0.356\alpha_1 + 0.130\alpha_3 + 0.373\alpha_4 + 0.085\alpha_5 + 0.072\alpha_7 - 0.0018 \tag{3.4}$$

where α_n indicate the atmospheric corrected spectral radiance of band n ($n = 1,3,4,5,7$). Band 2 is removed from this equation since the standard deviation of its coefficient is too big.

3.4.2 Fractional vegetation cover

Fractional vegetation cover (FVC) is defined as the percentage of vegetation covering the ground area in the vertical projection. It is an important indicator for characterizing the land surface vegetation cover and for assessing plants growth condition (Zhang et al., 2013). To derive FVC, the normalized difference vegetation index (NDVI) is the basic element. NDVI is a remote sensing based vegetation index used to quantify the density of plant growth on the earth. It is derived from the surface reflectance of visible (red) spectrum a_{vis} (wavelength λ in 0.5-0.7 μm) and the surface reflectance of near-infrared spectrum a_{nir} (λ in 0.7-0.9 μm). The visible spectrum absorbs the chlorophyll of plants and the mesophyll leaf structure scatters the near infrared spectrum. NDVI is formulated as:

$$NDVI = \frac{a_{nir} - a_{vis}}{a_{nir} + a_{vis}} \tag{3.5}$$

The range of NDVI is [-1,1]. Land use types can be simply identified with NDVI as water, soil and vegetated surfaces. A low but positive NDVI approximates 0.5-0.24 represents soil surfaces; negative values represents open water; and high values close to 1 indicate very high density of green plants. Plant species, leaf area, soil reflectance and shadows affect NDVI estimation (Jasinski, 1990). Sellers (1985) concluded that NDVI is a near linear indicator of minimal canopy resistance and photosynthetic capacity. A good linear relationship between NDVI and ETA was found by (Kerr et al., 1989), with a time laps of 20 days.

However, NDVI is an unsuitable indicator of the vegetation cover since it is more related to the chlorophyll of leaves rather than the vegetation coverage – for same vegetation coverages with identical FVC values, the NDVI values may be different due to the different chlorophyll contents (Glenn et al., 2007). The equation for FVC computation is written as (Carlson et al., 1995):

$$F_r = (\frac{NDVI - NDVI_0}{NDVI_s - NDVI_0})^2 \tag{3.6}$$

where F_r is the fractional vegetation cover (FVC); $NDVI_s$ indicates the NDVI values at 100 % vegetation cover and $NDVI_0$ indicates the NDVI values for bare soil. The NDVI values are divided into three intervals according to different cases (Sobrino et al., 2001): (1) $NDVI < 0.2$, the pixel valued in this range indicates the bare soil; (2) $NDVI > 0.5$, the pixel valued in this range indicates the full vegetated land; (3) $0.2 \leq NDVI \leq 0.5$, the pixel valued in this interval is considered to represent the vegetation and soil mixed surface. Therefore in Equation 3.6, we used the values that $NDVI_s = 0.5$ and $NDVI_s = 0.2$ for data processing.

3.4.3 Land surface temperature and emissivity

The land surface temperature (LST) is a key parameter in the land surface processes, e.g., the heat exchange and the water cycling between land surface and atmosphere (Sun, 2011). LST has been widely used in the meteorological and environmental studies: (1) to monitor the kinetic temperature trend at spatial and temporal scale on the land surface; (2) to indicate and predict the climate change; (3) to monitor the vegetation water stress; (4) to estimate the sensible heat flux and subsequently the latent heat flux (Boulet et al., 2007; Jin, 2004; Norman and Becker, 1995; Sun and Pinker, 2003). Matsui et al. (2003) found a strong negative connection between LST and precipitation in a monthly time step – about +4 K change in LST decreased the rainfall in 1 mm per day, and this connection was attributed to the positive soil moisture-rainfall feedback. LST has also been frequently used to indirectly indicate the crop water stress (Boulet et al., 2007; Yuan et al., 2004). In the ET process, the canopy surface temperature decreases and the surrounding air temperature increases. Under

the water-stress conditions, the ET reduces and the canopy temperature increases. Moreover, the absorbed solar radiation warms the air temperature above the canopy surface due to the surface energy balance principle. This theory has been subsequently extended to the LST and ET. LST is thus commonly used for ET retrieving due to its correlation with soil moisture.

The remote sensing thermal infrared (TIR) bands directly record the radiance emitted by the surface, and are commonly used for LST retrieving. Infrared thermometry was firstly used by Tanner (1963) to retrieve leaf temperature. Fuchs and Tanner (1966) used infrared thermometers with a bandpass filter to measure the real vegetation surface temperature. The TIR-based LST is found more accuracy than the microwave-retrieved LST, since the low variation of land surface emissivity (LSE) of TIR data and the high correlation between its recorded radiance and temperature (Sun, 2011). With contrast to the sea surface temperature (SST) that is available in global scale for a long term, LST is difficult to obtain due to the high-heterogeneity of land surface, unknown emissivity and atmospheric conditions (Jin, 2004). The methods for LST estimation require consideration containing both atmospheric effects and land surface emissivity (Li and Becker, 1993). Numbers of methods were proposed to retrieve LST from remote sensing TIR data. Methods based on multiple thermal bands as well as methods based on single thermal band are two main types of the methods for LST retrieving that applied for data from different remote sensors. Split-window method is the most commonly used multiple-thermal-band method, which estimates LST from two adjacent channels. (Sobrino et al., 2004) compared three methods for LST retrieving based on the sole TIR band of Landsat 5 TM – radiative transfer equation, mono-window algorithm (Qin et al., 2001), and the single-channel method (Jiménez-Muñoz and Sobrino, 2003), and found the single-channel method performed the best in both LST and LSE estimation. For the single-channel method, accurate LSE and atmospheric profiles are necessary (Gao et al., 2013). Based on the Landsat TM/ETM+ images with single thermal band, in this study, the single-channel method was used for LST retrieving. LSE (ε) was obtained in terms of the high emissivity in vegetated surfaces and the relatively low emissivity in bare soil and is formulated as (Brunsell and Gillies, 2002):

$$\varepsilon = F_r \cdot \varepsilon_v + (1 - F_r) \cdot \varepsilon_s \tag{3.7}$$

where ε_v is the emissivity of full vegetation and ε_s is the emissivity of bare soil. For ET/ETM+ band 6, $\varepsilon_v = 0.99$, $\varepsilon_s = 0.97$ (Sobrino et al., 2004).

LST estimation is mainly affected by atmosphere, angular and emissivity (Valor and Caselles, 1996). The equation is given as (Sobrino et al., 2004):

$$T_s = \gamma[\varepsilon^{-1}(\psi_1 L_{sensor} + \psi_2) + \psi_3] + \delta \tag{3.8}$$

with

$$\gamma = \{\frac{c_2 L_{sensor}}{T_{sensor}^2}[\frac{\lambda^4}{c_1}L_{sensor} + \lambda^{-1}]\}^{-1} \tag{3.9}$$

$$\delta = -\gamma L_{sensor} + T_{sensor} \tag{3.10}$$

$$\psi_1 = -0.147w^2 - 0.15583w + 1.1234 \tag{3.11}$$

$$\psi_2 = -1.836w^2 - 0.37607w - 0.52894 \tag{3.12}$$

$$\psi_3 = -0.04554w^2 + 1.8719w - 0.39071 \tag{3.13}$$

where T_s is LST in K; L_{sensor} is the satellite radiance in $\mathrm{W\,m^{-2}\,sr^{-1}\,\mu m}$; T_{sensor} is the satellite brightness temperature in K; λ is the effective spectral wavelength, $\lambda = 11.457$ μm for TM band 6 and $\lambda = 11.269$ μm for ETM+ band 6; c_1 and c_2 are constants, $c_1 = 1.19104 \times 10^8$ in $\mathrm{W\,\mu m^4\,m^{-2}\,sr^{-1}}$ and $c_2 = 14387.7$ in $\mu\mathrm{m\,K}$; ψ_1, ψ_2 and ψ_3 are the atmospheric functions; w is the total atmospheric water vapor content, which was obtained by MOD 05 (MODIS Precipitable Water product).

LST is strongly linked with evapotranspiration through surface budget. While land surface temperature is higher than air temperature, the energy used for evapotranspiration is lower than the net radiation; whereas if it is lower than air temperature, the energy used for evapotranspiration is higher than the net radiation (Hatfield et al., 1983). In this remote sensing-based method, the maximal and mean LST values were subsequently used for surface energy fluxes (e.g. net radiation, sensible heat flux) retrieving (Figure 3.2).

3.5 Surface energy components

3.5.1 Surface energy balance equation

For most remote sensing techniques, surface energy balance equation is the physical basis for evapotranspiration estimation – latent heat flux (corresponding to evapotranspiration) is obtained as the residual of energy budget, and other energy components are calculated by means of ground measuring, remote sensing or modeling. The surface energy balance equation is written as:

$$R_n = LE + H + G \tag{3.14}$$

where all terms are expressed in $\mathrm{W\,m^{-2}}$; R_n is the net radiant energy, namely the total solar radiation absorbed by surface; LE is the latent heat flux, which is numerically equal to the sum energy consumption for evapotranspiration; H is the sensible heat flux and G is the soil heat flux, which are energy consumption for heat exchange in atmosphere and soil, respectively. Evapotranspiration is thereby obtained as the energy residual between the totally absorption (R_n) and consumption (sum of H and G) on the surface. In the equation, the energy consumption for photosynthesis and heat stored in vegetation are not taken into account. In general, LE is larger than H or G over vegetated surfaces.

In surface energy balance equation, two observed surface types should be considered for radiant and convection fluxes estimation – single layer surface and multiple layers surface. The former indicates a sole component observed surface while the latter contents two sources components of both soil and vegetation, in which the vegetation can be divided into several layers according to the canopy degrees.

3.5.2 Net radiation

Solar radiation is the total energy supplier for energy exchange on the earth. Net radiation (R_n) is the solar radiation balance between incoming (from atmosphere to surface) and outgoing (from surface to atmosphere) radiation. To obtain R_n, the radiation balance equation is used:

$$R_n = (R_s\downarrow - R_s\uparrow) + (R_l\downarrow - R_l\uparrow) \tag{3.15}$$

with

$$R_s\downarrow + R_s\uparrow = (1-\alpha)R_s\downarrow \tag{3.16}$$

$$R_l\downarrow = \varepsilon_a \sigma T_{am}^4 \tag{3.17}$$

$$R_l\uparrow = \varepsilon \sigma T_{sm}^4 \tag{3.18}$$

where R_s is the shortwave radiation and R_l is the longwave radiation, both in $\mathrm{W\,m^{-2}}$, with $\downarrow$ and $\uparrow$ indicate the incoming and outgoing directions; α is the shortwave surface albedo (dimensionless); ε_a is the effective atmospheric emissivity (dimensionless) while ε is the surface emissivity (dimensionless); T_{am} and T_{sm} are respectively the mean air and land surface temperature, both in $^{\mathrm{o}}\mathrm{C}$. Equation 3.17 is a empirical equation for downward longwave radiation estimation in terms of only the near surface meteorological data. The approximate

effective mean atmospheric temperature T_{am} is calculated by a simply linear relationship to the near surface (about 2 m above the surface) air temperature T_0 (Qin et al., 2001):

$$\text{For mid-latitude summer} \quad T_a = 16.0110 + 0.92621T_0 \tag{3.19}$$

$$\text{For mid-latitude winter} \quad T_a = 19.2704 + 0.91118T_0 \tag{3.20}$$

Brutsaert (1975) presented a derivation for effective atmospheric emissivity ε_a under cloudy-free conditions. The functions are (Richter, 1998):

$$\varepsilon_a = 1.24 \times (\frac{p_{wv}}{T_a})^{1/7} \tag{3.21}$$

$$p_{wv} = RHe_s/100 \tag{3.22}$$

$$e_s(T_a) = 6.1078exp[\frac{17.26939(T_a - 273.16)}{T_a - 35.86}] \tag{3.23}$$

where p_{wv} is the water vapor partial pressure in millibar; T_a is the air temperature in Kevin; p_{wv} is calculated as a function of the relative humidity RH (Equation 3.22); e_s is the water vapor pressure in saturated air (Equation 3.23), (Murray, 1967)).

Equation 3.18 is a simple method proposed by Lagouarde and Brunet (1993) for daily upward longwave radiation estimation under cloudless conditions. It requires only the remote sensing-retrieved land surface temperature (LST, T_s) in the early afternoon.

3.5.3 Sensible heat flux

Sensible heat flux H is the key term in this method. Jackson et al. (1977) firstly proposed a simple approach for accumulated daily evapotranspiration estimation. The basic idea of this approach is that the sensible heat flux H is proportional to the difference between the instantaneous plant canopy surface temperature and air temperature measured at midday $(T_s - T_a)$. $(T_s - T_a)$ is commonly used as an indicator of vegetation water status, This so-called simplified method neglects the soil heat flux over 24 hours period and is written as:

$$LE = R_n - B(T_s - T_a) \tag{3.24}$$

where T_c is the remote sensing-based canopy temperature measured daily between 1330 and 1400 h, in ^oC; T_a is the air temperature measured 150 cm above the soil surface, in ^oC; B is a dimensionless constant, which indicates that $(T_s - T_a)$ is linearly related to H.

This simplified method has been modified by numbers of studies (Carlson et al., 1995; Nieuwenhuis et al., 1985; Seguin and Itier, 1983) and written as:

$$R_{n24} - LE_{24} = B(T_{013} - T_{a13})^n \tag{3.25}$$

where R_{n24} and LE_{24} are respectively the integrated net radiation and latent heat flux over 24 hours; T_{013} and T_{a13} are respectively the surface radiant and the air temperature 50 m above the surface at 1300 h local time; B and n are pseudo constants derived from the fractional vegetation cover. Relevant functions are formulated as below:

$$B = 0.0109 + 0.051F_r \tag{3.26}$$

$$n = 1.067 - 0.372F_r \tag{3.27}$$

Since LST is very difficult to determine as well as remote sensing TIR data is the only means to retrieve LST in large-scale regions, Penman equation combined both aerodynamic and surface energy techniques to estimate evapotranspiration on the basis of the meteorological variables but jumped the calculation of LST.

3.5.4 Soil heat flux

For estimation in daily scale (over 24 hours), the soil heat flux (G) is always considered as negligible. However, in this study, since the instantaneous LST retrieved from remote sensing images in midday was used to estimate the accumulated surface energy fluxes in 24-hours period, the amount of G should be taken into account. Under full canopy covered conditions, G may be in the same order of magnitude as H once well-watered as well as may be in the same order of magnitude as LE for senescent plants (Kustas and Daughtry, 1990).

Soil heat flux is found to linearly relate to net radiation. In vegetated regions, G is 5-10 % of R_n and is 30-50 % of R_n in bare soil (Choudhury et al., 1986). Boegh et al. (2002) further assumed that the ratio of soil heat flux to net radiation (G/R_n) is related to the fractional vegetation cover (FVC). The generalized formula for all surface types is written as:

$$(G/R_n) = F_r(G/R_n)_{veg} + (1 - F_r)(G/R_n)_{soil} \tag{3.28}$$

with $(G/R_n)_{veg} = 0.1$ and $(G/R_n)_{soil} = 0.5$. Ratio (G/R_n) for vegetation is less than that for bare soil is due to the partial decreased net radiation for vegetation surface.

3.5.5 Latent heat flux (actual evapotranspiration)

Thus, in this study, the ultimate equation for daily evapotranspiration estimation via remote sensing images is formulated as (Casper and Vohland, 2008):

$$\int_0^{24h} LE = \int_0^{24h} R_n - G - B(T_{s(max)} - T_{a(max)})^n \tag{3.29}$$

with $B = 0.0109 + 0.051F_r$ and $n = 1.067 - 0.372F_r$; $T_{s(max)}$ is the maximum land surface temperature in ^{o}C; $T_{a(max)}$ is the maximum air temperature in ^{o}C; $\int_0^{24h} LE$ and $\int_0^{24h} R_n$ are in cm.

3.6 Results and discussion

In Figure 3.3 and 3.4, the remote sensing-retrieved surface properties and surface energy components on five sample dates for both forest types are shown. In the boxplots of surface albedo on five samples dates (Figure 3.3a), it is shown that for each day, the surface albedo of deciduous forest is always higher than that of coniferous forest. In the WaSiM-ETH model, the parameter setting is alike (Table 2.4) – for deciduous forest, the default surface albedo is 0.2, and for coniferous forest it is 0.1. In the model setting, the default surface albedo values keep constant for each month in an entire year. However, the surface albedo is related to the vegetation properties and the atmospheric conditions (Liang, 2001); a significant albedo-climate coupling and feedback mechanism between the land surface and the atmosphere is also found by Cess (1978). The actual surface albedo is thereby assumed to vary over the time steps (e.g. daily, monthly) according to the changes in the meteorological variables. This assumption is confirmed by the remote sensing-retrieved surface albedo. On the three dates in 2003, significant high albedo (the median values were around 0.15 for each) were shown in contrast to on the other two dates (less than 0.1). Since the increase of surface albedo has been found to reduce the regional precipitation in several publications (Charney et al., 1977; Dirmeyer and Shukla, 1994; Sud and Fennessy, 1982), the extremely dry climate condition (with rare precipitation) in the summertime of 2003 is assumed to be attributed to a significant albedo increase. However, the verification of this assumption requires more observations in a long-time period. In this study, these remote sensing-retrieved surface albedo on five sample dates are in poor temporal resolution and far from enough.

In Figure 3.3b and c, the appearances of NDVI and FVC for both forest types on 5 sample dates confirmed the assertion that the NDVI is more related to the chlorophyll of leaves rather than the vegetation coverage (Glenn et al., 2007). It is shown that there were significant variances in NDVI on 5 dates whereas with regard to FVC, the variances were very small. In terms of the FVC, a relatively smaller vegetation coverage is indicated in coniferous forest than in deciduous forest for each day. This can be simply attributed to the features of both forest type – the deciduous forest, also called board-leaf forest, is superior in area covering than the coniferous forest with small-leaf plants. However, in WaSiM-ETH, the default setting values of FVC in the model for deciduous forest are always smaller than those for coniferous forest (Table 2.4). To verify the features of FVC for both forest types, observations in higher temporal resolution are also required.

In Figure 3.4a, it is shown that there was adequate energy supply on May 15, 2000, July 05, 2001 and July 19, 2003, whose R_n values were all over 5 mm per day. On the other two dates in 2003, the R_n were very low, especially on September 21, its R_n was not more than 2 mm per day. The amount order of R_n on sample dates was not consistent with the SSD measurements (Figure 1.7c). For example, on July 05, 2001, the R_n was the top of all but its SSD was the lowest; whereas on the two dates in August and September in 2003, their R_n were very low (less than 3 mm) but the SSD were relatively high. This can be attribute to the surface albedo, which determines the amount of effective incident solar radiation. Therefore, R_n is more accurately than SSD to quantify the effective energy supply for ET. In publications, R_n has been frequently used to represent measurements in solar radiation to explore the relative importance in ET estimation (Bakhtiari et al., 2012; Saxton, 1975). In terms of the surface albedo, it is found that the absorbed net radiation (R_n) of deciduous forest was consequently always lower than that of coniferous forest (in Figure 3.4a).

It is known that in general, 2/3 of the R_n will transfer as the latent heat flux to support the ET process (Gash and Shuttleworth, 2007). The change trend of LE (Figure 3.4d) over five sample days was consistent with R_n and confirmed this. The G also exhibited similar change trend over time to R_n, since daily G is linearly related to R_n. The H depends on the temperature difference between land surface and air. Therefore, the highest and lowest values of H respectively indicate the large temperature gap on August 04, 2003 and slight temperature difference on September 21, 2003.

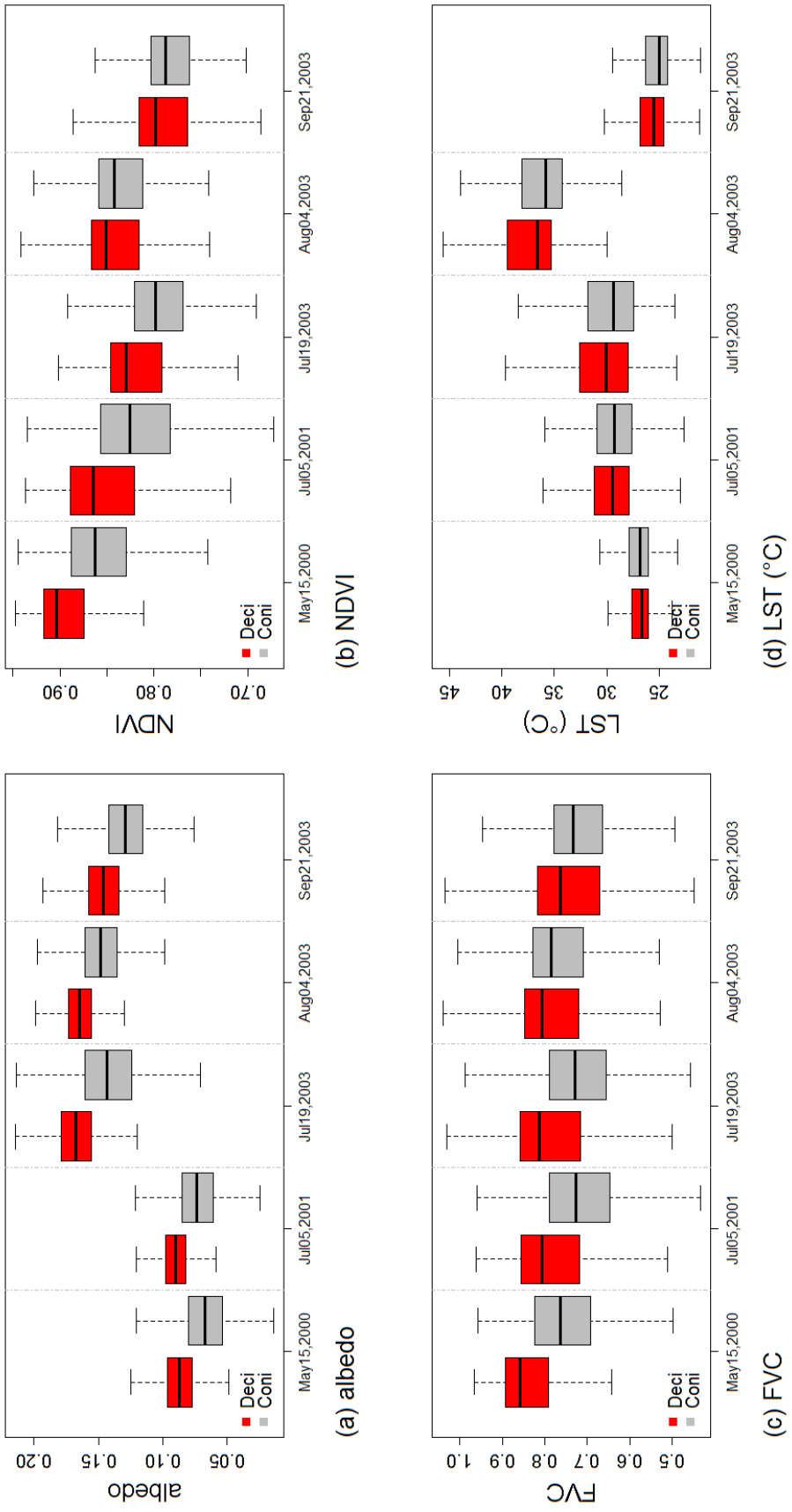

Fig. 3.3 Surface properties (a) α, (b) NDVI, (c) FCOV, (d) LST on five sample dates in deciduous and coniferous forest of the Nahe catchment.

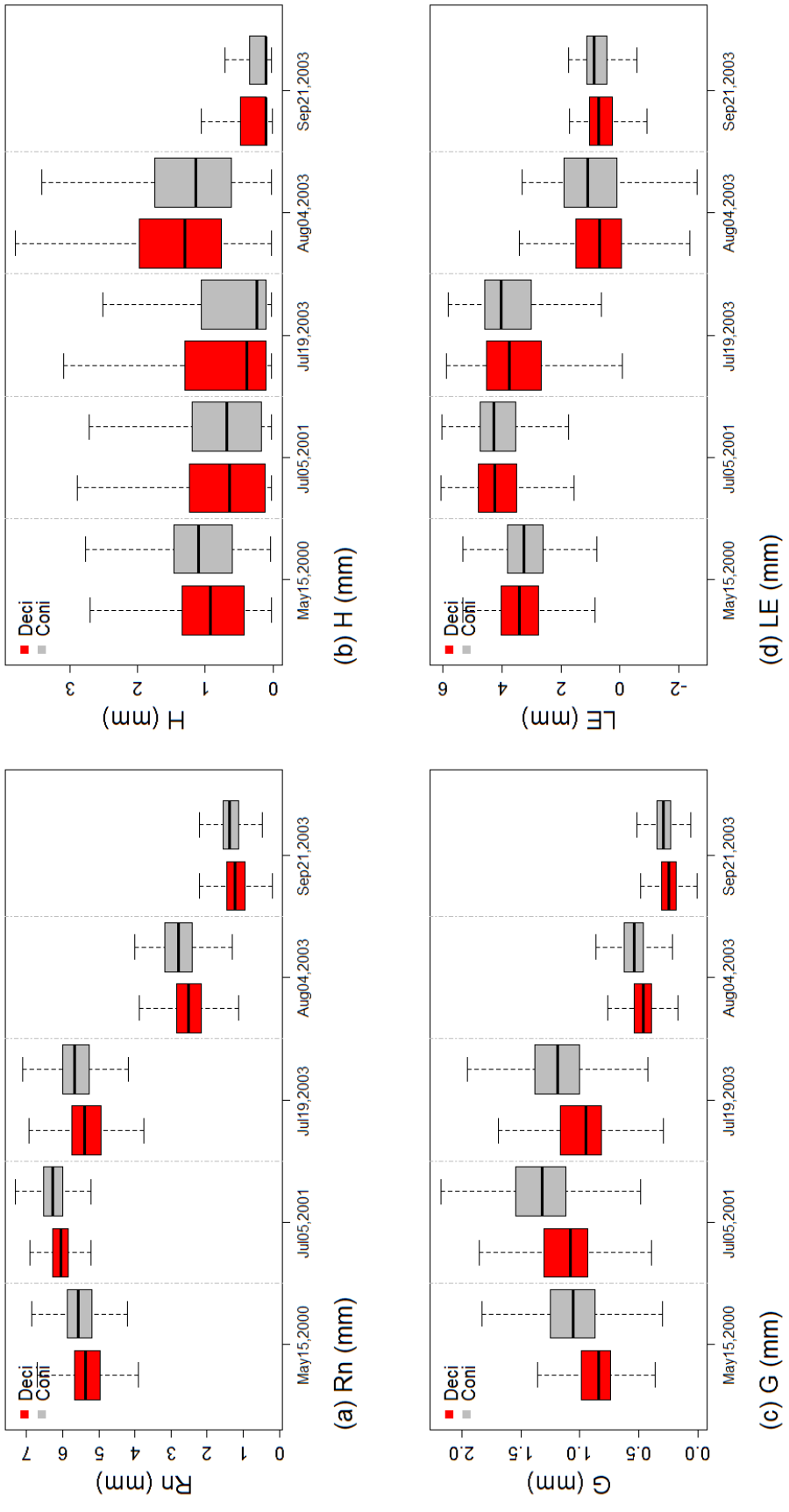

Fig. 3.4 Surface energy components (a) R_n, (b) H, (c) G, (d) LE on five sample dates in deciduous and coniferous forest of the Nahe catchment.

3.7 Summary and conclusion

In this chapter, we introduced the main remote sensing techniques for ETA estimation. The basic principle of the remote sensing-based method is to estimate ETA as latent heat flux through the surface energy balance equation with retrieved surface properties, such as surface albedo, fractional vegetation cover (FVC) and land surface temperature (LST). LST is the most important variable in this method, which was retrieved from the TM/ETM+ TIR band by the single-channel method (Jiménez-Muñoz and Sobrino, 2003). The daily sensible heat flux (H) is linearly related to the difference between daily maximal LST and air temperature. The mean LST was also used to calculate the outgoing longwave radiation and subsequently the R_n. The contribution of the soil heat flux G was estimated as a fraction of R_n. The ETA rate was finally obtained as latent heat flux through the surface budget.

The performances of surface properties and surface energy components on five sample dates were discussed. Between deciduous and coniferous forest, there were significant differences for each day: (1) the surface albedo of deciduous forest were consistently higher than those of coniferous forest, and the R_n and G in deciduous forest were thereby always lower than in coniferous forest; (2) the vegetation cover indicated by FVC values in deciduous forest were always higher than in coniferous forest. These differences between forest types were attributed to the different vegetation properties of plants in deciduous and coniferous forest.

With regard to the change trend over five sample days, it is shown that: (1) On the three days in 2003, the surface albedo were much higher than on the other two days; (2) surface albedo is very dependent on the surface properties and the climate conditions, and it controls the net radiation R_n. The amount of soil heat flux (G) and latent heat flux (LE) exhibited similar change trend over time to R_n, since the amount of G were linearly related to R_n and in general, major R_n supplies for evapotranspiration as latent heat flux. Sensible heat flux is very dependent on the simultaneous temperature difference between land surface and surrounding air. On August 04, the H was the highest.

Chapter 4

Surface resistance calibration in WaSiM-ETH

4.1 Introduction

The calibration of a physically based hydrological model is a process of adjusting parameters to find their optimal values or ranges – the simulations generated by the model should show an agreement with the observations as good as possible. There are two important parts involved: to evaluate the "closeness" between the simulations and observations as well as to adjust the parameters in the aims of improving the "closeness" between the paired variables (Boyle et al., 2000). Calibration is necessary for models applied in different regions and scales (e.g. Cullmann et al. (2006)). Ideal observations for the model calibration depend on not the data length but whether they contain enough information, e.g., multiple climate conditions (Gan et al., 1997) and critical events (Singh et al., 2012). Boyle et al. (2000) has classified the model parameter estimation schemes into three levels: (1) Level zero, to determine the approximate ranges of the parameters by examining the values obtained from previous experiences or similar calibrated watershed; (2) Level 1, to refine the parameter ranges obtained in lever zero by identifying the dominant effect of individual parameters on outputs in time series; (3) level 2, to further refine the parameter value ranges by detailed analysis in the parameter interactions and the model performances. Manual and automatic strategies are two commonly means for model calibration. The manual method is also termed as the "manual-expert" approach, for which expertises, knowledges and experiences are necessary. In contrast to the traditional single-criterion automatic calibration methods, excellent results are always obtained by employing manual approaches. However, the manual approaches are time and labor consuming. The traditional automatic approaches are superior

in the speed and powerful computation ability, objective in determination, and time and labor saving but the results may not be acceptable due to the single-criterion assessment (Gupta et al., 2003).

Model performance evaluation through comparing the model simulations with the corresponding observations is the foundation for model calibration or validation. The model performance evaluation is carried out to provide: (1) the quantitative estimate of a model's ability in simulating watershed behaviors; (2) a means for evaluating the improvements in model performance during a calibration process; (3) a mechanism for current efforts comparison (Dawson et al., 2007; Krause et al., 2005). Boyle et al. (2000); Legates and McCabe (1999); Willmott (1981) suggested to use multiple evaluation techniques for model performance evaluation. Graphical and statistical techniques are two primary evaluation means. The most frequently used visual assessment is inspecting the differences between two variables plotted in time series. Loague and Green (1991) discussed four commonly graphical means for model performance evaluation: (1) to plot modelled and observed data sets over time; (2) to plot medians and ranges of the modelled and observed data; (3) to plot the matched integrated modelled and observed data; (4) to plot the cumulative distribution of the integrated values. These methods can be respectively displayed as hydrographs, box plots, bar graphs and scatter plots. The hydrographs are the most frequently used graphical formal in model performance comparison, by which modelled and observed data sets in a time series are directly plotted. They compare variables in the specific time steps (daily, weekly, monthly or yearly). The hydrographs help the identification of model bias, differences, peak flows and recessions (Committee et al., 1993; Legates and McCabe, 1999). The agreements and disagreements on timing and magnitude between the compared variables can be easily recognized at first glance. The box plots provide detailed information in statistical distribution, in which the dispersion degree, the distribution skewness and the outliers are shown. The bar graphs indicate the frequency of data distribution in specific values, which also provide information on population distribution. The scatter plots provide a most effective way to display the correlation between two variables. There are three types of the correlations: curvilinear, exponential and linear. The Pearson's correlation coefficient (r) and its square coefficient of determination (R^2) are frequently used regression measures to indicate the linear relationship between variables.

In the last decades, dozens of statistical measures have been proposed for the hydrological model performance evaluation. The statistical measures are very good supplements to graphical techniques. Fox (1981) suggested that the model performance evaluation should be based on the differences between the simulated and observed variables - the average bias, the variance (noise), and the gross variability are necessary. The most frequently used measures

for evaluating the "goodness-of-fit" for the hydrological models in publications, r and R^2, are found to be oversensitive to the extreme values and insensitive to the additive and proportional differences between simulated and observed data sets (Legates and McCabe, 1999; Willmott, 1981). To overcome their shortages for model evaluation, Willmott (1981) proposed the index of agreement (d) as an alternative statistical index. Legates and McCabe (1999) also suggested using d and the Nash-Sutcliffe efficiency (NSE) proposed by Nash and Sutcliffe (1970) to replace r and R^2. The root mean square error (RMSE) and the mean absolute error (MAE) are both considered as effective measures for average gross differences between two variables estimation and have been widely used over the time. RMSE is more sensitive to extreme values than MAE, since the impact on the latter is reduced due to the absence of the exponent (Willmott, 1982; Willmott and Matsuura, 2005). Legates and McCabe (1999) suggested that a complete model performance assessment should include both goodness-of-fit or relative error measures (e.g. d or NSE) and absolute error measures (e.g. RMSE or MAE) with additional supporting information. Krause et al. (2005) used several efficiency criteria such as R^2, NSE, d and their modified forms in stream flow investigation and suggested a combination of different efficiency criteria for model performance evaluation. Dawson et al. (2007) has divided different metrics for model performance evaluation in three categories: (1) the statistical measures of the modelled and observed data sets in time series, (2) the statistical measures of the residual errors between modelled and observed data sets in time series, (3) the dimensionless coefficients of the model performance in compare to the recognized standards. Analogously, Moriasi et al. (2007) briefly divided them into three main categories: standard regression, dimensionless and error indices; and the statistics such as NSE, ratio of the root mean square error to the standard deviation (RSR), and percent bias (PBIAS) were finally recommended. The standard regression measures have been used for indicating the linear relationship between two variables, e.g., the regression line method, r and R^2. Error indices provide statistical information based on the differences between simulations and observations. Mean bias error (MBE), MAE, RMSE and their derivations are included in this category. The dimensionless measures evaluate the model performance with a relative value of assessment, whose ranges are always not more than 1. For example, the ranges of d and NSE are between 0 and 1 as well as from $-\infty$ to 1, respectively. For both indices, a value of 1 indicates perfect model performance that simulations and observations fit the 1:1 line. A general satisfied range for model performance evaluation were recommended by Moriasi et al. (2007) as: $NSE > 0.5$, $RSR \leq 0.7$ and $PBIAS < \pm 25$ % for stream flow.

The simulated and observed data sets used in this study are still the actual evapotranspiration (ETA) estimated by the WaSiM-ETH model and LE (latent heat flux, corresponded to ETA) retrieved from remote sensing images on 5 samples dates (May 15, 2000, July 05,

2001 and July 19, August 04 and September 21 in 2003). The weakness of the observations IS that they are available in a limited number and are discontinuous in time series. However, the observations are representative for multiple climate conditions – wet, medium wet and dry. Gan et al. (1997) used data included wet, average and dry year for model calibration and suggested that ideal observations could not be in a large amount but should contain enough information. Singh et al. (2012) used critical events replacing the whole time series to successfully calibrated the WaSiM-ETH model. Thus, the purposes of this chapter are: (1) to find appropriate methods (graphical and statistical techniques combined) for model performance evaluation based on the observations; (2) to calibrate the surface resistance for both forest types in WaSiM-ETH. Moreover, due to the advantage of the observations in spatial accuracy, model performance at the spatial scale were also be investigated.

In this chapter, we carried out manual calibration of the WaSiM-ETH model. The calibrated parameter is the surface resistance, which can be further divided into the canopy surface resistance r_{sc} and the soil surface resistance r_{se}. r_{sc} is related to the transpiration of plants and r_{se} is related to the evaporation of bare soil. Values of r_{sc} and r_{se} were adjusted in terms of our previous experiences. 12 representative different surface resistance combinations (consisted of different values of r_{sc} and r_{se}) for each forest type were selected as samples for plotting and discussion. The box plots were used for a graphical overview of the model performance at spatial-temporal scale. The statistical techniques were also applied to supply additional information for model performance assessing. To distinguish the simulations and the observations, we used ETA to denote the simulations generated by the WaSiM-ETH model and LE (latent heat flux) to denote the corresponding observations retrieved from remote sensing images.

4.2 Review of statistical techniques for model performance evaluation

4.2.1 Basic index

The measures of model performance evaluation are derived on the basis of the differences/errors between the simulations (P) and the observations (O). To easily identify the average model-performance tendency (over- or underestimated), $(P - O)$ was used in this paper to represent the differences between two variables. Fox (1981) suggested that the measures such as the MBE, the mean variance of error distribution (S_d^2), RMSE, and MAE should be calculated

for model evaluation. These indices are calculated as below (Fox, 1981):

$$MBE = N^{-1} \sum_{i=1}^{N} (P_i - O_i) \tag{4.1}$$

$$S_d^2 = (N-1)^{-1} \sum_{i=1}^{N} (P_i - O_i - MBE)^2 \tag{4.2}$$

$$RMSE = \sqrt{N^{-1} \sum_{i=1}^{N} (P_i - O_i)^2} \tag{4.3}$$

$$MAE = N^{-1} \sum_{i=1}^{N} \left| P_i - O_i)^2 \right| \tag{4.4}$$

where N is the number of cases. With regards to these indices, Willmott (1982) suggested that RMSE and MAE are the best overall measures of all, since they provided enough diagnostic information while MBE and S_d^2 do not. Positive and negative MBE values describes the average model-performance of overestimation and underestimation, respectively. S_d^2 indicates the mean variance to MBE, form which the degree of disperse is also indicated. Willmott (1982) mentioned that MAE is less sensitive to extreme values than RMSE since it avoids the exponentiation. Willmott and Matsuura (2005) further recommended that dimensioned evaluations and inter-comparisons of average model-performance error should be based on MAE since RMSE is unambiguous. To date, RMSE and MAE have been widely used for model performance evaluation in publications to describe the mean differences in the same units of P and O.

4.2.2 Correlation measures

The correlation measures have been frequently used in model performance evaluation but they have often been questioned. The correlation measures quantitatively estimated the association or agreement between two variables while the difference measures estimate the size of differences (Fox, 1981). The r and R^2 are commonly used correlation measures. r describes the linear relationship between two variables. It ranges from -1 to 1. A value of 0 indicates that there is no linear association between two variables while $r = -1 \text{or} 1$ indicates that simulations are perfect linearly (negative or positive) correlated to the observations. The coefficient of determination R^2, which is the square of Pearson's correlation coefficient, describes the proportion of the variance in observed data explained by the model. The value of R^2 ranges from 0 to 1, the higher value the less error variance indicated. The r and R^2 are

calculated as:

$$R^2 = (r)^2 = \left(\frac{\sum_{i=1}^{N}(P_i - \bar{P})(O_i - \bar{O})}{\sqrt{\sum_{i=1}^{N}(P_i - \bar{P})^2}\sqrt{\sum_{i=1}^{N}(O_i - \bar{O})^2}}\right)^2 \tag{4.5}$$

where $\bar{P}$ and $\bar{O}$ are mean values of P and O , respectively. Fox (1981) suggested using r in model performance evaluation at the scales of time, space, and time and space combined. Nonetheless, r and R^2 have been subsequently considered as inappropriate measures in several publications (Krause et al., 2005; Legates and McCabe, 1999; Willmott, 1982), since these statistics are oversensitive to high extreme values and insensitive to additive and proportional differences between simulations and observations.

4.2.3 Index of agreement

In order to overcome the less interpretation of r and R^2 in distinguishing the pair-wised P and O, Willmott (1981) proposed the d to describe the relative differences between these two variables. The index d is dimensionless and calculated as (Willmott, 1981):

$$d = 1 - \frac{\sum_{i=1}^{N}(P_i - O_i)^2}{\sum_{i=1}^{N}(\left|P_i - \bar{O}\right| + \left|O_i - \bar{O}\right|)^2} = 1 - N \cdot \frac{MSE}{PE} \tag{4.6}$$

with $\left|P_i - \bar{O}\right| + \left|O_i - \bar{O}\right|)^2$ indicates the total potential errors variance (PE) of both P and O ($0 \leq MSE \leq N^{-1} \cdot PE$ (Willmott, 1982). The index of agreement d ranges from 0 to 1 that indicates the residual ratio of error $(P_i - O_i)^2$ to PE. The computed d with a value of 0 represents a totally disagreement of P and O while $d = 1$ indicates that a perfect agreement. It represents a decided improvement over r and R^2 but also be sensitive to extreme values, owing to the squared difference.

Legates and McCabe (1999) suggested an adjusted d_1 in order to reduce the effect of squared terms. The modified index of agreement is formed as:

$$d_1 = 1 - \frac{\sum_{i=1}^{N}|P_i - O_i|}{\sum_{i=1}^{N}(\left|P_i - \bar{O}\right| + \left|O_i - \bar{O}\right|)} = 1 - N \cdot \frac{MAE}{PE} \tag{4.7}$$

4.2.4 Nash-Sutcliffe efficiency

The Nash-Sutcliffe efficiency (NSE) is proposed by Nash and Sutcliffe (1970) and indicates the simulation ability of a hydrological model by contrasting the simulation to the paired observed data - how well the observations versus simulations fit to the 1:1 line. NSE is also

dimensionless and describes the relative error between P and O. It is computed as:

$$E = 1 - \frac{\sum_{i=1}^{N}(P_i - O_i)^2}{\sum_{i=1}^{N}(O_i - \bar{O})^2} = 1 - \frac{N \cdot RMSE^2}{N \cdot \sigma_O^2} = 1 - (\frac{RMSE}{\sigma_O})^2 \tag{4.8}$$

with σ_O is the standard deviation of observation, $\sigma_O = \sqrt{\sum_{i=1}^{N}(O_i - \bar{O})^2}$. NSE indicates the normalized ratio of residual variance ("noise", $(P_i - O_i)^2$) to the observation variance ($(O_i - \bar{O})^2$). NSE ranges between $-\infty$ and 1. Model performance with E value between 0 and 1 are considered acceptable. Less error between P and O always leads to higher E and better model-performance. It is notable that NSE with a negative value indicates bad model performance that is not even better than the mean value of observed variable.

Legates and McCabe (1999) suggested an adjusted Nash-Sutcliffe efficiency E_1 in order to reduce the effect of squared terms. The modified E_1 is formed as:

$$E_1 = 1 - \frac{\sum_{i=1}^{N}|P_i - O_i|}{\sum_{i=1}^{N}|O_i - \bar{O}|} = 1 - \frac{N \cdot MAE}{N \cdot MAD_O} = 1 - \frac{MAE}{MAD_O} \tag{4.9}$$

with MAD_O is the mean absolute deviation of observation.

4.2.5 Percent bias

Percent bias (PBIAS) indicates the average tendency of model simulations in contrast to the corresponding observations in percentage. The optimal PBIAS value is 0, the more PBIAS approaches to 0, the less error between P and O it indicates. Positive value expresses overestimation model behavior while negative value means underestimation (Gupta et al., 1999). It is calculated as:

$$PBIAS = \frac{\sum_{i=1}^{N}(P_i - O_i)}{\sum_{i=1}^{N} O_i} \cdot 100 = \frac{N \cdot MBE}{N \cdot \bar{O}} \cdot 100 = \frac{MBE}{\bar{O}} \cdot 100 \tag{4.10}$$

PBIAS is derived as the ratio between MBE and average O ($\bar{O}$). PBIAS is recommended to evaluate watershed models as long as the measured data uncertainty has been considered (Moriasi et al., 2007).

4.2.6 RMSE-observations standard deviation ratio

RMSE-observations standard deviation ratio (RSR) is also recommended by Moriasi et al. (2007) in model performance evaluation. It is calculated as the ratio between RMSE and standard deviation of measured data, it was formulated as below:

$$RSR = \frac{\sqrt{\sum_{i=1}^{N}(P_i - O_i)^2}}{\sqrt{\sum_{i=1}^{N}(O_i - \bar{O}_i)^2}} = \frac{RMSE}{\sigma_O} \tag{4.11}$$

where lower RSR value indicates a better model performance.

Likewise, the MAE-observations standard deviation ratio (MSR) is modified to overcome the sensitivity to extremely values. The modified index can be denote as MAE-observations standard deviation ratio, which is written as:

$$MSR = \frac{\sum_{i=1}^{N}|P_i - O_i|}{\sum_{i=1}^{N}|O_i - \bar{O}_i|} = \frac{MAE}{\sigma_O^2} \tag{4.12}$$

4.3 Results and discussion

4.3.1 Graphical overview of model performance

In Figure 4.1, the spatial and temporal distribution of daily ETA (in mm) on 5 separate sample dates (May 15, 2000, July 05, 2001, and July 19, August 04, and September 21, in 2003) are shown with boxplots. Two sources of pair-wise data sets are included: the model-simulated ETA and the corresponding remote sensing-based observations, LE. Each data group consists of 5 sample days' daily data. In WaSiM-ETH, for each forest type, 12 representative groups of ETA were generated from 12 different surface resistance combinations. These surface resistance combinations were selected by experiences. For deciduous forest, they are denoted as: 80_200, 100_200, 100_500, 100_1500, 150_250, 150_300, 150_400, 150_1000, 200_300, 200_1000, 200_1500, 300_600, with the first number in front of the underline represents the canopy surface resistance r_{sc} (in $\mathrm{s\,m^{-1}}$) and the second number followed the underline represents the soil surface resistance r_{se} (in $\mathrm{s\,m^{-1}}$). For coniferous forest, the selected 12 surface resistance combinations are: 160_300, 160_500, 240_300, 240_1000, 300_600, 300_650, 300_750, 320_1000, 320_1500, 350_600, 350_750, 400_750. In the following text, each 5-day ETA group simulated by the specific surface resistance combination is denoted by " ETA + resistance combination" (e.g. ETA set simulated by surface resistance combination 80_200 is denoted by " ETA 80_200").

For both forest types, the 5-day LE groups show similar features in the variation trend over time (Figure 4.1). The daily regional (indicated the entire Nahe catchment) median values of LE are sorted as: July 05, 2001 > July 19, 2003 > May 15, 2000 > August 04, 2003 > September 21, 2003. In addition, the significant decline of LE amount from July 19 to August 04 in 2003 should be noted. Under well-watered conditions, the ET amount always reaches its annual top in the summer due to the abundant sunshine radiation, high air temperature, dry air humidity, and frequent rainfall in the season. However, LE on August 04, 2003 was abnormally low, whose basic meteorological variables such as the relative sunshine duration (SSD, dimensionless), the air temperature (T, in ^oC), the relative humidity (RH, dimensionless) were inconsistent with the common case in summer (Figure 1.7). It is attributed to the extreme climate condition of the summer of 2003, which was very warm and dry (introduced in Chapter 1) - rare precipitation resulted in less soil water content and thereby more amount was reduced from ETP to ETA.

In Table 4.1, the detailed regional mean and median values of LE are listed. It is shown that there is no large difference between the daily mean and median value of LE for each date, which indicates that LE_i (i denotes the pixel index within an daily LE grid data, $i = 0, 1, 2, ...$) are evenly distributed in their value ranges and there are few extreme values (otherwise it would lead the mean value far away form the median value). This spatial pattern of LE is attributed to its high spatial accuracy. It is also found that on three dates of 2003, LE of the coniferous forest were a little higher than that of the deciduous forest on the same dates. It is supposed due to the better drought-endurance of the coniferous forest.

In contrast to daily LE, the distribution of ETA in deciduous forest shows features that (Figure 4.1a): (1) major ETA_i (i denotes the pixel index within an daily ETA grid data, $i = 0, 1, 2, ...$) spread in the area closing to the minimal value of its range on May 15, 2000. The significant variation between its median and mean differs from the corresponding LE_i distribution. On the other four dates for each surface resistance, the daily medians of ETA also exhibit different degrees of variation from their mean values. For the ETA data sets, the median values are more representative than the means in describing the daily spatial distribution, since the median is insensitive to the outliers and represents the behaviours of major LE_i; (2) For LE, the LE_i on September 21, 2003 are in the most compact value range while on July 19, 2003, the LE_i are the most widely scattered, which can be quantified by their mean standard deviation. For ETA, it is noted that on July 19, 2003, for some resistance combinations, the ETA_i are significantly widely scattered. In Figure 4.1b for coniferous forest, similar spatial features to those for deciduous forest are shown. These spatial features are attributed to the simulation accuracy of the WaSiM-ETH model at the spatial scale. Unlike LE, ETA is simulated on the basis of the ground measurements, therefore

its spatial accuracy depends on the density of climate station network as well as the accuracy of collected meteorological data.

To select the ETA sets with the similar variation trend over time to LE, two important criteria should be met based on the median values of ETA: (1) sorted the 5-day ETA rates as: July 05, 2001 > July 19, 2003 > May 15, 2000 > August 04, 2003 > September 21, 2003; (2) included the extreme event that the significant decline of ETA rates between July 19, 2003 and August 04, 2003. For deciduous forest, it is found that two ETA sets with the surface resistance combinations that r_{sc} at 150 $\mathrm{s\,m^{-1}}$, r_{se} at 250 $\mathrm{s\,m^{-1}}$ (denoted by surface resistance combination 150_250) as well as r_{sc} at 150 $\mathrm{s\,m^{-1}}$, r_{se} at 300 $\mathrm{s\,m^{-1}}$ (denoted by surface resistance combination 150_300) virtually exhibit similar variation features over time to LE. In the coniferous forest (Figure 4.1b), ETA 300_600 set, ETA 300_650 set, ETA 300_750 set and ETA 350_600 set are found to match the both criteria.

		LE (mm)				
		May15	Jul.05	Jul.19	Aug.04	Sep.21
Deci	mean	3.46	4.07	3.60	1.26	0.80
	median	3.52	4.30	3.88	1.16	0.87
Coni	mean	3.33	4.08	3.78	1.48	0.89
	median	3.38	4.30	4.12	1.48	0.97

Table 4.1 The regional mean and median values of 5-day daily LE (in mm) for deciduous and coniferous forest of the Nahe catchment.

4.3.2 Statistical model performance evaluation

In Section 4.2, a various of commonly used statistical measures were reviewed. Based on the assessment by the graphical means, the statistical measures supply additional information on model performance evaluation. Multiple techniques were suggested to be used for model evaluation (Boyle et al., 2000; Legates and McCabe, 1999; Willmott, 1981). Conventionally, mean values of both simulated and observed variables in the specific time steps have been always used for model performance at the temporal scale evaluation. However, due to the low simulation accuracy of WaSiM-ETH in the spatial scale, it is found that there are significant variations between mean and median values of the daily ET_i (Figure 4.1), and the median values better describe the spatial distribution of the daily ET_i than the corresponding mean values. Thus in this study, to take both spatial and temporal patterns into account, we used the median values of the pairwise ETA and LE over time to calculate the statistical indices

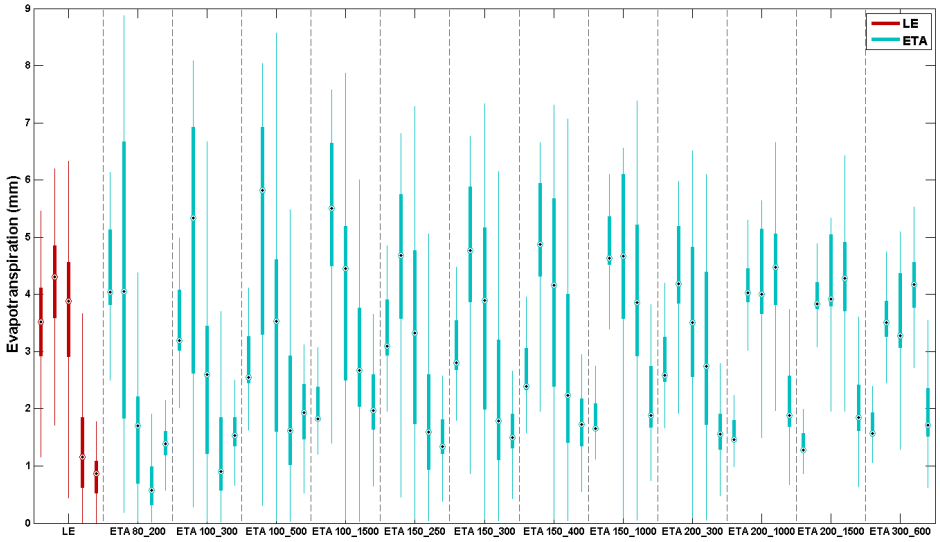

(a) Deciduous forest

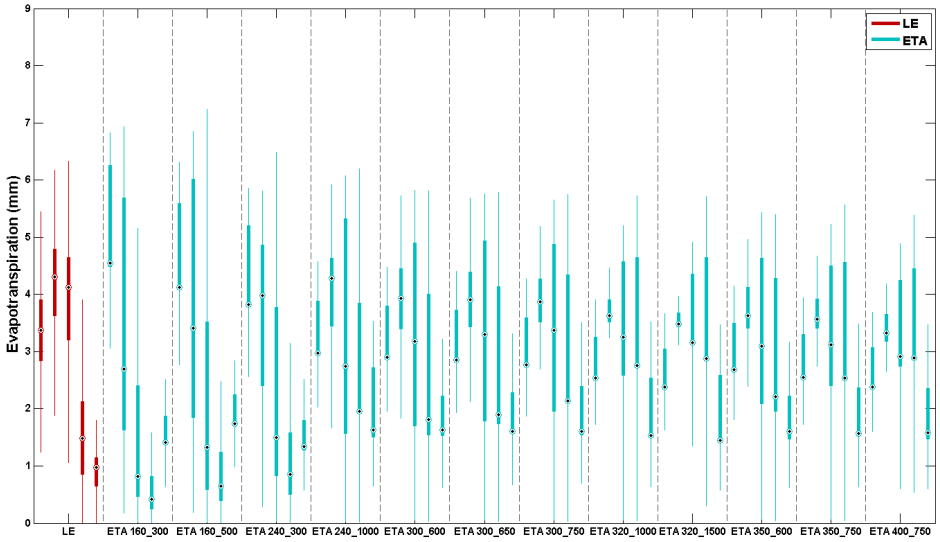

(b) Coniferous forest

Fig. 4.1 Two sources of daily ETA (in mm, with each group consists of 5-sample-day daily values) in the Nahe catchment. The red boxplots are LE group as well as the 12 green boxplot groups are ETA groups simulated with 12 different surface resistance combinations by WaSiM-ETH.

for model performance evaluation. All the values for both forest types are listed in Table 4.2 and 4.3.

In Table 4.2, except for the bias error indices, MBE and PBIAS, the optimal values of all statistical measures consistently point out that the ET 150_250 set exhibits the best model performance of all for the deciduous forest. Based on a variety of previous studies, Moriasi et al. (2007) proposed a general performance rating criteria in terms of NSE, RSR and PBIAS in a monthly time step for streamflow (Table 4.4). In the WaSiM-ETH manual (Schulla and Jasper, 2007), NSE has also been recommended for model evaluation between simulated and observed data. Due to the lack of systematic studies on model evaluation in a daily time step for ETA simulation, this rating criteria was used in this study as a most reliable reference. ETA 150_250 set with values of NSE, RSR and PBIAS at 0.90, 0.32 and 2.26 %, respectively, is considered as "very good" in the model performance. Moreover, R^2 for ETA 150_250 is more than 0.9, which is also much higher than the commonly considered acceptable value 0.5 (Santhi et al., 2001; Van Liew et al., 2003). It is noted that the value of MAE, and the modified statistical indices, E_1, d_1 and MSR, show slightly less agreements on the model performance in contrast to their corresponding indices RMSE, E, d and RSR, respectively. It is because of the characteristics of the observations that are in a limited number but representative for multiple climate conditions (Legates and McCabe, 1999; Willmott, 1982; Willmott and Matsuura, 2005), which requires the statistical indices to be sensitive to the extreme values (wet and dry).

For coniferous forest (Table 4.3), ETA 300_600 and ETA 300_650 exhibit approximate simulation ability at the temporal scale, with the identical MAE, d_1, d, E_1 and MSR values. Focusing on the general recommended indices, NSE, RSR and PBIAS, ETA 300_650 is evaluated as the optimal as well as is rated as "Very good" ($E = 0.81$, $RSR = 0.42$ and $PBIAS = -4.77$ %). Comparing statistics for both forest types, MBE, S_d^2, RMSE, d_2, NSE, PBIAS and RSR consistently point out that the simulations in deciduous forest perform a little better than in coniferous forest. However, a completely opposite conclusion is drawn in terms of R^2. It is attributed to the disadvantage of R^2 that it is oversensitive to the outliers and insensitive to the proportional differences (Legates and McCabe, 1999). Thereby, for model performance evaluation in the daily time step for ETA simulation, MBE, S_d^2, RMSE, d, E, PBIAS and RSR are considered as appropriate statistical indices to provide additional information to the boxplots. The surface resistances were calibrated as $r_{sc} = 150\ \mathrm{s\,m^{-1}}$, $r_{se} = 250\ \mathrm{s\,m^{-1}}$ in the deciduous forest as well as $r_{sc} = 300\ \mathrm{s\,m^{-1}}$, $r_{se} = 650\ \mathrm{s\,m^{-1}}$ in the coniferous forest.

	MBE	S_d^2	MAE	RMSE	R^2	d_1	d	E_1	E	PBIAS	MSR	RSR
80_200	-0.40	1.22	0.81	1.07	0.58	0.71	0.86	0.42	0.45	-14.57	0.39	0.74
100_300	-0.04	0.83	0.71	0.81	0.73	0.73	0.92	0.49	0.68	-1.31	0.34	0.57
100_500	0.34	1.02	0.87	0.97	0.66	0.67	0.89	0.37	0.55	12.45	0.42	0.67
100_1500	0.54	1.66	1.21	1.27	0.46	0.54	0.79	0.12	0.22	19.52	0.59	0.88
150_250	0.06	0.25	0.45	0.45	0.91	0.82	0.97	0.68	0.90	2.26	0.22	0.32
150_300	0.21	0.32	0.49	0.55	0.88	0.80	0.96	0.65	0.85	7.50	0.24	0.38
150_400	0.33	0.75	0.78	0.84	0.71	0.68	0.90	0.44	0.66	12.09	0.38	0.59
150_1000	0.59	2.68	1.34	1.58	0.19	0.52	0.68	0.04	-0.21	21.56	0.65	1.05
200_300	0.17	0.96	0.74	0.89	0.67	0.65	0.84	0.47	0.61	6.05	0.36	0.62
200_1000	0.42	3.87	1.36	1.81	0.02	0.49	0.55	0.02	-0.59	15.44	0.66	1.26
200_1500	0.28	3.88	1.37	1.78	0.02	0.48	0.54	0.01	-0.54	10.27	0.66	1.24
300_600	0.10	3.65	1.44	1.71	0.01	0.39	0.50	-0.04	-0.42	3.71	0.70	1.19

Table 4.2 Statistical indices for model evaluation at temporal scale between regional median ETA and LE on 5 sample dates in deciduous forest of the Nahe catchment.

	MBE	S_d^2	MAE	RMSE	R^2	d_1	d	E_1	E	PBIAS	MSR	RSR
160_300	-0.87	3.09	1.52	1.80	0.16	0.47	0.63	-0.17	-0.72	-30.60	0.81	1.31
160_500	-0.60	2.15	1.20	1.44	0.27	0.54	0.72	0.07	-0.11	-21.05	0.64	1.05
240_300	-0.55	1.55	0.88	1.24	0.44	0.67	0.80	0.33	0.18	-19.23	0.47	0.90
240_1000	-0.13	0.66	0.59	0.74	0.76	0.71	0.89	0.55	0.71	-4.63	0.31	0.54
300_600	-0.16	0.42	0.56	0.60	0.94	0.73	0.93	0.57	0.81	-5.68	0.30	0.44
300_650	-0.14	0.39	0.56	0.58	0.96	0.71	0.93	0.57	0.82	-4.77	0.30	0.42
300_750	-0.10	0.48	0.62	0.63	0.94	0.69	0.92	0.53	0.79	-3.37	0.33	0.46
320_1000	-0.11	0.95	0.84	0.88	0.69	0.55	0.82	0.35	0.59	-3.93	0.45	0.64
320_1500	-0.18	1.15	0.93	0.98	0.57	0.50	0.77	0.28	0.49	-6.25	0.49	0.71
350_600	-0.20	0.68	0.75	0.77	0.91	0.61	0.86	0.42	0.69	-7.16	0.40	0.56
350_750	-0.18	0.89	0.85	0.86	0.78	0.55	0.82	0.35	0.60	-6.39	0.45	0.63
400_750	-0.23	1.37	1.04	1.07	0.48	0.41	0.69	0.20	0.39	-8.07	0.55	0.78

Table 4.3 Statistical indices for model evaluation at temporal scale between regional median ETA and LE on 5 sample dates in coniferous forest of the Nahe catchment.

Performance Rating	RSR	NSE	PBIAS %
Very good	$0.00 \leq RSR \leq 0.50$	$0.75 < NSE \leq 1.00$	$PBIAS < \pm 10$
Good	$0.50 \leq RSR \leq 0.60$	$0.65 < NSE \leq 0.75$	$\pm 10 \leq PBIAS < \pm 15$
Satisfactory	$0.60 \leq RSR \leq 0.70$	$0.50 < NSE \leq 0.65$	$\pm 15 \leq PBIAS < \pm 25$
Unsatisfactory	$RSR > 0.70$	$NSE \leq 0.50$	$PBIAS \geq \pm 25$

Table 4.4 General performance ratings for recommended statistics for a monthly time step (Moriasi et al., 2007).

4.3.3 Model evaluation at space scale

An apparent advantage for the remote sensing-based observations used in this study is the relatively higher spatial accuracy than the model outputs. Actually, ETA and LE are two sources of actual ET rates that generated by different estimation techniques and with different basic materials. ETA was simulated based on the interpolated meteorological data sets, the spatial accuracy of which depends on the locations and the numbers of available climate stations. LE was retrieved by Landsat images, whose spatial resolution is 30 m for visible and NIR bands as well as it is respectively 120 m and 60 m for the TIR band of TM and ETM+. Their spatial differences are shown in the frequency distribution of daily ETA and LE (Figure 4.2 and 4.3). It is obviously that the most spatial difference between daily ETA and LE is the continuity of distribution - for each day, LE_i are always continuous distributed while ETA_i are not, especially in the coniferous forest (Figure 4.31). In order to investigate the detailed model performance in the spatial scale, the statistical indices related to errors such as mean bias error MBE, mean variance of error distribution S_d^2 and MAE were employed. RMSE was not taken into account since it is more sensitive to the outliers than MAE (Willmott, 1982; Willmott and Matsuura, 2005). Unlike the evaluation index requirement in the temporary scale, the measures that be less affected by outliers are appropriate in spatial pattern evaluation. In Figure 4.4, the distributions of errors between daily ET and LE are shown, with the dash lines indicate MBE and $MBE \pm S_d^2$. MBE indicates the bias of error as well as the S_d^2 indicates the deviation degree of all errors to the mean bias. It is shown that less MBE and S_d^2 leads to a better MAE, which is recommended to be the best overall measures similar to RMSE that provides enough diagnose information containing both MBE and S_d^2 (Willmott, 1982). Therefore, an ideal error distribution between ET and LE is expected to approximate to the normal distribution, with $MBE = 0$, S_d^2 values as small as possible and consequently low MAE. Therefore MAE is considered as appropriate measure for model evaluation at the spatial scale.

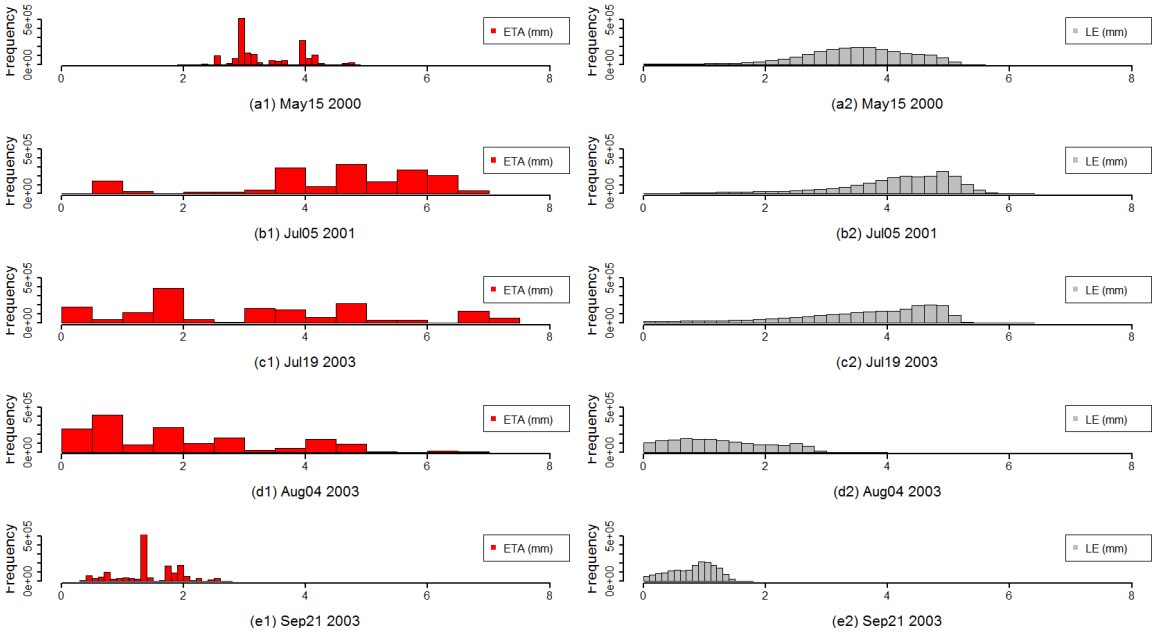

Fig. 4.2 Frequency distribution of daily (1) ETA 150_250 and (2) LE (both in mm) on 5 sample dates (a-e) in deciduous forest of the Nahe catchment.

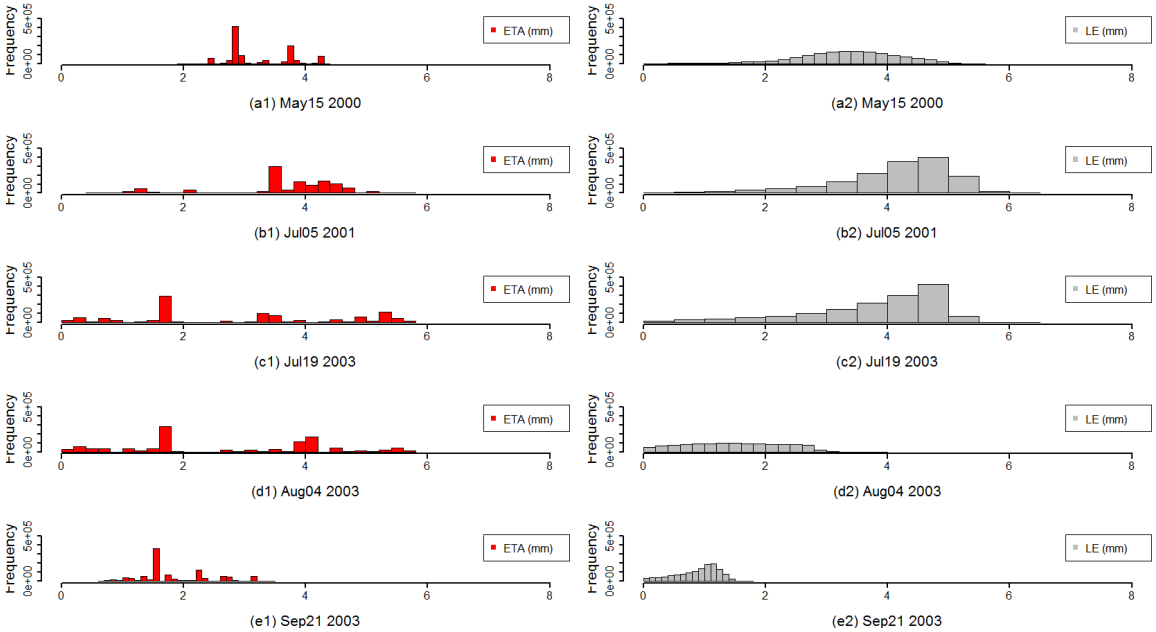

Fig. 4.3 Frequency distribution of daily (1) ETA 300_650 and (2) LE (both in mm) on 5 sample dates (a-e) in coniferous forest of the Nahe catchment .

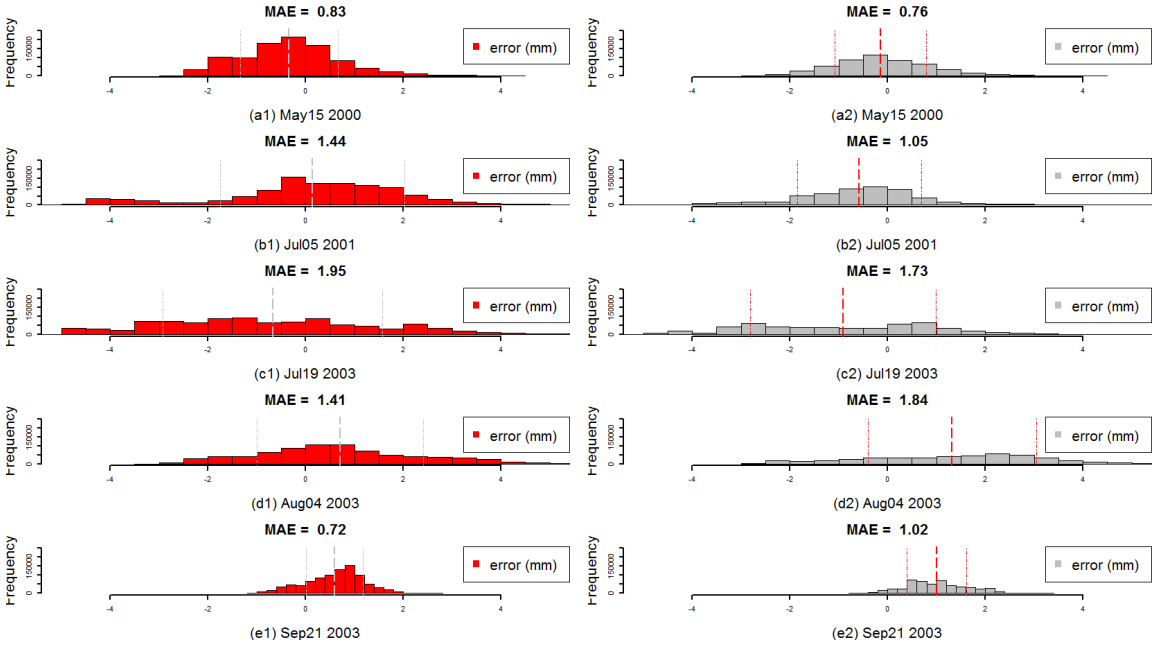

Fig. 4.4 Frequency distribution of difference (error, in mm) between (1) ETA 150_250 and LE in deciduous forest and (2) ETA 300_650 and LE in coniferous forest of the Nahe catchment on 5 sample dates (a-e).

To take both the temporal pattern and the detailed spatial pattern into account for model performance evaluation, we calculated the MAE between daily ETA and LE on 5 sample dates and plotted them over time (Figure 4.5). For deciduous forest, both ETA 150_250, ETA 150_300 exhibit relatively better overall model performance than ETA simulated with other surface resistance combinations – the MAE of five days are all in relatively small ranges (below the horizontal dash line, Figure 4.5a). Likewise, ETA 300_600 and ETA 300_650 show better overall model performance in time scale for coniferous forest (Figure 4.5b). In terms of the temporal and high-accuracy spatial information, ETA 150_250 and ETA 300_650 are confirmed as the optimal simulations for deciduous and coniferous forest, respectively. Therefore, for model performance evaluation at the temporal-spatial scale, using the median value of daily ETA to replace its daily spatial pattern is feasible.

4.4 Conclusion

In the WaSiM-ETH model, the meteorological variables - solar radiation, air temperature, air humidity, wind speed and precipitation as well as the property parameters - aerodynamic resistance and surface resistance are important input for ETA estimation. Especially in the forest regions, the surface resistance played a leading role in affecting ETA compared to the

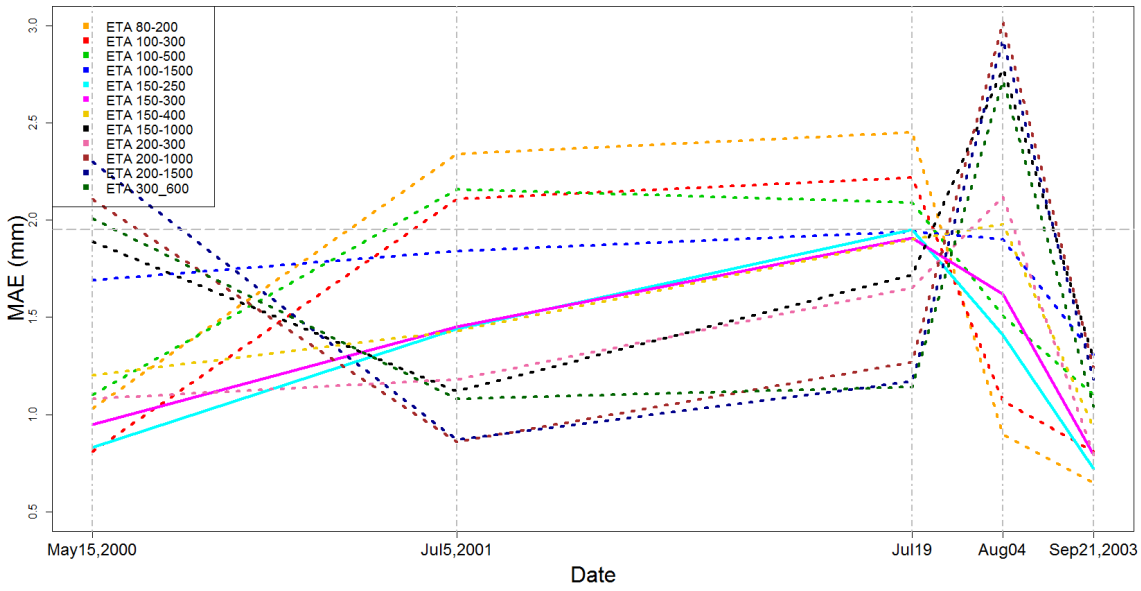

(a) Deciduous forest

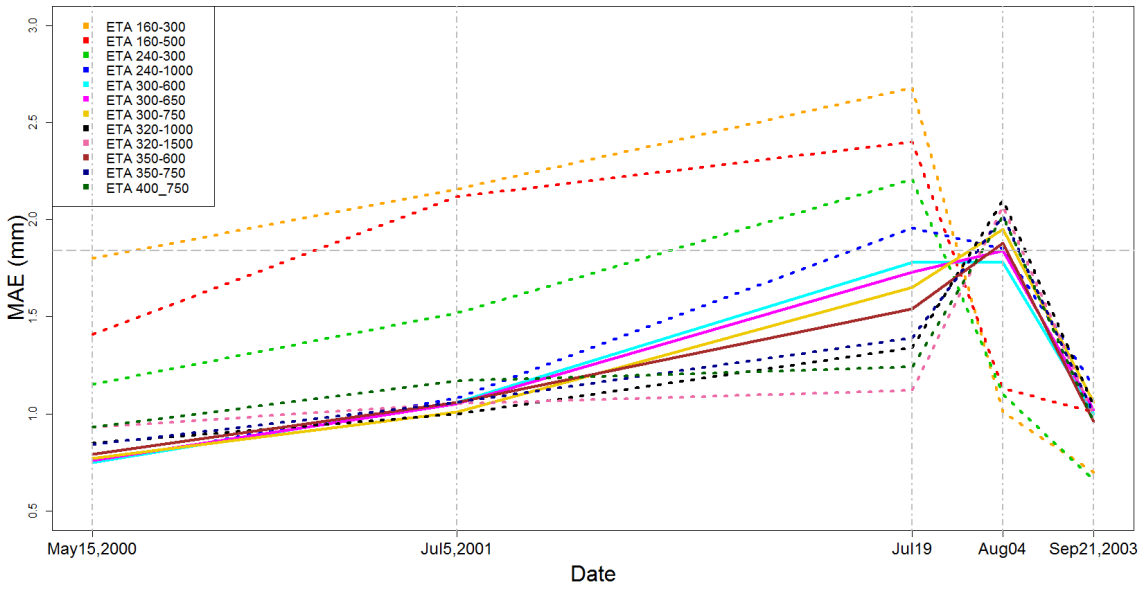

(b) Coniferous forest

Fig. 4.5 Five days' MAE (mean absolute error) between ETA (simulated from 12 surface resistance combinations) and LE in the Nahe catchment.

aerodynamic resistance as well as the meteorological variables (Beven, 1979). Moreover, in WaSiM-ETH, the aerodynamic resistance is calculated by a function of wind speed for high crop surface (e.g. forest). Thus, surface resistance is the sole and most significant parameter and was calibrated in this study. The calibrated surface resistance included two parameters - the canopy surface resistance r_{sc} and the soil surface resistance r_{se}, which correspond to the transpiration of plants and the evaporation of soil, respectively. The simulated and observed data are ETA simulated by the WaSiM-ETH model and LE retrieved from remote sensing images on five sample dates. With regard to the observations, low accuracy at temporal scale is the biggest problem while processing model evaluation and calibration. However, the weather conditions on the sample dates contained multiple events such as wet, medium wet and dry were expected to fill in the gaps. On August 04, 2003, the abnormal low ETA in summertime was also considered as significant extreme event.

As multiple evaluation techniques were suggested for model performance evaluation (Boyle et al., 2000; Legates and McCabe, 1999; Willmott, 1981), graphical and statistical techniques were used in this study. Boxplots indicated the model performance at both spatial and temporal scales well. ETA 150_250 and ETA 150_300 for deciduous and ETA 300_600, ETA 300_650, ETA 300_750 and ETA 350_600 were found to graphically exhibit similar spatial and temporal patterns to the corresponding daily LE for 5 sample days. The regional median value was more appropriate than the mean value to represent the spatial pattern of daily ET due to the relatively low simulation accuracy of WaSiM-ETH in spatial scale. An important statistical evaluation reference is the general satisfied model performance criterion proposed by Moriasi et al. (2007) - $NSE > 0.5$, $RSR \leq 0.7$ and $PBIAS < \pm 25$ %. NSE was considered as the most important statistical index since it is also recommended in WaSiM-ETH manual. Met the requirement that be sensitive to the extreme values, the statistical indices such as MBE, S_d^2, RMSE, d, NSE, PBIAS and RSR were considered as appropriate measures to provide additional information to the boxplots.

Due to the high accuracy of remote sensing based LE in spatial pattern, model performance evaluation was also carried out in spatial scale. The spatial accuracy of ET was relatively low and depended on the density of climate station networks. Moreover, the appropriate statistical index for spatial pattern evaluation between daily ET and LE was MAE. MAE was found as good overall indicator that provide enough information containing mean bias error and standard deviation, and insensitive to the extreme values in contrast to RMSE. It is shown that the daily median value of ETA simply represents its spatial distribution and is recommended to be employed in model evaluation in time series.

Chapter 5

Sensitivity analysis

5.1 Introduction

Sensitivity analysis is useful in all phases of modelling a physical hydrological cycle system: model formulation, model calibration and model validation, with the definition of the sensitivity is a measure of the effect of changes in one factor on another factor (McCuen, 1973). To understand parameters through sensitivity analysis, especially their relative roles in the model, is a good preparation to understand the characteristics of a mathematical equation or a model (Saxton, 1975). Sensitivity analysis is conducted to answer the following questions: (1) which parameters significantly impact the model outputs and should be paid more attention to; (2) which parameters are insignificant and can be eliminated in the modelling process; (3) which input components contribute the most to the variations of model outputs; (4) which parameters are the most highly correlated with the model outputs; (5) what consequence would be if changing an input parameter (Hamby, 1994). By focusing on those significant factors that a model is most sensitive to, the future studies, e.g., model calibration and validation, can be simplified and accelerated. A distinction between "sensitive" and "important" parameters was introduced by Crick and Hill (1987) – the sensitive parameters significantly affect the model outputs and the important parameters substantially contribute to the uncertainties of model outputs. The former is related to the parameter sensitivity analysis and the latter is related to the parameter uncertainty analysis. An important parameter is always sensitive whereas a sensitive parameter may not be important if it has been well calibrated thereby contributes very little to the uncertainties in model outputs (Hamby, 1994).

There are a variety of parameter sensitivity analysis methods and the direct method is the fundamental of them all. It is also referred to as the differential analysis, with which a direct investigation of the variances between the model outputs and the base case is conducted. The simplest method for the sensitivity analysis is to perturb one parameter at a time while

keeping the other parameters in constant. The method is also termed as the "one-at-a-time" method.

The Penman-Monteith equation (Monteith et al., 1965) is the most frequently used and recommended approach for evapotranspiration (ET) estimation (Allen et al., 1989, 1998; Droogers and Allen, 2002). Several components are employed in this equation: (1) the surface energy balance components – the net radiation (R_n), the sensible heat flux (H), the soil heat flux (G) and the latent heat flux (LE); (2) the ground-measured meteorological variables – the sunshine duration, the air temperature, the vapor pressure and the wind speed; (3) the atmospheric factors – the phychrometric constant, the dry air density and the specific heat capacity of the dry air; (4) the resistance parameters – the bulk surface resistance and the aerodynamic resistance. A successful modelling of the Penman-Monteith ET is very dependent on the aerodynamic resistance and the canopy resistance (Beven, 1979; Rana and Katerji, 1998). The aerodynamic resistance is related to the transfer of heat and water vapor from the evaporating surfaces into the air above. The bulk surface resistance describes the resistant ability of the vapor diffusion from the surfaces while transpiring and evaporating. Beven (1979) found that in a broadly humid temperate forested region, the Penman-Monteith actual evapotranspiration (ETA) was highly sensitive to the canopy resistance, with the diurnal and monthly relative sensitivity coefficient S_r uniformly approximated to -1, whereas the relative importance of the aerodynamic resistance remained very small. In a study under the semi-arid climate conditions, Rana and Katerji (1998) found that: (1) for well-watered short crops, the aerodynamic resistance played a leading role for influencing the Penman-Monteith ETA estimation while canopy resistance played a secondary role; (2) for water stressed tall crops, the canopy resistance was the most important parameter that should be precisely modelled with considering the climatic, canopy and soil water features, since it leaded to the major relative errors. Moreover, in the WaSiM-ETH model, for tall crops higher than 2 m, the aerodynamic resistance is a function of the wind speed.

ET is also very dependent on the meteorological variables. The meteorological variables are subject to different sources of errors (Hupet and Vanclooster, 2001). To investigate the error variances associated within ET estimation, Beven (1979) has divided the errors that contributed to a model into four sources: (1) instrument errors, (2) site errors, (3) measurement model errors, (4) modelling errors. The errors in the meteorological variables are found to result in less uncertainties in the estimated evaporation rate by the Penman equation (McCuen, 1974). A series of publications have reported the relative importances of the meteorological variables for ET estimation: Bakhtiari et al. (2012); Beven (1979); Saxton (1975) reported that the net radiation was the most important variable; Gleick (1986); Goyal (2004); McCuen (1974); Piper (1989); Revelle and Waggoner (1983); Samani (2000) reported

that the air temperature was the most important variable; Gong et al. (2006); McCuen (1974) reported that the relative humidity was the most sensitive variable; wind speed or wind profile parameters was reported as the least sensitive variable in publications (Gong et al., 2006; McCuen, 1974; Saxton, 1975).

In this chapter, the parameter sensitivity analysis was conducted for two parameters in the WaSiM-ETH water balance model for each forest type: the canopy surface resistance (r_{sc}) and the soil surface resistance (r_{se}). The purposes of this chapter are: (1) to verify the optimal values of the surface resistance; (2) to verify the previously recommended statistical measures (Chapter 4) for evaluating the model performance; (3) to determine the appropriate range boundaries of r_{sc} and r_{se} for both forest types; (4) to suggest the satisfied value ranges of the recommended statistical indices that concluded in Chapter 4 for model evaluation; (5) to explore the relative importances of r_{sc} and r_{se} in both forest types.

5.2 Method and material

The parametric sensitivity was expressed by a sensitivity coefficient. The sensitivity coefficient is the ratio of the changes in the model outputs to the changes in a parameter, with the other parameters all remain constant (Krieger et al., 1978). There are two forms of the sensitivity coefficient – absolute and relative. The former indicates the magnitude changes of the model outputs resulted from the magnitude changes of the investigated parameter. It is used to compare the sensitivities of the same or similar parameters (e.g. with a same unit), which is written as (McCuen, 1974):

$$S_a = \frac{\partial P_i}{\partial f_i} \tag{5.1}$$

where S_a is the coefficient of the absolute sensitivity; f_i indicates the model input parameters which the hydrologists are interested in and varies in its acceptable value range that always determined by experiences; P_i is the model outputs that corresponded to f_i.

The relative sensitivity coefficient has been frequently used in publications to compare the sensitivity of different parameters in different units and value ranges. It relates the relative changes (in percentage) in the model outputs to the relative changes in the parameters. It is written as (McCuen, 1974):

$$S_r = \frac{\partial P_i}{\partial f_i} \times \frac{f_o}{P_o} \tag{5.2}$$

In the equation, S_r is the dimensionless relative parametric sensitivity, f_o and P_o respectively indicate the optimal values of parameter f and the corresponding output. Usually, f_o is valued

as the mean of its experimental value range. Lenhart et al. (2002) ranked the sensitivity coefficient into four classes: small to negligible, medium, high and very high (Table 5.1).

Class	Index	Sensitivity
I	$0.00 \leq \|I\| < 0.05$	Small to negligible
II	$0.05 \leq \|I\| < 0.20$	Medium
III	$0.20 \leq \|I\| < 1.00$	High
IV	$\|I\| \geq 1.00$	Very High

Table 5.1 Sensitivity classes (Lenhart et al., 2002).

In the WaSiM-ETH manual (Schulla and Jasper, 2007), a one-at-a-time perturbation method was used in the sensitivity analysis of the surface resistance. The canopy surface resistance (r_{sc}) was varied between 25 % and 200 % of its optimal value to study the impact on potential evapotranspiration (ETP), ETA, interception evaporation and runoff. The Nash-Sutcliffe efficiency (NSE) proposed by Nash and Sutcliffe (1970) was employed as the sole statistical index for the model performance evaluation between the modelled and observed runoff data sets. In this chapter, we used a similar one-at-a-time perturbation method on the parameter sensitivity analysis of r_{sc} and r_{se} for both deciduous and coniferous forest. The optimal values were previously determined in Chapter 4: for deciduous forest, $r_{sc} = 150$ $\mathrm{s\,m^{-1}}$, $r_{se} = 250$ $\mathrm{s\,m^{-1}}$; for coniferous forest, $r_{sc} = 300$ $\mathrm{s\,m^{-1}}$, $r_{se} = 650$ $\mathrm{s\,m^{-1}}$. For both forest types, continuous perturbation of ± 25 $\mathrm{s\,m^{-1}}$ for r_{sc} and continuous perturbation of ± 50 $\mathrm{s\,m^{-1}}$ for r_{se} were conducted to find their appropriate upper and lower bounds, until the model performance was considered as unsatisfactory. Paired simulations and observations are still daily ETA and LE (latent heat flux retrieved by remote sensing images, corresponded to the ETA) on 5 sample dates. To evaluate the model performance as well as to determine the appropriate value ranges of r_{sc} and r_{se}, we used the general satisfactory criterion recommended by Moriasi et al. (2007) – $NSE > 0.5, RSR \leq 0.7, PBIAS < \pm 12$ (RSR is the RMSE-observations standard deviation ratio and PBIAS is the percent bias (Moriasi et al., 2007)). Both absolute and relative sensitivity coefficients were subsequently calculated for each resistance.

5.3 Value range determination

As mentioned before, the parameter setting of r_{sc} in the WaSiM-ETH model follows a seasonal variation rule that (Table 2.3): for each forest type, r_{sc} rises to the maximum during November to February and falls down to the the minimum during May to September.

Nonetheless, r_{se} in the model always remains the same for a whole year. In Table 5.2, the estimated appropriate value ranges of r_{sc} and r_{se} for both forest types are listed, with the annual maximal (in November-February) and minimal (in May-September) values. For deciduous forest, the annual maximal acceptable value ranges of r_{sc} and r_{se} are respectively [100,225] and [50,450], as well as for coniferous forest are respectively [225,375] and [350,1200]. It is apparent that in either deciduous or coniferous forest, for a value change in each $\mathrm{s\,m^{-1}}$, r_{sc} results in much more variances in transpiration than r_{se} results in evaporation. It is attributed to that transpiration is always the majority of total ET rate, especially in the forested regions, the ratio of transpiration to ET is in general 80-90 % (Kurpius et al., 2003; Szilagyi, 2000; Wilson et al., 2001).

In Figure 5.1-5.4, the performances of each statistical index with perturbed r_{sc} and r_{se} values are shown. An appropriate statistical index (except for the bias indices, e.g. the mean bias error (MBE) and PBIAS) always points out the best performed model outputs with its maximal or minimal value. For instance, in Figure 5.1, the recommended indices such as NSE, RSR separately exhibit an upside-down "v" and "v" curvilinear trend over the x axis (perturbed r_{sc} values), with their troughs or peaks corresponded to the optimal $r_{sc} = 150$ $\mathrm{s\,m^{-1}}$ (marked with dash lines). Therefore, the mean variance of error distribution (S_d^2), the root mean square error (RMSE) and the index of agreement (d) are considered as appropriate indices due to their "v"-curve performance. As mentioned in Chapter 4, to take full advantage of the multiple climate conditions of the observations such as wet, medium wet and dry, the statistical indices that being sensitive to the extreme values (e.g. the significant low value on August 04, 2003 with compare to the general annual high value in the summer time) were required. As concluded in Chapter 4, the modified NSE ($E1$) that corresponded to NSE (E), the MAE-observations standard deviation ratio (MSR) that corresponded to RSR, the mean absolute error (MAE) that corresponded to RMSE and the modified index of agreement ($d1$) that corresponded to d were considered as the misleading statistics in this study due to their relatively smaller sensitivity to the extreme values than their corresponding indices (Legates and McCabe, 1999; Willmott, 1982; Willmott and Matsuura, 2005). It is also shown that those indices that without an exponential in calculation exhibit apparent misleading in model performance evaluation (e.g. Figure 5.1a v.s. 5.1b, Figure 5.1c v.s. 5.1b). In addition, as a controversial index, R^2 has been repeatedly reported as an inappropriate index in publications (Krause et al., 2005; Legates and McCabe, 1999; Willmott, 1982)), but it still has been frequently used in studies for model performance assessment. In Figure 5.1h, the variation trend of R^2 exhibits disagree with other "appropriate" indices. Therefore it is an unacceptable measure for model evaluation in this study. MBE and PBIAS exhibit similar performances in bias between the simulated and observed data sets. Unlike others, the

bias indices always evaluate model performance within a certain value range. For instance, Moriasi et al. (2007) rated $PBIAS < \pm 25$ % for streamflow, $PBIAS < \pm 55$ for sediment, and $PBIAS < \pm 70$ for nitrogen and phosphorus as satisfactory for model performance evaluation. In this study, in terms of the evaluation performance of the statistical indices for r_{sc} and r_{se} for both forest types, $S_d^2 < 1.11$, $RMSE < 9.97$, $d > 0.79$, $MBE < \pm 0.45$ and $PBIAS < \pm 15$ are recommended as additional evaluation criteria to $NSE > 0.5, RSR \leq 0.7$ for the model performance evaluation.

		lower bound		optimal		upper bound	
		max	min	max	min	max	min
Deci	r_{sc} ($s\,m^{-1}$)	100	65	150	98	225	148
	r_{se} ($s\,m^{-1}$)	50	50	250	250	450	450
Coni	r_{sc} ($s\,m^{-1}$)	225	155	300	206	375	258
	r_{se} ($s\,m^{-1}$)	350	350	650	650	1200	1200

Table 5.2 Estimated value ranges for canopy surface resistance r_{sc} and soil surface resistance r_{se} for deciduous and coniferous forest, "max" indicates the maximal value during wintertime (November-February) and "min" indicates the minimal value in summertime (May-September).

5.4 Sensitivity analysis

5.4.1 Sensitivity of potential evapotranspiration to surface resistance

In Figure 5.5, the fluctuations of the daily relative sensitive coefficient Sr of ETP to r_s are shown. It is obviously that ETP is generally more sensitive to r_{sc} than to r_{se}, especially in the coniferous forest (except for the days during May in the deciduous forest). We infer that the potential transpiration of the plants in forest areas dominates in ETP generation. And it was reported in several studies that the transpiration contributed 80-90 % to ET in the full-canopy regions (Kurpius et al., 2003; Szilagyi, 2000; Wilson et al., 2001). In terms of the grading standard proposed by Lenhart et al. (2002), in deciduous forest, r_{sc} and r_{se} are ranked as high-sensitive parameters ($0.2 \leq Sr < 1$) since their Sr approximately range in [-0.5,-0.3] and [-0.3,-0.2], respectively, whereas in coniferous forest, r_{sc} that ranged in [-0.7,-0.5] plays a relatively more important role than r_{se} ranged in [-0.25,-0.15]. Therefore, an increase of 10 % in r_{sc} leads to a decrease of ETP of 3-5 % and 5-7 % in deciduous and coniferous forest, respectively, and an increase of 10 % in r_{se} leads to a decrease of ETP of

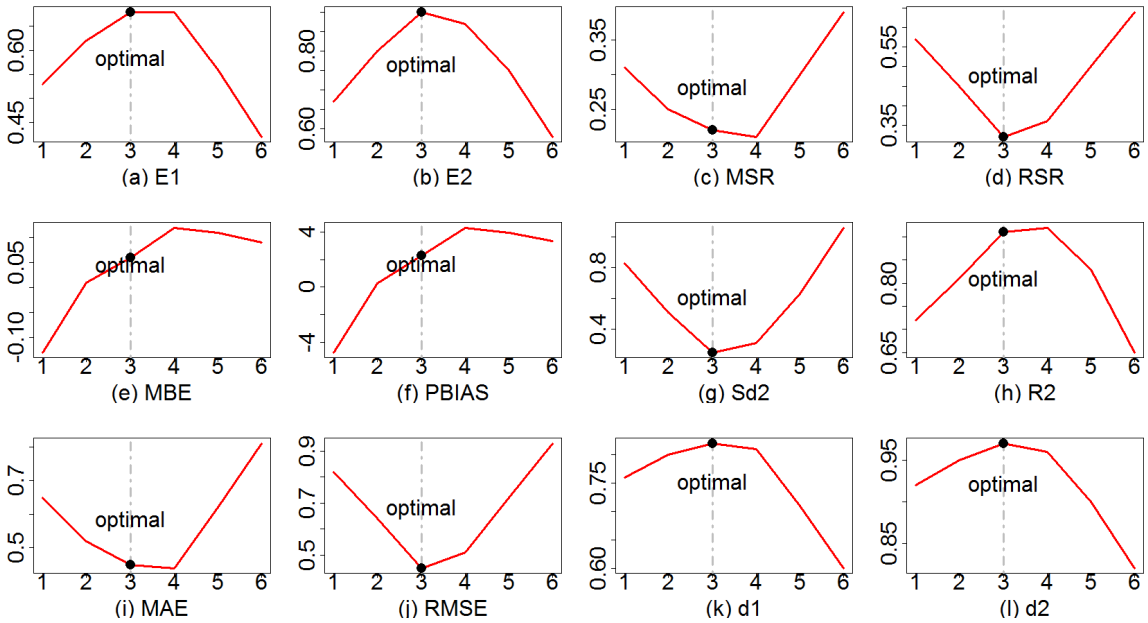

Fig. 5.1 Model performance evaluation between ETA simulated with perturbed r_{sc} values in [100,225] $\mathrm{m\,s^{-1}}$ and LE on 5 sample days at temporal scale for deciduous forest, the x axis indicates the perturbed r_{sc} values.

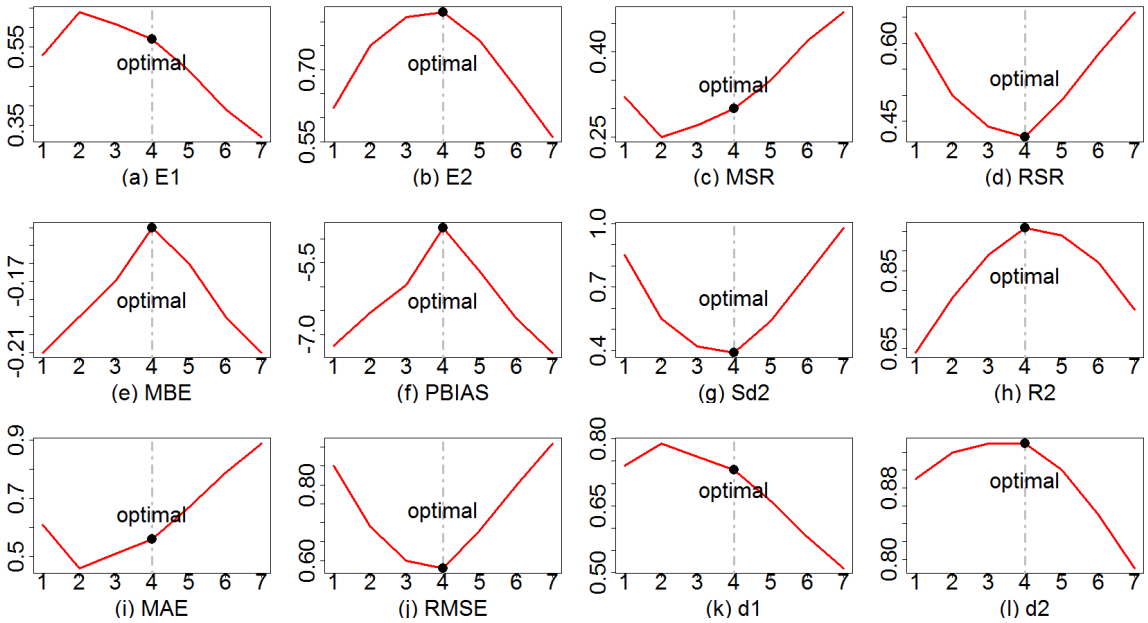

Fig. 5.2 Model performance evaluation between ETA simulated with perturbed r_{se} values in [50,450] $\mathrm{m\,s^{-1}}$ and LE on 5 sample days at temporal scale for deciduous forest, the x axis indicates the perturbed r_{se} values.

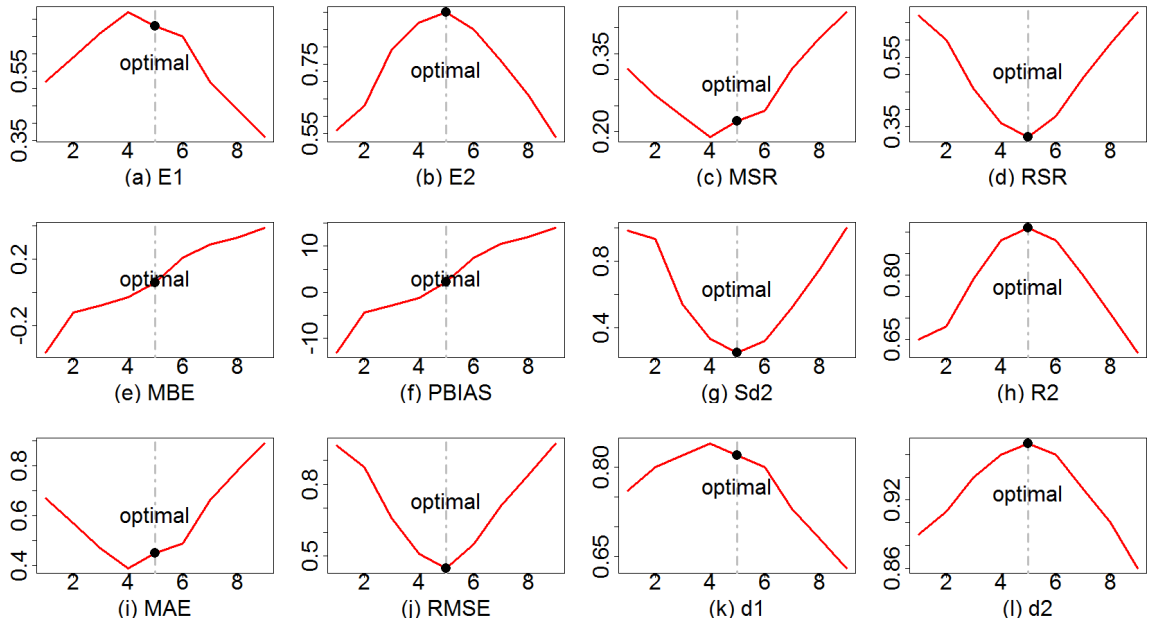

Fig. 5.3 Model performance evaluation between ETA simulated with perturbed r_{sc} values in [225,375] $\mathrm{m\,s^{-1}}$ and LE on 5 sample days at temporal scale for coniferous forest, the x axis indicates the perturbed r_{sc} values.

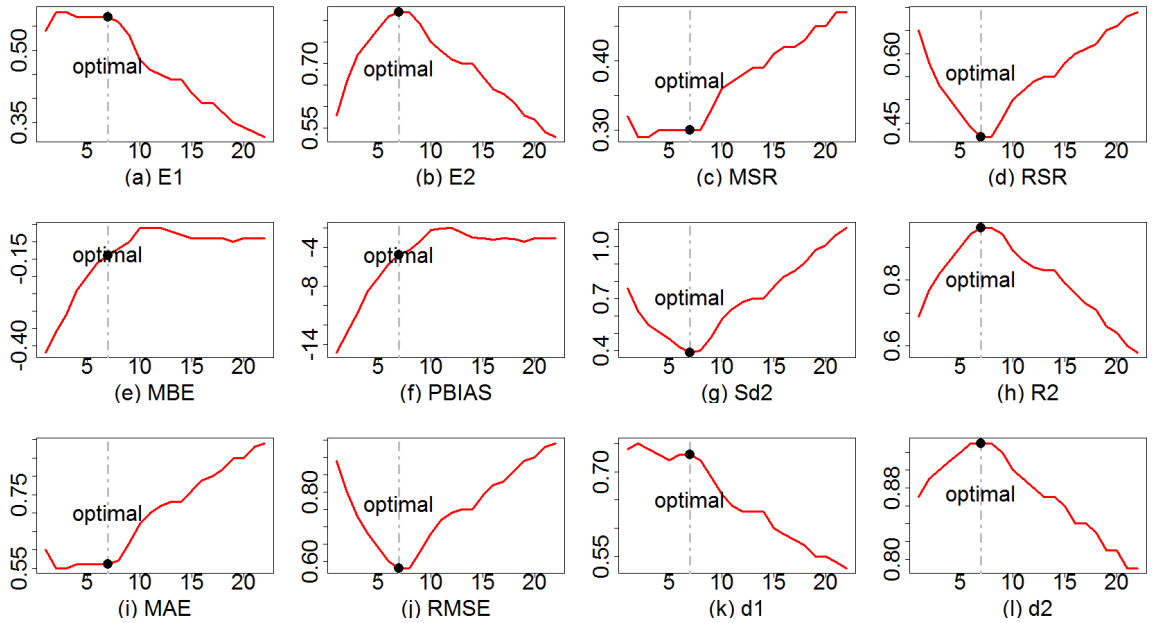

Fig. 5.4 Model performance evaluation between ETA simulated with perturbed r_{se} values in [350,1200] $\mathrm{m\,s^{-1}}$ and LE on 5 sample days at temporal scale for coniferous forest, the x axis indicates the perturbed r_{se} values.

2-3 % and 1.5-2.5 % in deciduous and coniferous forest, respectively. The differences of the relative importances for r_{sc} and r_{se} between deciduous and coniferous forest are due to the ratio of optimal r_s to ETP. The relative coefficient is very dependent on this ratio, and the ratio for each surface resistance and forest type is very different. Assuming the ETP rates for both forests are almost the same due to their similar meteorological variables, r_{sc}/ETP in coniferous forest is more than two times of the ratio in deciduous forest as well as r_{se}/ETP in coniferous forest is also more than two times of the ratio in deciduous forest.

To parallel compare the sensitivities of r_{sc} and r_{se} for both forests, we further studied the absolute responses of ETP to their perturbations. In Figure 5.6, it is apparent that according to an increase of r_{sc} in each $\mathrm{s\,m^{-1}}$, ETP increases much more in the absolute magnitude in the deciduous forest than in the coniferous forest. This agrees with the calibrated canopy surface resistance values of both forests – $r_{sc} = 150\ \mathrm{s\,m^{-1}}$ for deciduous forest and $r_{sc} = 300\ \mathrm{s\,m^{-1}}$ for coniferous forest, which indicate that the resistance of plant canopy while transpiring in coniferous forest are two times of that in deciduous forest. The impact on ETP resulted from r_{se} are relatively small – S_a of r_{se} are about one order smaller than those of r_{sc} (e.g. -0.012 v.s. -0.0017 $\mathrm{s\,m^{-1}}$), in terms of which we confirm the dominated contribution of transpiration in ET. In the S_a curves, the troughs present the most sensitive events (with big negative values). In both forests, the extremely sensitive events (troughs in curves that corresponded to both r_{sc} and r_{se}) occurred in June of 2000, July of 2001 as well as July and August of 2003. In 2003, more significant seasonal variability in deciduous forest exhibit than in coniferous forest. The activity of Sa_{sc} rises from May to July and August then fall down again from September, which is associated with the variation of T. Moreover, in the extremely warm and dry year 2003, r_{sc} exhibits much more activity in affecting ETP than in 2000. Air temperature is therefore assumed as a very dependent impact variable.

The absolute sensitive coefficients of both surface resistances are assumed to depend on the generated daily ETP rate. In Figure 5.7 and 5.8, the extreme values of $S_a < -0.03$ in deciduous forest, $S_a < -0.01$ in coniferous forest, were pointed out with dash lines and associated to the basic meteorological variances and ETP simulated by the calibrated surface resistances (ETP 150_250 for deciduous forest and ETP 300_650 for coniferous forest). It is shown that, high absolute sensitivity of r_{sc} appears with amount peaks in T and simultaneous relative humidity troughs, which consequently leads to the amount peaks in ETP. In the same periods, there are also high SSD values, but no significant associations are shown with WS. S_a is thus very dependent on the ETP rates, whose fluctuation is assumed highly controlled by air temperature and relative humidity.

To verify the assumption, the correlations between meteorological variables and ETP were shown in Figure 5.9 and 5.10. For both forest types, the correlations between RH and

ETP were the most fitting 1:1 line, with $r \geq 0.87$. In several publications, RH has been reported as the most sensitive meteorological variable for ET estimation (Gong et al., 2006; McCuen, 1974). Air temperature T also exhibits very high correlation with ETP in 2001 and 2003, whose correlation coefficient r are more than 0.8 that followed RH. However, in May to September in 2000, less correlation is shown between T and ETP, with r less than 0.7. SSD and WS are followed in orderly, with r approximately ranges in [0.6,0.8] and less than 0.3, respectively. The net radiation R_n has been always applied to replace SSD to explore the relative importance of solar radiation in the Penman-Monteith ET generation and is found as a very sensitive factor (McCuen, 1974). Wind speed has been always reported as the least sensitive variable of all to ETP (Gong et al., 2006; McCuen, 1974; Saxton, 1975). For both forests, the correlation coefficients between each meteorological variable and ETP are more or less the same.

5.4.2 Sensitivity of actual evapotranspiration to surface resistance

(Beven, 1979) concluded that in forest regions, r_{sc} was the most sensitive parameter of ETA generated by the Penman-Monteith equation, which significantly controlled ETA under the dry-canopy conditions, and its relative sensitive coefficients approximated to -1.0 in the hourly and monthly time steps. The relative importances of r_{sc} and r_{se} in ETA simulation in WaSiM-ETH were shown (in Figure 5.11). In deciduous forest, no large variance appears during May to September in 2000 and the *Sr* approximately ranges in [-0.5,0]. It is noted that in July and August in 2001 and 2003, a number of high positive *Sr* appear. Especially in August of 2003, the peak value exceeds 1.5 in deciduous forest and is close to 2.0 in coniferous forest, which represent that an 10 % increase of r_{sc} leads to an 15 % and 20 % increase in deciduous and coniferous forest, respectively. However, these positive *Sr* are abnormal. In coniferous forest, in 2000, r_{se} exhibits very low sensitivity with *Sr* values approximated to 0 and the *Sr* curve is relatively flat that with small fluctuations. In 2001 and 2003, there are even more high positive *Sr*. ETA in August of 2003 is extremely sensitive to r_{sc}. With regard to the absolute sensitivity (Figure 5.12), for each $\mathrm{s\,m^{-1}}$ change in r_{sc} or r_{se}, the response changes in ETA are sorted from large to small as: r_{sc} for deciduous, r_{sc} for coniferous, r_{se} for deciduous and r_{se} for coniferous. Moreover, the impact of r_{se} for coniferous on ETA were very small.

Likewise, the daily absolute sensitivities of both surface resistances are assumed to depend on the generated daily ETA rate. In Figure 5.13 and 5.14, the negative extreme values of S_a ($S_a < -0.015$ in deciduous forest, $S_a < -0.008$ in coniferous forest), were marked out with dash lines in grey and associated to the precipitation, the model outputs such as ETP, ET and decline between ETP to ETA (deETP) simulated with the calibrated surface resistance

combination 150_250 for deciduous forest and 300_650 for coniferous forest. It is shown that, in deciduous forest (Figure 5.13), high negative absolute sensitivities of r_{sc} appear with peaks in ETP, ETA, and a moderate deETP with not more than 4 mm. In coniferous forest (Figure 5.13), high negative absolute sensitivity of r_{sc} appear with also peaks in ETP and ET, as well as the deETP not more than 1 mm. The abnormal positive high values of S_a ($S_a > 0.02$ in deciduous forest, $S_a > 0.005$ in coniferous forest, marked out with dash lines in red) frequently occurred in dry periods with rare precipitation, especially in 2003. Those r_{sc} always appeared with simultaneous extremely high ETP and deETP, with which the little water content in root zone for evapotranspiration were inferred. And the positive value is attributed to the coupling and feedback between evapotranspiration and soil modules in WaSiM-ETH - under dry soil moisture conditions, in a long-term period, increasing the surface resistance will reduce the actual evapotranspiration and subsequently increase the soil water content; however, the increased soil water content will subsequently feedback to the actual evapotranspiration due to the water balance strategy in WaSiM-ETH. Therefore, under dry-soil conditions, an increase of r_{sc} may lead to an increase of ETA in WaSiM-ETH model.

Correlation between meteorological variables and ET were shown in Figure 5.15 and 5.16. With respect to the correlation with ETP, the introduction of soil water content reduced the correlation between meteorological variables and ET. In deciduous forest, in 2000 and 2001, ET was highest correlated with T, followed by RH, SSD and WS. In 2003, all variables were less correlated due to the dry climate conditions. In coniferous forest, the correlation sorted from high to low is also as: T, RH, SSD and WS in 2000 and 2001. However, in the wet year 2000, r corresponding to RH and SSD were much lower than those for deciduous forest. Thus, the correlation between ETA and meteorological variables were dependent on the ratio of ETA to ETP - under wet and medium wet soil moisture conditions and the ratio is thereby big, the correlation between ETA and meteorological variables are better than under dry soil moisture conditions.

5.5 Conclusion

In this chapter, parameter sensitivity analysis was conducted on surface resistance in WaSiM-ETH model. Two parameters were studied - canopy surface resistance (r_{sc}) and soil surface resistance (r_{se}). A one-at-a-time perturbation method was employed. For both forests, continuous perturbation of $r_{sc} \pm 25\ \mathrm{s\,m^{-1}}$ and $r_{sc} \pm 50\ \mathrm{s\,m^{-1}}$ were respectively carried out in WaSiM-ETH. In terms of the general satisfactory criterion recommended by Moriasi et al. (2007) - $NSE > 0.5, RSR \leq 0.7, PBIAS < \pm 25$, the appropriate surface resistance

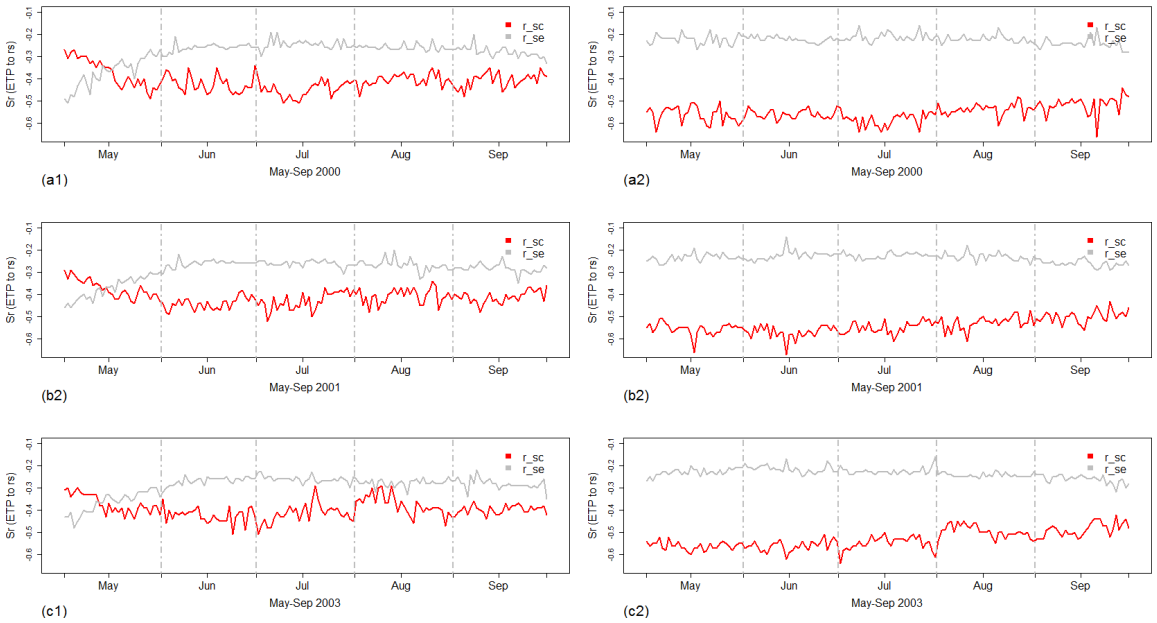

Fig. 5.5 Daily relative sensitive coefficient (Sr, dimensionless) of ETP to surface resistance (r_s) in May-September in year (a) 2000, (b) 2001, (c) 2003 in (1) deciduous and (2) coniferous forest.

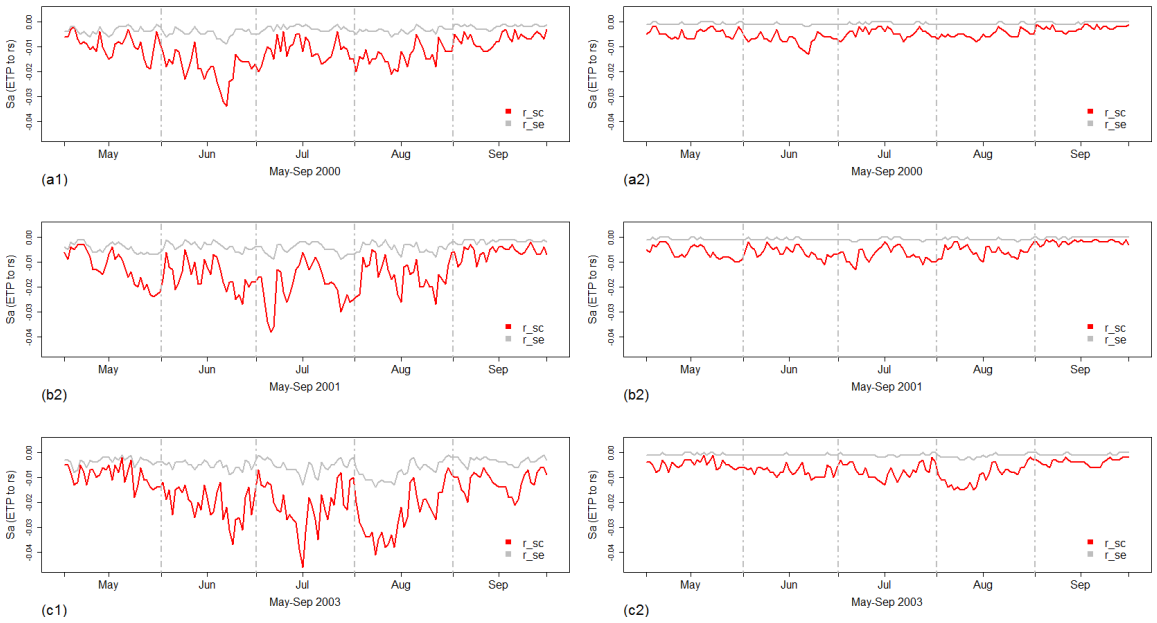

Fig. 5.6 Daily absolute sensitive coefficient (Sa, in mm/s m^{-1}) of ETP to surface resistance (r_s) in May-September in year (a) 2000, (b) 2001, (c) 2003 in (1) deciduous and (2) coniferous forest.

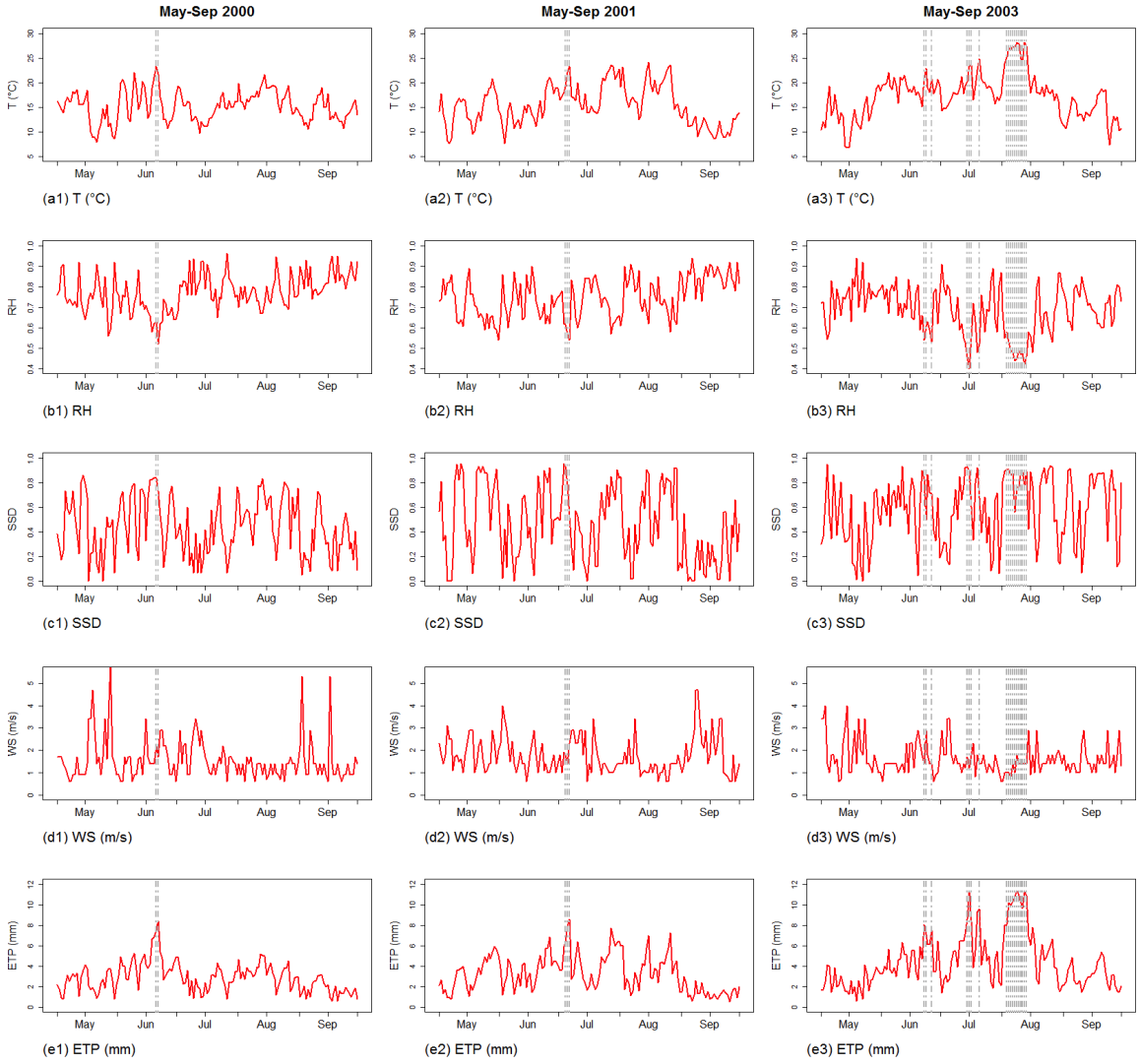

Fig. 5.7 Meteorological variables (a) T (in ^{o}C), (b) RH, (c) SSD (d) WS (in $\mathrm{m\,s^{-1}}$), and (e) ETP 150_250 (in mm), during May-September in (1) 2000, (2) 2001, (3) 2003 in deciduous forest, with the large negative values of *Sa* (ETP to r_{sc}) were marked with dash lines.

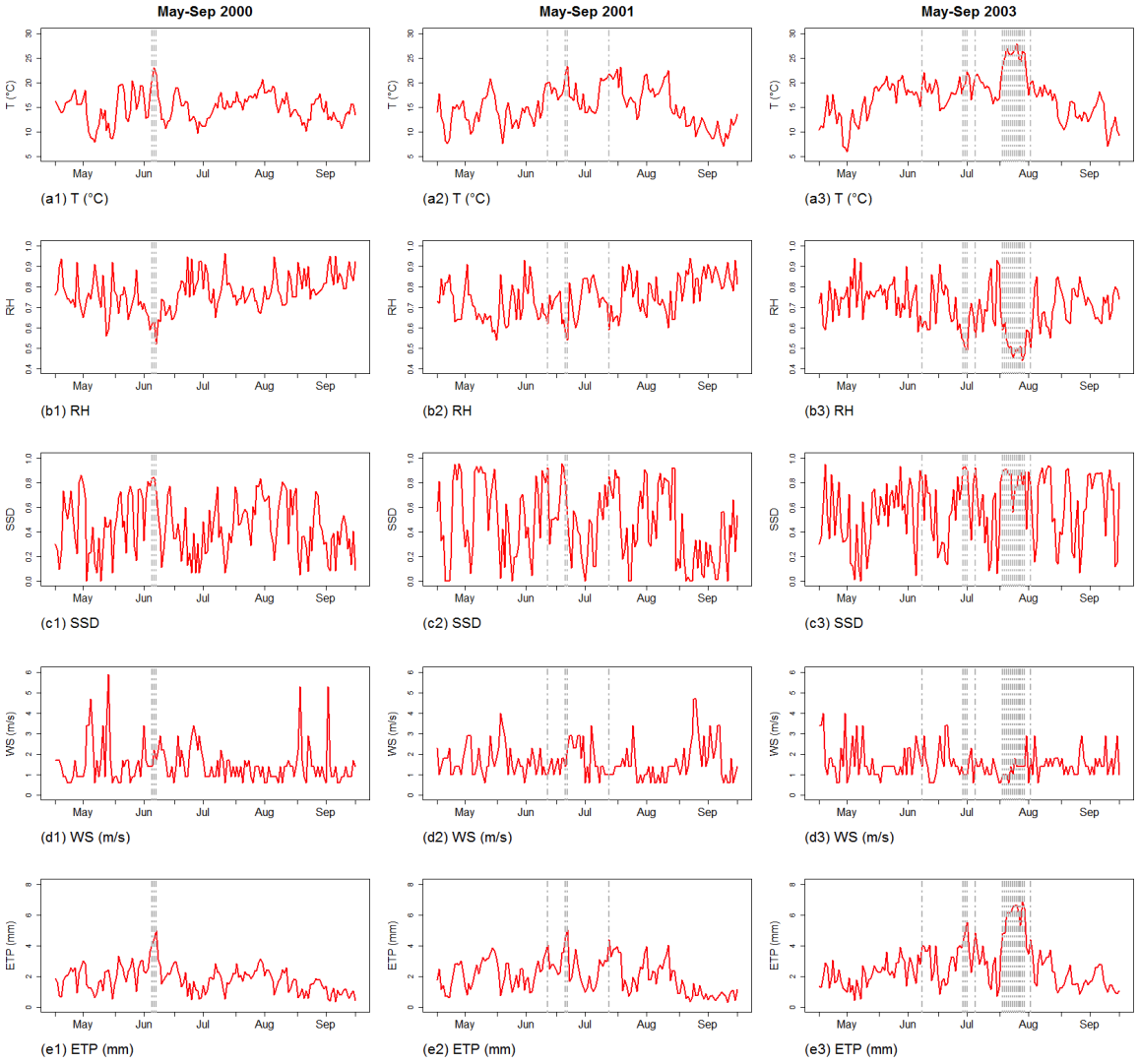

Fig. 5.8 Meteorological variables (a) T (in ^{o}C), (b) RH, (c) SSD (d) WS (in $\mathrm{m\,s^{-1}}$), and (e) ETP 300_650 (in mm), during May-September in (1) 2000, (2) 2001, (3) 2003 in coniferous forest, with the large negative values of *Sa* (ETP to r_{sc}) were marked with dash lines.

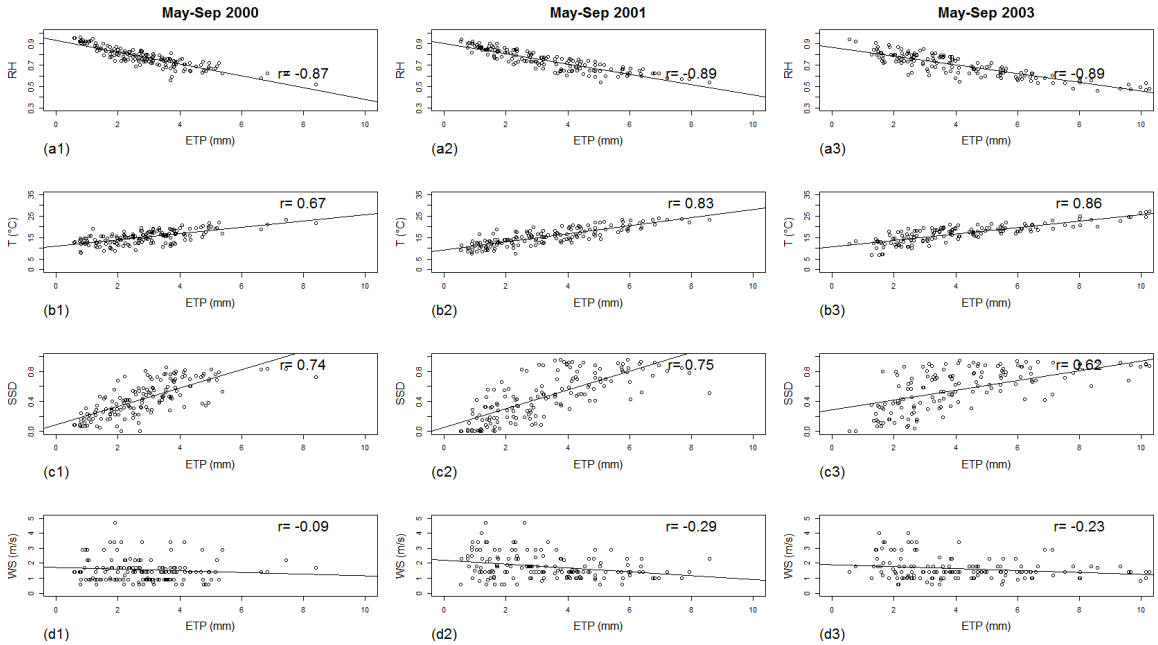

Fig. 5.9 Scatter plot between ETP and (a) RH, (b) T (in ^{o}C), (c) SSD and (d) WS (in m s^{-1}), during May-September in (1) 2000, (2) 2001, (3) 2003 in deciduous forest.

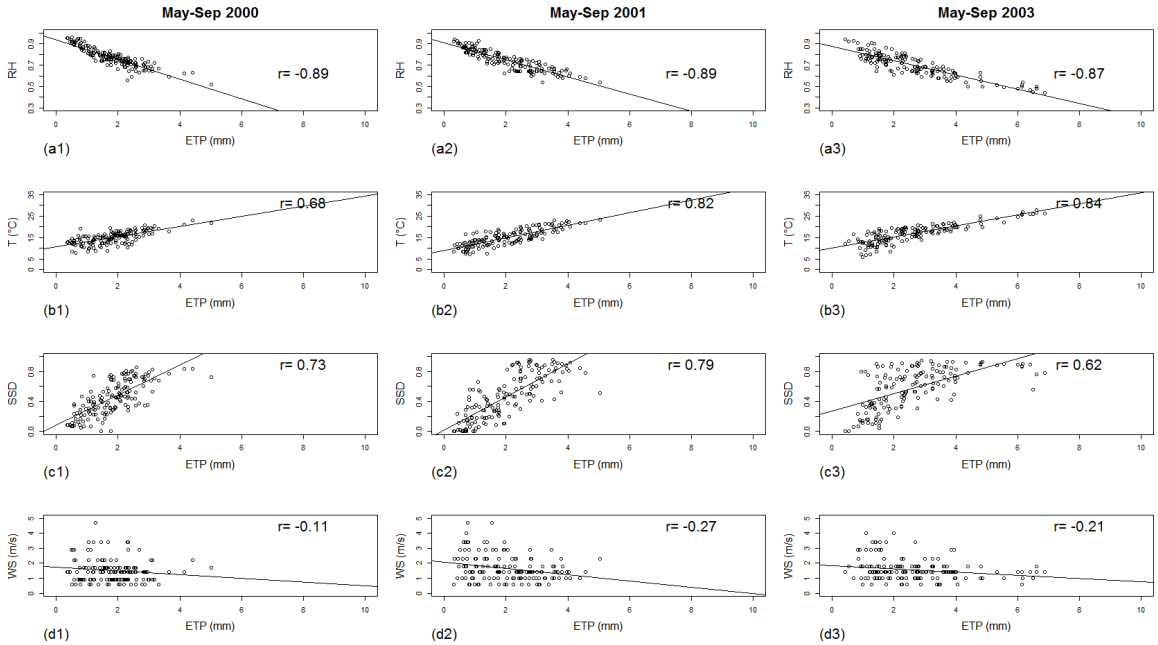

Fig. 5.10 Scatter plot between ETP and (a) RH, (b) T (in ^{o}C), (c) SSD and (d) WS (in m s^{-1}), during May-September in (1) 2000, (2) 2001, (3) 2003 in coniferous forest.

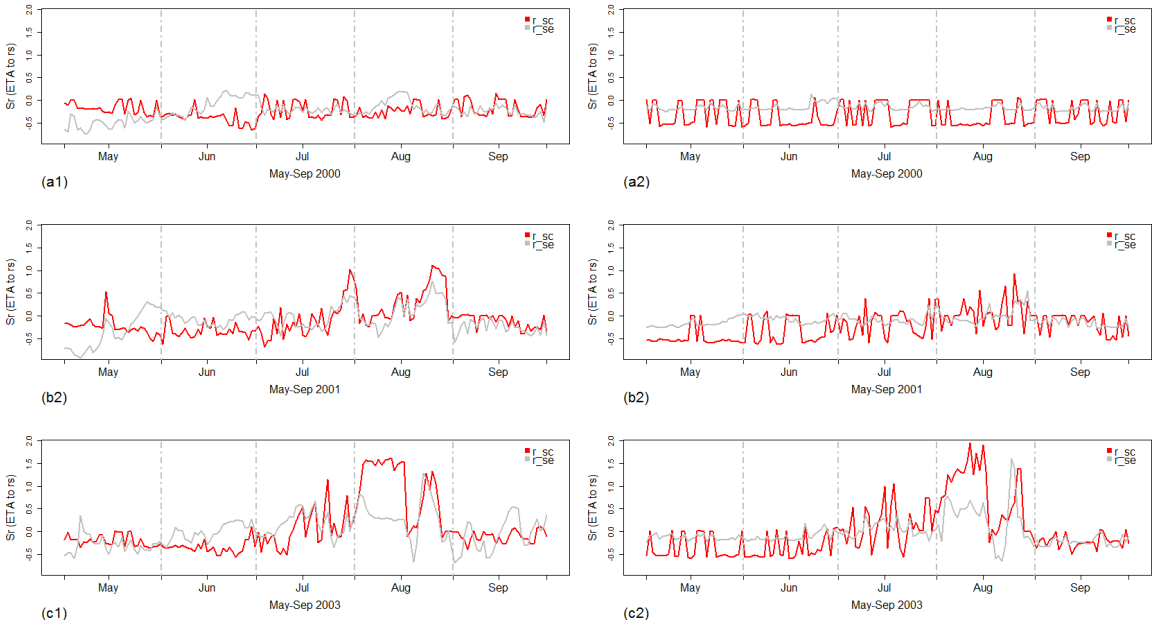

Fig. 5.11 Daily relative sensitive coefficient (*Sr*, dimensionless) of ETA to surface resistance (r_s) in May-September in year (a) 2000, (b) 2001 and (c) 2003 in (1) deciduous and (2) coniferous forest.

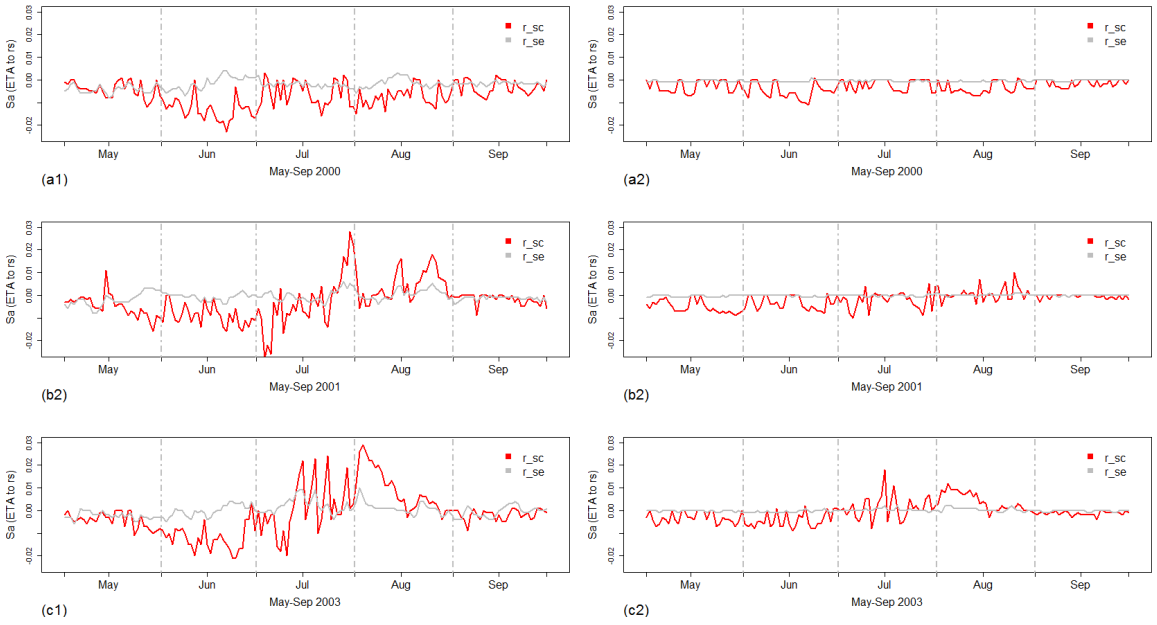

Fig. 5.12 Daily absolute sensitive coefficient (*Sa*, in mm/s m^{-1}) of ETA to surface resistance (r_s) in May-September in year (a) 2000, (b) 2001 and (c) 2003 in (1) deciduous and (2) coniferous forest.

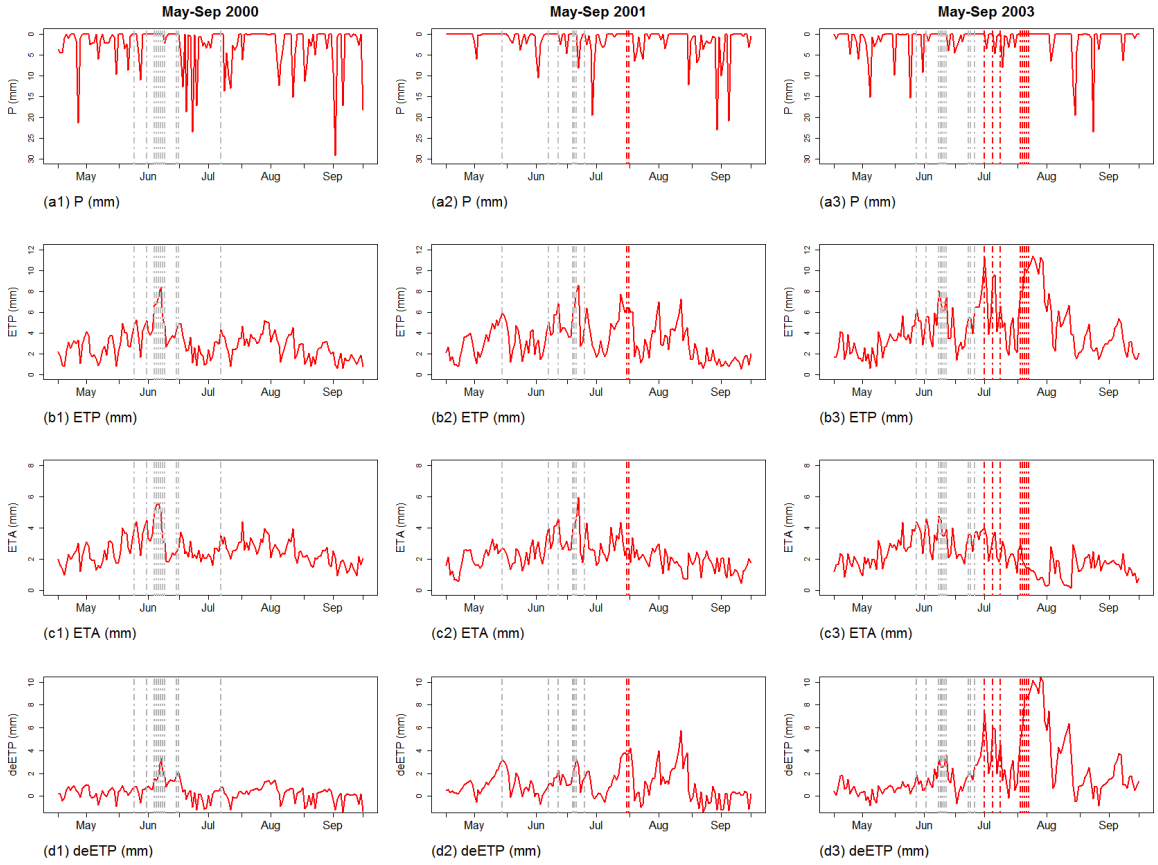

Fig. 5.13 (a) P (in mm), (b) ETP 150_250 (in mm), (c) ETA 150_250 (in mm), and (d) deETP 150_250 (in mm) during May-September in (1) 2000, (2) 2001, (3) 2003 in deciduous forest, with the large negative and positive values of *Sa* (ETA to r_{sc}) were respectively marked with dash lines in grey and red.

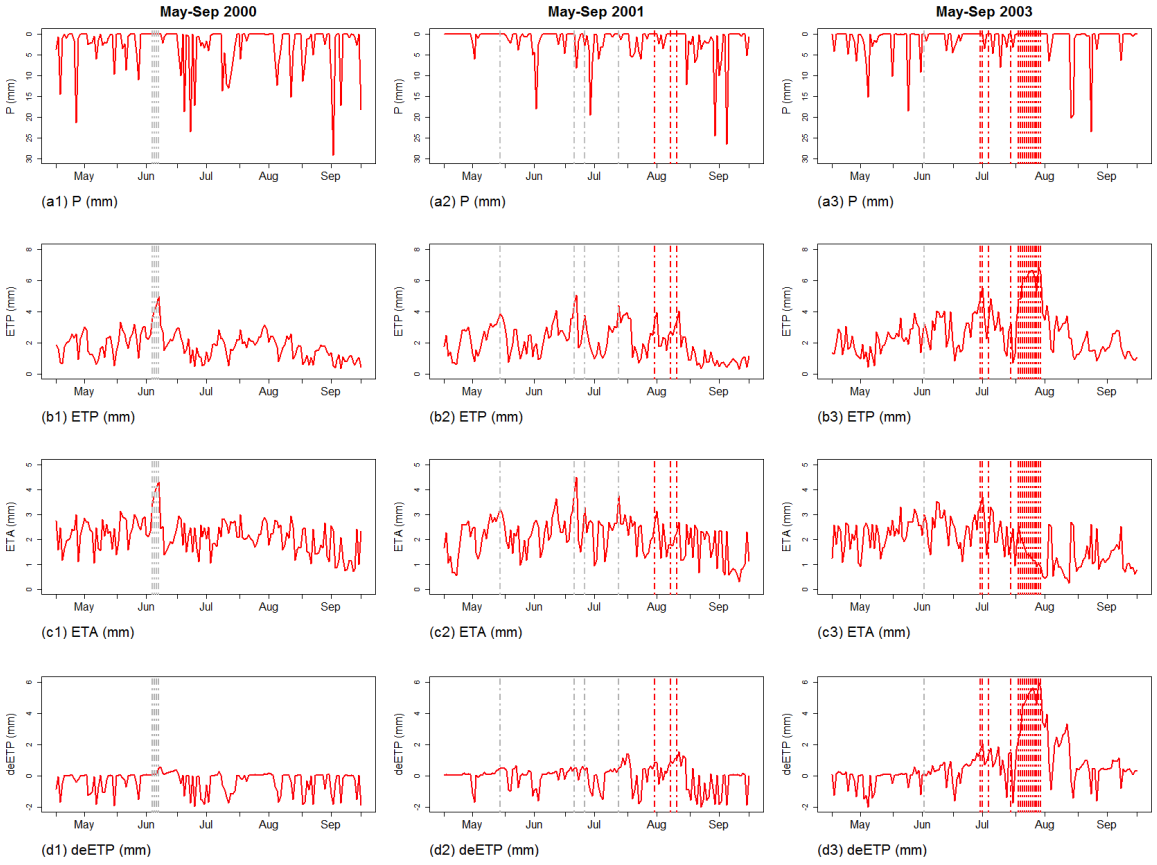

Fig. 5.14 Meteorological variables (a) T (in ^{o}C), (b) RH, (c) SSD (d) WS (in $\mathrm{m\,s^{-1}}$), and (e) ETA 300_650 (in mm), during May-September in (1) 2000, (2) 2001, (3) 2003 in coniferous forest, with the large negative and positive values of Sa (ETA to r_{sc}) were respectively marked with dash lines in grey and red.

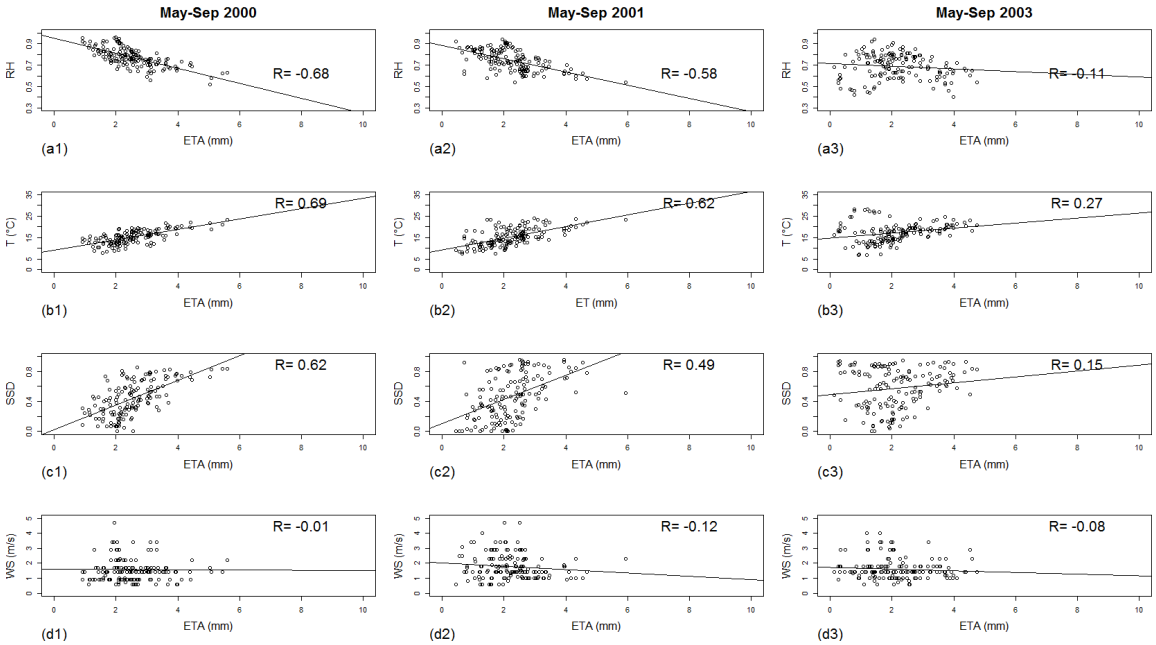

Fig. 5.15 Scatter plot between ETA and (a) RH, (b) T (in ^{o}C), (c) SSD and (d) WS (in m s^{-1}), during May-September in (1) 2000, (2) 2001, (3) 2003 in deciduous forest.

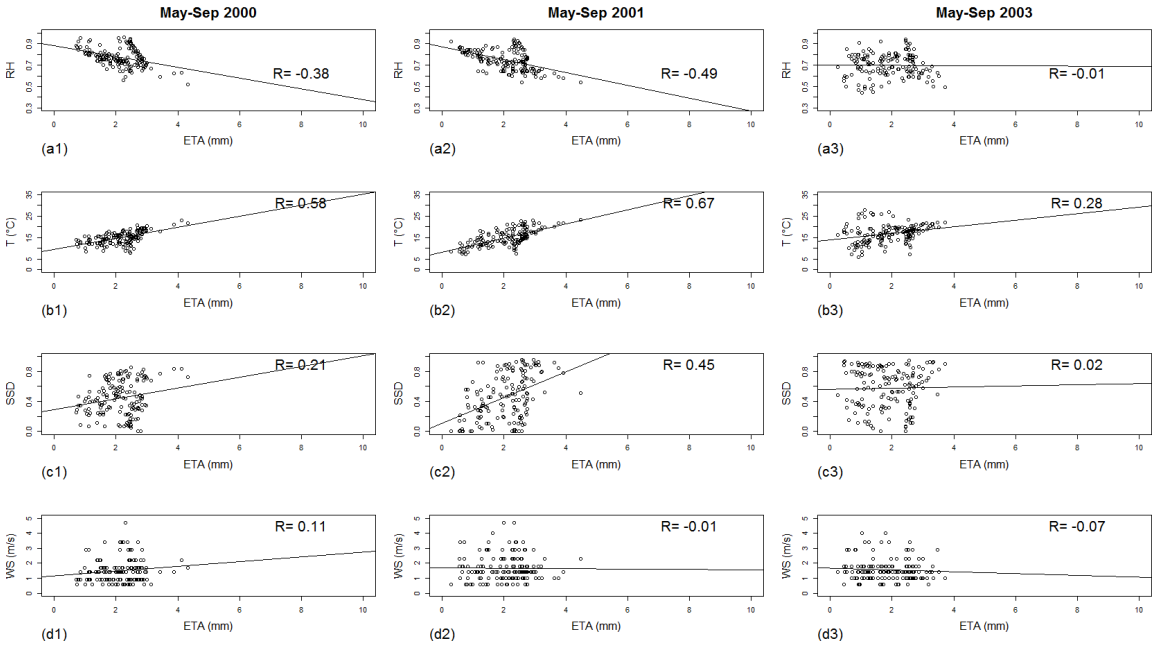

Fig. 5.16 Scatter plot between ETA and (a) RH, (b) T (in ^{o}C), (c) SSD and (d) WS (in m s^{-1}), during May-September in (1) 2000, (2) 2001, (3) 2003 in coniferous forest.

value ranges during May-September (annual minimal) were determined as: in deciduous forest, [100,225] for r_{sc} and [50,450] for r_{se} as well as in coniferous forest, [225,375] for r_{sc} and [350,1200] for r_{se}. The previously recommended statistical evaluation indices such as NSE (E), RSR, PBIAS, MBE, the mean variance of error distribution (S_d^2), index of agreement (d), and RMSE were confirmed as appropriate indices. The model performance can be judged as satisfactory if $NSE > 0.5, RSR \leq 0.7, PBIAS < \pm 12, MBE < \pm 0.45, S_d^2 < 1.11, d > 0.79, RMSE < 9,97$. E_1, MSR, MAE and R^2 were misleading indices due to their relatively insensitivity to extreme values. In terms of those recommended indices, the previously calibrated surface resistance values were also confirmed.

For both forest types, r_{sc} played a more important role than r_{se} in ETP estimation. In terms of the grading standard proposed by (Lenhart et al., 2002), r_{sc} were ranked as high-sensitive parameters in ETP estimation, whereas the relative sensitivity coefficient of ETP to r_{se} in coniferous forest were partly lower than the high-sensitive level. In deciduous forest, an increase of r_{sc} in 10 % will lead to a decrease of ETP in 3-5 % whereas an increase of r_{se} in 10 % will lead to a decrease of ETP in 2-3 %. In coniferous forest, an increase of r_{sc} and r_{se} in 10 % will respectively result to 5-7 % and 1.5-2.5 % reduction in ETP. Since the relative sensitive coefficient is very dependent on the ratio that r_{so}/ETP_o (with o indicated the optimal values), the absolute sensitive coefficient were further investigated. The absolute sensitivity of ETP to r_{sc} were about one order bigger than the absolute sensitivity of ETP to r_{se} (e.g. -0.012 $\mathrm{s\,m^{-1}}$ vs. -0.0017 $\mathrm{s\,m^{-1}}$). It was found that the fluctuations of absolute sensitivity coefficients of ETP to r_{sc} were dependent on the generated ETP rate. Moreover, the daily ETP were found the most highly correlated with RH, followed by T, SSD and WS.

With regard to the ETA, r_{sc} also played a more important role than r_{se} for both forest types. This importance difference was attributed to that transpiration always dominates in ETA rates, especially in forest regions (Kurpius et al., 2003; Szilagyi, 2000; Wilson et al., 2001). Under wet meteorological conditions, the daily absolute sensitivity of r_{sc} were also dependent on the generated ET rates. However, under dry soil moisture conditions, an increase of r_{sc} may may lead to an increase of ETA due to the coupling and feedback between the evapotranspiration and soil modules in WaSiM-ETH model. The correlation between ETA and meteorological variables were dependent on the ratio of ETA to ETP. Under wet and medium wet conditions, the ETA were found the most correlated with T, followed with RH, SSD and WS. Under dry conditions, weak correlations were shown.

Chapter 6

Summary

The main works we have done in this thesis are: (1) calibrated the canopy surface resistance r_{sc} and the soil surface resistance r_{se} in the WaSiM-ETH model for both forest types - the calibrated values are $r_{sc} = 150\ \mathrm{s\,m^{-1}}$, $r_{se} = 250\ \mathrm{s\,m^{-1}}$ for deciduous forest; $r_{sc} = 300\ \mathrm{s\,m^{-1}}$, $r_{se} = 650\ \mathrm{s\,m^{-1}}$ for coniferous forest; (2) determined the appropriate value ranges of r_{sc} and r_{se} (annual maximum) – [100,225] $\mathrm{s\,m^{-1}}$ for r_{sc} and [50,450] $\mathrm{s\,m^{-1}}$ for r_{se} in deciduous forest, as well as [225,375] $\mathrm{s\,m^{-1}}$ for r_{sc} and [350,1200] $\mathrm{s\,m^{-1}}$ for r_{se} in coniferous forest; (3) found appropriate statistical indices and determined their value ranges for model performance evaluation – the model performance can be judged as satisfactory if $NSE > 0.5, RSR \leq 0.7, PBIAS < \pm 12, MBE < \pm 0.45, S_d^2 < 1.11, d > 0.79, RMSE < 9,97$; (4) investigated the relative importances of r_{sc} and r_{se} – r_{sc} played an more important role than r_{se} in potential evapotranspiration (ETP) and actual evapotranspiration (ETA) estimation by the Penman-Monteith equation; (5) investigated the correlation relationships between meteorological variables and ETP/ETA – the ETP estimation was found the most correlated to the relative humidity (RH), followed by air temperature (T), relative sunshine duration (SSD) and wind speed (WS). Under wet or medium wet climate conditions, the ETA estimation was found the most correlated to T, followed by RH, SSD and WS. Under water-stress conditions, there were very small correlations between ETA and meteorological variables.

6.1 Comparison of two techniques for ETA estimation

In this thesis, two different techniques were employed for ETA estimation. One is the conventional method in the WaSiM-ETH model – to firstly estimate the ETP rate and the soil water content, and subsequently to obtain the ETA by reducing ETP according to the soil water content. The Penman-Monteith equation was used for ETP calculation. The other is using remote sensing images combing with the ground-measured meteorological data to

retrieve the surface properties and the surface energy components, and estimate latent heat flux (LE, corresponding to ETA) through the surface energy balance equation. Since it is frequently reported that much different evapotranspiration (ET) rates are always generated by different methods, the remote sensing-based method is required to be as similar to the Penman-Monteith equation as possible. The Penman-Monteith equation combined both aerodynamic- and surface energy-based techniques, with which ETP is on the one hand calculated as the turbulent transport of vapor and on the other hand estimated through the surface energy equation. In the equation, the meteorological variables such as sunshine duration, air temperature, relative humidity and wind speed are basic input data. The biggest difficulty in estimating ETP by the Penman-Monteith equation is the determination of surface resistance (Brown, 1974). In the remote sensing- based method, the TM/ETM+ thermal infrared (TIR) band was used for land surface temperature (LST) retrieving, which is a critical variable for sensible heat flux (H) estimation. The daily H is calculated in terms of the temperature difference between the maximal LST and air temperature, which is also related to the aerodynamic techniques. Based on the retrieved surface properties such as surface albdeo, fractional vegetation cover (FVC) and LST as well as the ground-measured meteorological data, the LE was obtained through the surface energy equation. Using remote sensing TIR data is the only means for a large-scale LST retrieving. In the Penman-Monteith equation, the introduction of the aerodynamic-based technique eliminates the difficulty in LST determinate and makes the ETP estimation possible only based on meteorological data (Penman, 1948).

6.2 Features of simulations and observations

The simulations are the ETA generated by the WaSiM-ETH model with different surface resistance combinations (including both r_{sc} and r_{se}) in a daily time step. The value adjustments of r_{sc} and r_{se} were conducted in a manual model calibration process on the basis of previous works and experiments. In this thesis, 12 representative surface resistance combinations were selected for each forest type for research. The observations are remote sensing-retrieved daily LE . Due to the high-quality and cloudy-free requirements for remote sensing image selection as well as the overlapping cycle of TM/ETM+ sensor is 16 days, images on only 5 dates were available during 1971-2003 (model run). Comparing both data, the features of simulations and observations are: (1) the model-simulated ETA are in good temporal resolution that are continuous in a long time series in a daily time step, whereas the observations are noncontinuous in time series and only available in a limited number; (2) the observations are superior in spatial resolution to the simulations since for the former, the spatial resolution are on the

basis of TM/ETM+ images, whose general spatial resolution are 30 $\times$ 30 m; whereas for the latter, the basic input data are meteorological measurements, whose spatial resolution are mainly dependent on the density of climate station networks. Singh et al. (2012) successfully calibrated the WaSiM-ETH model by using critical events replaced the whole time series. Furthermore, the observations were found to represent multiple climate conditions such as wet, medium wet and dry as well as the extremely low ETA rate on August 04, 2003 in contrast to the previously years during the same time was considered as extreme event. These features are great supplements to overcome the poor temporal resolution of the observations.

6.3 Impact and feedback of meteorological variables

In 2000, there were abundant precipitation and relatively high air humidity, whereas in the summer of 2003, there were rare precipitation, relatively high air temperature and low air humidity. To judge the moisture degree of a climate, the amount of both precipitation and ETA should be taken into account (Thornthwaite, 1948). The decline between model simulated ETP and ETA (deETP) in a daily time step was considered as a good indicator – deETP values describes the water-stress degree that the bigger the deETP is, the more the amount of effective precipitation is smaller than ETA. In terms of the model outputted deETP simulated with 12 different surface resistance combinations, a consistent assumption was proposed that the meteorological condition on August 04, 2003 was dry whereas on May 15, 2000, was very wet - 12 deETP values on that day uniformly approximated to 0.9 (in Figure 2.2 and 2.3).

Meteorological variables such as SSD, T, RH and WS are basic input data for ETP estimation. It is found that the fluctuations of daily ETP generated by the Penman-Monteith equation was very dependent on the changes in the meteorological variables, especially the changes in T and RH. Numbers of publications reported the importances of meteorological variables in ET estimation, especially their relative importances in contrast to others. R_n, RH and T was respectively reported as the most sensitive variable in several publications (Bakhtiari et al., 2012; Gong et al., 2006; Goyal, 2004; McCuen, 1974; Saxton, 1975), whereas in most cases, WS was reported as the least sensitive variable (Gong et al., 2006; McCuen, 1974; Saxton, 1975). In the WaSiM-ETH model, ETP estimation was found the most correlated to the RH, followed by T, SSD and WS. R_n was suggested to replace SSD to quantify the total energy supply in surface energy budget. Under non-water-stress condition, ETA estimation was found the strongest correlated to T, followed by RH, SSD and WS. Under water-stress condition, there were very small correlations between ETA and meteorological variables.

The meteorological variables are not the only critical input data for ET estimation, but also affected by the ET feedback. It was found that in the long-time period during May 01, 2000 to September 30, 2003, there were significant differences respectively in T, RH and WS between two forest types - there were higher T, lower RH and more rapid WS in deciduous forest than in coniferous forest. Since the local air temperature, air humidity and cloud formation are always affected by ET (Rabin et al., 1990; Segal and Arritt, 1992), these differences were assumed not only as the causes of more ET generated in deciduous forest than in coniferous forest, but also as the result from the feedbacks of the generated different ET rates in two forest types in a long-time period. On the five sample dates, in general, higher T and lower RH were also exhibited in deciduous forest in contrast to in coniferous forest. However, there was opposite appearance that on the three days of 2003, the ET rates generated in deciduous forest were less than in coniferous forest. This appearance was assumed attributed to the higher drought-tolerance of plants in coniferous forest under soil water-stress conditions.

6.4 Features of WaSiM-ETH model

In the WaSiM-ETH model, the flow for ETA estimation was simplified in three steps: (1) to calculate the ETP on the basis of the meteorological variables such as SSD, T, RH and WS by the Penman-Monteith equation; (2) to simulate the soil water content in one-dimension in the vertical direction by the Richards equation; (3) to reduce the ETP to ETA according to the actual soil water content. In the process of ETA estimation in WaSiM-ETH, the meteorological variables are critical input data as well as the aerodynamic resistance and the surface resistance are important parameters.

Aerodynamic resistance and surface resistance are the most important parameter in the Penman-Monteith equation, however, the surface resistance plays a leading role in the forest regions (Beven, 1979; Rana and Katerji, 1998). In WaSiM-ETH, the aerodynamic resistance for forest regions is a function of the wind speed. Duo to the smallest sensitivity of WS in the Penman-Monteith ETP and ETA estimation, the aerodynamic resistance was also inferred as insensitive parameters for forested regions. Since the transpiration and evaporation are separately calculated with the Penman-Monteith equation, the surface resistance were divided into the canopy surface resistance r_{sc} and the soil surface resistance r_{se}, with the interception surface resistance was not taking into account. The perturbations of the surface resistance were found to impact the model simulated ETP, SM and deETP mainly in magnitude but keep their fluctuations reflecting the impact of the changes in meteorological variables. Both surface resistances were calibrated to find their optimal values and appropriate values ranges

respectively for both forest types in the WaSiM-ETH model. It was also found that in both forests, r_{sc} played a much important role than r_{se}, which was attributed to the knowledge that transpiration always dominates the ET, especially in a forest area (Kurpius et al., 2003; Szilagyi, 2000; Wilson et al., 2001). For instance, an increase of 10 % of r_{sc} leaded to an decrease in ETP of 3-5 % in deciduous forest and 5-7 % in coniferous forest, as well as an increase of 10 % of r_{se} leaded ETP to a reducing of 2-3 % in deciduous forest and 1.5-2.5 % in coniferous forest.

It is noted that in WaSiM-ETH, the simulation of ETA and soil moisture are closely linked. In a long time series, increasing the surface resistance to reduce the ET increases the soil moisture, since the water balance in terms of the total water supply from precipitation. Therefore in the extremely dry and warm summer of 2003, extremely high positive sensitive coefficients that described the response of ETA to r_{sc} were found - in a long time series, an increase of r_{sc} decreased the ET amount and maintain more water in the soil in the previous days, and subsequently increased the current soil moisture to supply more water for ET in water-stress days.

6.5 Important surface properties in ETA estimation

The surface properties such as surface albedo, fractional vegetation cover (FVC) and land surface temperature (LST) are critical parameters for ET estimation. Based on the remote sensing-retrieved surface properties on five sample dates, differences were shown for each property parameter between two forest types: the surface albedo, FVC in deciduous forest were always higher than in coniferous forest. With regard to the LST, on the three dates in the dry year 2003, LST in deciduous forest were higher than in coniferous forest, which were assumed due to the higher drought-tolerance of the plants in coniferous forest under water-stress conditions. In the WaSiM-ETH model, the default setting of surface albedo are consistently 0.2 and 0.1 respectively for deciduous and coniferous forest in each month, whereas default monthly FVC in deciduous forest were lower than those in coniferous forest. Due to these surface property differences between forest types as well as between model and remote sensing-retrieved values, future work of this thesis will extend in this direction.

6.6 Recommended model performance evaluation techniques

Using multiple evaluation techniques to assess model performance is widely suggested (Boyle et al., 2000; Legates and McCabe, 1999; Willmott, 1981). In this thesis, boxplot was found as a good graphical indicator that exhibited model performance at both spatial

and temporal scale. Due to the features of observations that containing multiple climate conditions such as wet, medium wet and dry, but in a limited number, the statistical indices for model performance evaluation in time series are required to be sensitive to extreme values. The Nush-Sutcliffe efficiency (NSE), RMSE-observations standard deviation ratio (RSR), percent bias (PBIAS), mean bias error (MBE), mean variance of error distribution (S_d^2), index of agreement (d), root mean square error (RMSE) were found to satisfy this requirement and are appropriate to provide additional evaluation information to boxplot. At the spatial scale, MAE was considered as appropriate index since it is an overall measure that provide enough diagnose information containing both MBE and S_d^2.

6.7 Sources of error

In this study, there are three primary sources of error in the data simulation by the WaSiM-ETH model: error resulted from the surface properties, error resulted from the model regionalization strategy, and error resulted from the measurements of field capacity. (1) error resulted from the surface properties. In Table 2.4, the default setting of the surface properties in the WaSiM-ETH model are shown. In the model, the surface properties such as surface albedo, leaf area index (LAI) and fractional vegetation cover (FVC) are monthly values and separately for both forest types. The surface albedo values of deciduous forest are keep in a constant for the whole year, whereas the albedo values of coniferous forest are also keep in a constant for each month but the values are only half of those in deciduous forest. For the FVC, in the growing period from May to September, the FVC values are bigger than the other seasons for both forest types. It is shown that the monthly FVC values of coniferous forest are always bigger than the values of deciduous forest. In Figure 3.3, the surface properties retrieved by the remote sensing images on five sample dates are shown. However, the values of surface albedo and FVC vary at daily scale. It is noted that the daily FVC values of deciduous forest are always bigger than those of coniferous forest, which is opposite to the parameter setting in the WaSiM-ETH model. Therefore, in the further work, the surface properties should be calibrated. Since the surface resistance for plants transpiration are very dependent on LAI and FVC, the surface properties calibration is also a follow-up work for surface resistance calibration. (2) error resulted from the model regionalization strategy. There are big differences in the spatial pattern between the model simulated ETA and the remote sensing-retrieved LE (Figure 4.2 and 4.3). It is obviously that LE is superior to ETA in spatial accuracy. In the WaSiM-ETH model, the spatial pattern of outputs is very dependent on the ground-measured precipitation and air temperature, the grid data sets of field capacity and soil slope. The future work is to improve the regionalization strategy to

reduce the error at spatial scale. (3) error resulted from the measurements of field capacity. In the WaSiM-ETH model, the field capacity of study area is divided into four classes: (1) 50 mm, (2) 100 mm, (3) 150 mm and (4) 200 mm. It is found that the the regions with a field capacity at 50 mm exhibited the worst model performance in ETA simulation. Actually, a field capacity at 50 mm is too low for the soil in the forest area. The field capacity grid data set is thereby supposed to contain errors.

References

Abtew, W. (1996). Evapotranspiration measurements and modeling for three wetland systems in south florida1.

Allen, R., Tasumi, M., Trezza, R., Waters, R., and Bastiaanssen, W. (2002). Sebal (surface energy balance algorithms for land). *Advance Training and Users Manual–Idaho Implementation, version*, 1:97.

Allen, R. G., Jensen, M. E., Wright, J. L., and Burman, R. D. (1989). Operational estimates of reference evapotranspiration. *Agronomy Journal*, 81(4):650–662.

Allen, R. G., Pereira, L. S., Howell, T. A., and Jensen, M. E. (2011). Evapotranspiration information reporting: I. factors governing measurement accuracy. *Agricultural Water Management*, 98(6):899–920.

Allen, R. G., Pereira, L. S., Raes, D., Smith, M., et al. (1998). Crop evapotranspiration-guidelines for computing crop water requirements-fao irrigation and drainage paper 56. *FAO, Rome*, 300:6541.

Bakhtiari, B., Baghizadeh, A., et al. (2012). Daily penman-monteith sensitivity analysis in many subclasses climates based on extended-de martonne classification. In *Soil and Water Engineering. International Conference of Agricultural Engineering-CIGR-AgEng 2012: agriculture and engineering for a healthier life, Valencia, Spain, 8-12 July 2012*, pages P–0024. CIGR-EurAgEng.

Bastiaanssen, W., Menenti, M., Feddes, R., and Holtslag, A. (1998a). A remote sensing surface energy balance algorithm for land (sebal). 1. formulation. *Journal of hydrology*, 212:198–212.

Bastiaanssen, W., Pelgrum, H., Wang, J., Ma, Y., Moreno, J., Roerink, G., and Van der Wal, T. (1998b). A remote sensing surface energy balance algorithm for land (sebal).: Part 2: Validation. *Journal of hydrology*, 212:213–229.

Batchelor, C. (1984). The accuracy of evapotranspiration estimated with the fao modified penman equation. *Irrigation Science*, 5(4):223–233.

Beven, K. (1979). A sensitivity analysis of the penman-monteith actual evapotranspiration estimates. *Journal of Hydrology*, 44(3):169–190.

Blaney, H. F. (1952). Determining water requirements in irrigated areas from climatological and irrigation data.

Boegh, E., Soegaard, H., and Thomsen, A. (2002). Evaluating evapotranspiration rates and surface conditions using landsat tm to estimate atmospheric resistance and surface resistance. *Remote Sensing of Environment*, 79(2):329–343.

Bosch, J. M. and Hewlett, J. (1982). A review of catchment experiments to determine the effect of vegetation changes on water yield and evapotranspiration. *Journal of hydrology*, 55(1):3–23.

Bouchet, R. (1963). Evapotranspiration réelle et potentielle, signification climatique. *IAHS Publ*, 62:134–142.

Boulet, G., Chehbouni, A., Gentine, P., Duchemin, B., Ezzahar, J., and Hadria, R. (2007). Monitoring water stress using time series of observed to unstressed surface temperature difference. *Agricultural and Forest Meteorology*, 146(3):159–172.

Boyle, D. P., Gupta, H. V., and Sorooshian, S. (2000). Toward improved calibration of hydrologic models: Combining the strengths of manual and automatic methods. *Water Resources Research*, 36(12):3663–3674.

Brown, K. (1974). Calculations of evapotranspiration from crop surface temperature. *Agricultural meteorology*, 14(1):199–209.

Brunsell, N. A. and Gillies, R. R. (2002). Incorporating surface emissivity into a thermal atmospheric correction. *Photogrammetric engineering and remote sensing*, 68(12):1263–1270.

Brutsaert, W. (1975). On a derivable formula for long-wave radiation from clear skies. *Water Resources Research*, 11(5):742–744.

Brutsaert, W. and Stricker, H. (1979). An advection-aridity approach to estimate actual regional evapotranspiration. *Water resources research*, 15(2):443–450.

Calcagno, G., Mendicino, G., Monacelli, G., Senatore, A., and Versace, P. (2007). Distributed estimation of actual evapotranspiration through remote sensing techniques. In *Methods and Tools for Drought Analysis and Management*, pages 125–147. Springer.

Calder, I. (1977). A model of transpiration and interception loss from a spruce forest in plynlimon, central wales. *Journal of Hydrology*, 33(3):247–265.

Carlson, T. N. and Buffum, M. J. (1989). On estimating total daily evapotranspiration from remote surface temperature measurements. *Remote Sensing of Environment*, 29(2):197–207.

Carlson, T. N., Capehart, W. J., and Gillies, R. R. (1995). A new look at the simplified method for remote sensing of daily evapotranspiration. *Remote Sensing of Environment*, 54(2):161–167.

Carlson, T. N., Dodd, J. K., Benjamin, S. G., and Cooper, J. N. (1981). Satellite estimation of the surface energy balance, moisture availability and thermal inertia. *Journal of Applied Meteorology*, 20(1):67–87.

Casper, M., Grigoryan, G., Heinemann, G., and Bierl, R. (2013). Auswirkungen des Klimawandels auf die Ressource Wasser in Rheinland-Pfalz. – RHEINLAND-PFALZ KOMPETENZ-ZENTRUM FÜR KLIMAWANDELFOLGEN [Eds.]: Schlussberichte des Landesprojekts Klima- und Landschaftswandel in Rheinland-Pfalz (KlimLandRP), Teil 2, Modul Wasser: 164 S.

Casper, M. and Vohland, M. (2008). Validation of a large scale hydrological model with data fields retrieved from reflective and thermal optical remote sensing data–a case study for the upper rhine valley. *Physics and Chemistry of the Earth*, 33(17):1061–1067.

Cess, R. D. (1978). Biosphere-albedo feedback and climate modeling. *Journal of the Atmospheric Sciences*, 35(9):1765–1768.

Chander, G., Markham, B. L., and Helder, D. L. (2009). Summary of current radiometric calibration coefficient for landsat mss, tm, etm+, and eo-1 ali sensors. *Remote sensing of enviroment*, 113(5):893–903.

Charney, J., Quirk, W. J., Chow, S.-H., and Kornfield, J. (1977). A comparative study of the effects of albedo change on drought in semi-arid regions. *Journal of the Atmospheric Sciences*, 34(9):1366–1385.

Chavez, P. S. (1996). Image-based atmospheric corrections-revisited and improved. *Photogrammetric engineering and remote sensing*, 62(9):1025–1035.

Choudhury, B., Reginato, R., and Idso, S. (1986). An analysis of infrared temperature observations over wheat and calculation of latent heat flux. *Agricultural and Forest Meteorology*, 37(1):75–88.

Committee, A. T. et al. (1993). Criteria for evaluation of watershed models. *Journal of Irrigation and Drainage Engineering*, 119(3):429–442.

Courault, D., Seguin, B., and Olioso, A. (2005). Review on estimation of evapotranspiration from remote sensing data: From empirical to numerical modeling approaches. *Irrigation and Drainage systems*, 19(3-4):223–249.

Covey, W. G. (1959). Testing a hypothesis concerning the quantitative dependence of evapotranspiration on availability of moisture. Master's thesis, A. & M. College of Texas.

Crick, M. and Hill, M. (1987). The role of sensitivity analysis in assessing uncertainty. In *Uncertainty analysis for performance assessments of radioactive waste disposal systems*.

Cullmann, J., Mishra, V., and Peters, R. (2006). Flow analysis with wasim-eth? model parameter sensitivity at different scales. *Advances in Geosciences*, 9:73–77.

Dawson, C. W., Abrahart, R. J., and See, L. M. (2007). Hydrotest: a web-based toolbox of evaluation metrics for the standardised assessment of hydrological forecasts. *Environmental Modelling & Software*, 22(7):1034–1052.

Dirmeyer, P. A. and Shukla, J. (1994). Albedo as a modulator of climate response to tropical deforestation. *Journal of Geophysical Research: Atmospheres (1984–2012)*, 99(D10):20863–20877.

Doorenbos, J. and Pruitt, W. O. (1977). Crop water requirements. fao irrigation and drainage paper 24. *FAO, Rome*, page 156.

Droogers, P. and Allen, R. G. (2002). Estimating reference evapotranspiration under inaccurate data conditions. *Irrigation and drainage systems*, 16(1):33–45.

Dyck, S. (1985). Overview on the present status of the concepts of water balance models. *IAHS-AISH publication*, (148):3–19.

Eagleson, P. S. (1978). Climate, soil, and vegetation: 1. introduction to water balance dynamics. *Water Resources Research*, 14(5):705–712.

Elfert, S. and Bormann, H. (2010). Simulated impact of past and possible future land use changes on the hydrological response of the northern german lowland 'hunte'catchment. *Journal of Hydrology*, 383(3):245–255.

Federer, C. A. and Lash, D. (1978). Brook: A hydrologic simulation model for eastern forests.

Ferretti, D., Pendall, E., Morgan, J., Nelson, J., Lecain, D., and Mosier, A. (2003). Partitioning evapotranspiration fluxes from a colorado grassland using stable isotopes: seasonal variations and ecosystem implications of elevated atmospheric co2. *Plant and Soil*, 254(2):291–303.

Ferrier, G. and Trahair, N. (1995). Evaluation of apparent surface reflectance estimation methodologies. *International Journal of Remote Sensing*, 16(12):2291–2297.

Fox, D. G. (1981). Judging air quality model performance. *Bulletin of the American Meteorological Society*, 62(5):599–609.

Fuchs, M. and Tanner, C. (1966). Infrared thermometry of vegetation. *Agronomy Journal*, 58(6):597–601.

Gan, T. Y., Dlamini, E. M., and Biftu, G. F. (1997). Effects of model complexity and structure, data quality, and objective functions on hydrologic modeling. *Journal of Hydrology*, 192(1):81–103.

Gao, C., Jiang, X., Li, Z.-L., and Nerry, F. (2013). Comparison of the thermal sensors of seviri and modis for lst mapping. In Kuenzer, C. and Dech, S., editors, *Thermal Infrared Remote Sensing*, volume 17 of *Remote Sensing and Digital Image Processing*, pages 233–252. Springer Netherlands.

Gash, J. H. C. and Shuttleworth, W. J. (2007). *Evaporation*. IAHS Press. International Association of Hydrological Sciences., Wallingford.

Gleick, P. H. (1986). Methods for evaluating the regional hydrologic impacts of global climatic changes. *Journal of hydrology*, 88(1):97–116.

Glenn, E. P., Huete, A. R., Nagler, P. L., Hirschboeck, K. K., and Brown, P. (2007). Integrating remote sensing and ground methods to estimate evapotranspiration. *Critical Reviews in Plant Sciences*, 26(3):139–168.

Gong, L., Xu, C.-y., Chen, D., Halldin, S., and Chen, Y. D. (2006). Sensitivity of the penman–monteith reference evapotranspiration to key climatic variables in the changjiang (yangtze river) basin. *Journal of Hydrology*, 329(3):620–629.

Goyal, R. (2004). Sensitivity of evapotranspiration to global warming: a case study of arid zone of rajasthan (india). *Agricultural Water Management*, 69(1):1–11.

Granger, R. (2000). Satellite-derived estimates of evapotranspiration in the gediz basin. *Journal of Hydrology*, 229(1):70–76.

Guitjens, J. C. (1982). Models of alfalfa yield and evapotranspiration. *Journal of the Irrigation and Drainage Division*, 108(3):212–222.

Gupta, H. V., Sorooshian, S., Hogue, T. S., and Boyle, D. P. (2003). Advances in automatic calibration of watershed models. *Calibration of watershed models*, pages 9–28.

Gupta, H. V., Sorooshian, S., and Yapo, P. O. (1999). Status of automatic calibration for hydrologic models: Comparison with multilevel expert calibration. *Journal of Hydrologic Engineering*, 4(2):135–143.

Gurney, R. and Camillo, P. (1984). Modelling daily evapotranspiration using remotely sensed data. *Journal of hydrology*, 69(1):305–324.

Gurtz, J., Zappa, M., Jasper, K., Verbunt, M., Badoux, A., Vitvar, T., and Lang, H. (2000). Modelling of runoff and its components and model validation in swiss pre-alpine and alpine catchments. In *International Workshop runoff generation and implications for river basin modelling*, pages 9–12.

Hamby, D. (1994). A review of techniques for parameter sensitivity analysis of environmental models. *Environmental monitoring and assessment*, 32(2):135–154.

Harbeck, G. E. (1962). *A practical field technique for measuring reservoir evaporation utilizing mass-transfer theory*. US Government Printing Office.

Hatfield, J., Perrier, A., and Jackson, R. (1983). Estimation of evapotranspiration at one time-of-day using remotely sensed surface temperatures. *Agricultural Water Management*, 7(1):341–350.

Haude, W. (1955). *Zur Bestimmung der Verdunstung auf möglichst einfachr Weise*.

Hibbert, A. R. (1965). *Forest treatment effects on water yield*. Coweeta Hydrologic Laboratory, Southeastern Forest Experiment Station.

Hunsaker, D. J., Pinter Jr, P. J., and Kimball, B. A. (2005). Wheat basal crop coefficients determined by normalized difference vegetation index. *Irrigation Science*, 24(1):1–14.

Huntington, T. G. (2006). Evidence for intensification of the global water cycle: review and synthesis. *Journal of Hydrology*, 319(1):83–95.

Hupet, F. and Vanclooster, M. (2001). Effect of the sampling frequency of meteorological variables on the estimation of the reference evapotranspiration. *Journal of Hydrology*, 243(3):192–204.

Irish, R. R. (2000). Landsat 7 science data users handbook. *National Aeronautics and Space Administration, Report*, pages 430–15.

Jackson, R., Reginato, R., and Idso, S. (1977). Wheat canopy temperature: a practical tool for evaluating water requirements. *Water Resources Research*, 13(3):651–656.

Jasinski, M. F. (1990). Sensitivity of the normalized difference vegetation index to subpixel canopy cover, soil albedo, and pixel scale. *Remote Sensing of Environment*, 32(2):169–187.

Jasper, K. (2005). *Hydrological modelling of Alpine river catchments using output variables from atmospheric models*. Diss. Naturwissenschaften, Eidgenössische Technische Hochschule ETH Zürich, Nr. 14385, 2002.

Jasper, K., Gurtz, J., and Lang, H. (2002). Advanced flood forecasting in alpine watersheds by coupling meteorological observations and forecasts with a distributed hydrological model. *Journal of hydrology*, 267(1):40–52.

Jensen, M. E., Burman, R. D., and Allen, R. G. (1990). Evapotranspiration and irrigation water requirements. ASCE.

Jiang, L. and Islam, S. (1999). A methodology for estimation of surface evapotranspiration over large areas using remote sensing observations. *Geophysical research letters*, 26(17):2773–2776.

Jiménez-Muñoz, J. C. and Sobrino, J. A. (2003). A generalized single-channel method for retrieving land surface temperature from remote sensing data. *Journal of Geophysical Research: Atmospheres (1984–2012)*, 108(D22).

Jin, M. (2004). Analysis of land skin temperature using avhrr observations. *Bulletin of the American Meteorological Society*, 85(4):587–600.

Jing, X., Yao, W.-Q., Wang, J.-H., and Song, X.-Y. (2011). A study on the relationship between dynamic change of vegetation coverage and precipitation in beijing's mountainous areas during the last 20 years. *Mathematical and Computer Modelling*, 54(3):1079–1085.

Karpouzli, E. and Malthus, T. (2003). The empirical line method for the atmospheric correction of iknos images. *International Journal of Remote Sensing*, 24(5):1143–1150.

Kerr, Y. H., Imbernon, J., Dedieu, G., Hautecoeur, O., Lagouarde, J., and Seguin, B. (1989). Noaa avhrr and its uses for rainfall and evapotranspiration monitoring. *International Journal of Remote Sensing*, 10(4-5):847–854.

Kite, G. and Droogers, P. (2000). Comparing evapotranspiration estimates from satellites, hydrological models and field data. *Journal of Hydrology*, 229(1):3–18.

Klok, E., Jasper, K., Roelofsma, K., Gurtz, J., and Badoux, A. (2001). Distributed hydrological modelling of a heavily glaciated alpine river basin. *Hydrological Sciences Journal*, 46(4):553–570.

Koster, R. D., Dirmeyer, P. A., Guo, Z., Bonan, G., Chan, E., Cox, P., Gordon, C., Kanae, S., Kowalczyk, E., Lawrence, D., et al. (2004). Regions of strong coupling between soil moisture and precipitation. *Science*, 305(5687):1138–1140.

Krause, P., Boyle, D., and Bäse, F. (2005). Comparison of different efficiency criteria for hydrological model assessment. *Advances in Geosciences*, 5(5):89–97.

Krieger, T., Durston, C., and Albright, D. (1978). Statistical determination of effective variables in sensitivity analysis.

Kurpius, M., Panek, J., Nikolov, N., McKay, M., and Goldstein, A. (2003). Partitioning of water flux in a sierra nevada ponderosa pine plantation. *Agricultural and Forest Meteorology*, 117(3):173–192.

Kustas, W. and Norman, J. (1996). Use of remote sensing for evapotranspiration monitoring over land surfaces. *Hydrological Sciences Journal*, 41(4):495–516.

Kustas, W. P. and Daughtry, C. S. (1990). Estimation of the soil heat flux/net radiation ratio from spectral data. *Agricultural and Forest Meteorology*, 49(3):205–223.

Lagouarde, J. and Brunet, Y. (1993). A simple model for estimating the daily upward longwave surface radiation flux from noaa-avhrr data. *International Journal of Remote Sensing*, 14(5):907–925.

Lagouarde, J.-P. (1991). Use of noaa avhrr data combined with an agrometeorological model for evaporation mapping. *International Journal of Remote Sensing*, 12(9):1853–1864.

Legates, D. R. and McCabe, G. J. (1999). Evaluating the use of "goodness-of-fit" measures in hydrologic and hydroclimatic model validation. *Water resources research*, 35(1):233–241.

Lenhart, T., Eckhardt, K., Fohrer, N., and Frede, H.-G. (2002). Comparison of two different approaches of sensitivity analysis. *Physics and Chemistry of the Earth, Parts A/B/C*, 27(9):645–654.

Li, Z.-L. and Becker, F. (1993). Feasibility of land surface temperature and emissivity determination from avhrr data. *Remote Sensing of Environment*, 43(1):67–85.

Liang, S. (2001). Narrowband to broadband conversions of land surface albedo i: Algorithms. *Remote Sensing of Environment*, 76(2):213–238.

Loague, K. and Green, R. E. (1991). Statistical and graphical methods for evaluating solute transport models: overview and application. *Journal of contaminant hydrology*, 7(1):51–73.

Loague, K. M. and Freeze, R. A. (1985). A comparison of rainfall-runoff modeling techniques on small upland catchments. *Water Resources Research*, 21(2):229–248.

Matsui, T., Lakshmi, V., and Small, E. (2003). Links between snow cover, surface skin temperature, and rainfall variability in the north american monsoon system. *Journal of Climate*, 16(11):1821–1829.

McCuen, R. H. (1973). The role of sensitivity analysis in hydrologic modeling. *Journal of Hydrology*, 18(1):37–53.

McCuen, R. H. (1974). A sensitivity and error analysis cf procedures used for estimating evaporation1.

Middelkoop, H., Daamen, K., Gellens, D., Grabs, W., Kwadijk, J. C., Lang, H., Parmet, B. W., Schädler, B., Schulla, J., and Wilke, K. (2001). Impact of climate change on hydrological regimes and water resources management in the rhine basin. *Climatic change*, 49(1-2):105–128.

Monteith, J. et al. (1965). Evaporation and environment. In *Symp. Soc. Exp. Biol*, volume 19, page 4.

Moriasi, D., Arnold, J., Van Liew, M., Bingner, R., Harmel, R., and Veith, T. (2007). Model evaluation guidelines for systematic quantification of accuracy in watershed simulations. *Trans. ASABE*, 50(3):885–900.

Morton, F. I. (1983). Operational estimates of areal evapotranspiration and their significance to the science and practice of hydrology. *Journal of Hydrology*, 66(1):1–76.

Murray, F. W. (1967). On the computation of saturation vapor pressure. *Journal of Applied Meteorology*, 6(1):203–204.

NASA (2015a). The enhanced thematic mapper plus. Accessed: 2014-11-20.

NASA (2015b). Mod 03 geolocation data set. Accessed: 2014-11-20.

NASA (2015c). Mod 05 total precipitable water. Accessed: 2014-11-20.

NASA (2015d). Mod 09 surface reflectance; atmospheric correction algorithm products. Accessed: 2014-11-20.

NASA (2015e). The thematic mapper. Accessed: 2014-11-20.

Nash, J. and Sutcliffe, J. (1970). River flow forecasting through conceptual models part i—a discussion of principles. *Journal of hydrology*, 10(3):282–290.

Nieuwenhuis, G., Smidt, E., and Thunnissen, H. (1985). Estimation of regional evapotranspiration of arable crops from thermal infrared images. *International Journal of Remote Sensing*, 6(8):1319–1334.

Norman, J. M. and Becker, F. (1995). Terminology in thermal infrared remote sensing of natural surfaces. *Remote Sensing Reviews*, 12(3-4):159–173.

Penman, H. and Long, I. (1961). Weather in wheat. *Quarterly Journal of the Royal Meteorological Society*, 87(371):111–112.

Penman, H. L. (1948). Natural evaporation from open water, bare soil and grass. *Proceedings of the Royal Society of London. Series A. Mathematical and Physical Sciences*, 193(1032):120–145.

Persaud, N. and Khosla, R. (1999). Partitioning soil-water losses in different plant populations of dry-land corn. *Agricultural water management*, 42(2):157–172.

Pike, J. (1964). The estimation of annual run-off from meteorological data in a tropical climate. *Journal of Hydrology*, 2(2):116–123.

Piper, B. (1989). Sensitivity of penman estimates of evaporation to errors in input data. *Agricultural water management*, 15(3):279–300.

Plegnière, S. and Casper, M. (2011). Erweiterung eines Verfahrens zur Bewertung des Einflusses der Klimaänderung auf die Wasserhaushaltssimulation von Waldstandorten. ForeStClim Project Report.

Popp, T. (1995). Correcting atmospheric masking to retrieve the spectral albedo of land surfaces from satellite measurements. *International Journal of Remote Sensing*, 16(18):3483–3508.

Priestley, C. and Taylor, R. (1972). On the assessment of surface heat flux and evaporation using large-scale parameters. *Monthly weather review*, 100(2):81–92.

Qin, Z.-h., Karnieli, A., and Berliner, P. (2001). A mono-window algorithm for retrieving land surface temperature from landsat tm data and its application to the israel-egypt border region. *International Journal of Remote Sensing*, 22(18):3719–3746.

Rabin, R. M., Stensrud, D. J., Stadler, S., Wetzel, P. J., and Gregory, M. (1990). Observed effects of landscape variability on convective clouds. *Bulletin of the American Meteorological Society*, 71(3):272–280.

Rana, G. and Katerji, N. (1998). A measurement based sensitivity analysis of the penman-monteith actual evapotranspiration model for crops of different height and in contrasting water status. *Theoretical and Applied Climatology*, 60(1-4):141–149.

Revelle, R. R. and Waggoner, P. E. (1983). Effects of a carbon dioxide-induced climatic change on water supplies in 7 the western united states. *Month*, 419:432.

Richards, L. A. (1931). Capillary conduction of liquids through porous mediums. *Journal of Applied Physics*, 1(5):318–333.

Richter, R. (1998). Value adding products derived from the atcor models. *Unpublished internal report at DLR, German Aerospace Center, Institute for Optoelectronics*.

Rößler, O. and Löffler, J. (2010). Potentials and limitations of modelling spatio-temporal patterns of soil moisture in a high mountain catchment using wasim-eth. *Hydrological processes*, 24(15):2182–2196.

Samani, Z. (2000). Estimating solar radiation and evapotranspiration using minimum climatological data. *Journal of Irrigation and Drainage Engineering*, 126(4):265–267.

Santhi, C., Arnold, J. G., Williams, J. R., Dugas, W. A., Srinivasan, R., and Hauck, L. M. (2001). Validation of the swat model on a large rwer basin with point and nonpoint sources1.

Saxton, K. E. (1975). Sensitivity analyses of the combination evapotranspiration equation. *Agricultural Meteorology*, 15(3):343–353.

Schulla, J. and Jasper, K. (2007). Model description wasim-eth. *Institute for Atmospheric and Climate Science, Swiss Federal Institute of Technology, Zürich*.

Segal, M. and Arritt, R. (1992). Nonclassical mesoscale circulations caused by surface sensible heat-flux gradients. *Bulletin of the American Meteorological Society*, 73(10):1593–1604.

Seguin, B. and Itier, B. (1983). Using midday surface temperature to estimate daily evaporation from satellite thermal ir data. *International Journal of Remote Sensing*, 4(2):371–383.

Sellers, P. J. (1985). Canopy reflectance, photosynthesis and transpiration. *International Journal of Remote Sensing*, 6(8):1335–1372.

Shukla, J. and Mintz, Y. (1982). Influence of land-surface evapotranspiration on the earth's climate. *Science*, 215(4539):1498–1501.

Singh, S. K., Liang, J., and Bárdossy, A. (2012). Improving the calibration strategy of the physically-based model wasim-eth using critical events. *Hydrological Sciences Journal*, 57(8):1487–1505.

Slatyer, R., McIlroy, I., et al. (1961). Practical microclimatology. *Practical Microclimatology.*

Smith, G. M. and Milton, E. J. (1999). The use of the empirical line method to calibrate remote sensed data to reflectance. *International Jornal of remote sensing*, 20(13):2653–2662.

Smith, M., Allen, R., and Pereira, L. (1998). Revised fao methodology for crop-water requirements.

Sobrino, J., Raissouni, N., and Li, Z.-L. (2001). A comparative study of land surface emissivity retrieval from noaa data. *Remote Sensing of Environment*, 75(2):256–266.

Sobrino, J. A., Jiménez-Muñoz, J. C., and Paolini, L. (2004). Land surface temperature retrieval from landsat tm 5. *Remote Sensing of environment*, 90(4):434–440.

Soer, G. (1980). Estimation of regional evapotranspiration and soil moisture conditions using remotely sensed crop surface temperatures. *Remote Sensing of Environment*, 9(1):27–45.

Sud, Y. and Fennessy, M. (1982). A study of the influence of surface albedo on july circulation in semi-arid regions using the glas gcm. *Journal of Climatology*, 2(2):105–125.

Sun, D. and Pinker, R. T. (2003). Estimation of land surface temperature from a geostationary operational environmental satellite (goes-8). *Journal of Geophysical Research: Atmospheres (1984–2012)*, 108(D11).

Sun, Y. (2011). Retrieval and application of land surface temperature.

Szilagyi, J. (2000). Can a vegetation index derived from remote sensing be indicative of areal transpiration? *Ecological Modelling*, 127(1):65–79.

Tanner, C. (1963). Plant temperatures. *Agronomy Journal*, 55(2):210–211.

Tanner, C. and Pelton, W. (1960). Potential evapotranspiration estimates by the approximate energy balance method of penman. *Journal of geophysical research*, 65(10):3391–3413.

Teillet, P. (1986). Image correction for radiometric effects in remote sensing. *International Journal of Remote Sensing*, 7(12):1637–1651.

Tetens, O. (1930). Uber einige meteorologische begriffe. *Z. Geophys.*, 6:297–309.

Thornthwaite, C. W. (1948). An approach toward a rational classification of climate. *Geographical review*, pages 55–94.

Turner, K. M. (1991). Annual evapotranspiration of natwe vegetation in a mediterranean-type climate1. *JAWRA Journal of the American Water Resources Association*, 27(1):1–6.

USGS (2015). Landsat thematic mapper (tm). Accessed: 2014-11-20.

Valor, E. and Caselles, V. (1996). Mapping land surface emissivity from ndvi: Application to european, african, and south american areas. *Remote sensing of Environment*, 57(3):167–184.

Van Bavel, C. (1966). Potential evaporation: the combination concept and its experimental verification. *Water Resources Research*, 2(3):455–467.

Van Bavel, C. (1967). Changes in canopy resistance to water loss from alfalfa induced by soil water depletion. *Agricultural Meteorology*, 4(3):165–176.

Van Genuchten, M. T. (1980). A closed-form equation for predicting the hydraulic conductivity of unsaturated soils. *Soil science society of America journal*, 44(5):892–898.

Van Liew, M., Arnold, J., and Garbrecht, J. (2003). Hydrologic simulation on agricultural watersheds: Choosing between two models. *Transactions of the ASAE*, 46(6):1539–1551.

Verbunt, M., Gurtz, J., Jasper, K., Lang, H., Warmerdam, P., and Zappa, M. (2003). The hydrological role of snow and glaciers in alpine river basins and their distributed modeling. *Journal of hydrology*, 282(1):36–55.

Vermote, E., Kotchenova, S., and Ray, J. (2011). Modis surface reflectance user's guide. *MODIS Land Surface Reflectance Science Computing Facility, version*, 1.

Vermote, E. F., Tanrè, D., Deuzè, J. L., Herman, M., and Morcette, J.-J. (1997). Second simulation of the satellite signal in the solar spectrum, 6s: An overview. *Geoscience and Remote Sensing, IEEE Transactions on*, 35(3):675–686.

Viviroli, D., Gurtz, J., and Zappa, M. (2007). *The Hydrological Modelling System PREVAH*. Geographica Bernensia.

Weast, R. C. (1969). Handbook of chemistry and physics. *The American Journal of the Medical Sciences*, 257(6):423.

Wendling, U. (1975). Zur messung und schätzung der potentiellen verdunstung. *Zeitschrift für Meteorologie*, 25(2):103–111.

Williams, D., Cable, W., Hultine, K., Hoedjes, J., Yepez, E., Simonneaux, V., Er-Raki, S., Boulet, G., De Bruin, H., Chehbouni, A., et al. (2004). Evapotranspiration components determined by stable isotope, sap flow and eddy covariance techniques. *Agricultural and Forest Meteorology*, 125(3):241–258.

Willmott, C. J. (1981). On the validation of models. *Physical geography*, 2(2):184–194.

Willmott, C. J. (1982). Some comments on the evaluation of model performance. *Bulletin of the American Meteorological Society*, 63(11):1309–1313.

Willmott, C. J. and Matsuura, K. (2005). Advantages of the mean absolute error (mae) over the root mean square error (rmse) in assessing average model performance. *Climate Research*, 30(1):79.

Wilson, J. S., Clay, M., Martin, E., Stuckey, D., and Vedder-Risch, K. (2003). Evaluating environmental influences of zoning in urban ecosystems with remote sensing. *Remote sensing of environment*, 86(3):303–321.

Wilson, K. B., Hanson, P. J., Mulholland, P. J., Baldocchi, D. D., and Wullschleger, S. D. (2001). A comparison of methods for determining forest evapotranspiration and its components: sap-flow, soil water budget, eddy covariance and catchment water balance. *Agricultural and Forest Meteorology*, 106(2):153–168.

Xu, C.-Y. and Singh, V. (2002). Cross comparison of empirical equations for calculating potential evapotranspiration with data from switzerland. *Water Resources Management*, 16(3):197–219.

Yepez, E. A., Williams, D. G., Scott, R. L., and Lin, G. (2003). Partitioning overstory and understory evapotranspiration in a semiarid savanna woodland from the isotopic composition of water vapor. *Agricultural and Forest Meteorology*, 119(1):53–68.

Yuan, G., Luo, Y., Sun, X., and Tang, D. (2004). Evaluation of a crop water stress index for detecting water stress in winter wheat in the north china plain. *Agricultural Water Management*, 64(1):29–40.

Zhang, L., Dawes, W., and Walker, G. (2001). Response of mean annual evapotranspiration to vegetation changes at catchment scale. *Water resources research*, 37(3):701–708.

Zhang, X., Liao, C., Li, J., and Sun, Q. (2013). Fractional vegetation cover estimation in arid and semi-arid environments using hj-1 satellite hyperspectral data. *International Journal of Applied Earth Observation and Geoinformation*, 21:506–512.

Weiwei Bie
Kleeburger Weg 102, 54296, Trier
+49 17695890980
bievivi@gmail.com

Birthday: May 16, 1984.

Birthplace: Chongqing, China.

EDUCATION

- Sep. 2011~ present Universität Trier, Department of Geography/Geosciences, Ph.D. in physical geography.

Thesis: ***Studies on surface resistance in a hydrological model with the evapotranspiration estimated by Penman-Monteith equation and remote sensing techniques in Nahe catchment forest area.***

- Sep. 2008~ Jun. 2006 China University of Mining & Technology, Beijing, College of Geoscience and Surveying Engineering, MSc. in Cartography and Geographic Information Science.

Thesis: ***Development of a spectrum library system based on geographic information and hyperspectral data.***

- Sep. 2002~ Jun. 2006, China University of Mining & Technology, Beijing, College of Faculties of Resources & Safety Engineering, BSc. in Resources Environment and the Management of Urban and Rural Planning.

Thesis: ***Ecological environment investigation of Nanjing City by remote sensing means.***

WORK EXPERIENCES

- Nov. 2005~ Jun. 2006 Beijing Mapuni Science and Technology Co. Ltd, Marketing, trainee.
- Jul. 2006~ Jun. 2008 Beijing Mapuni Science and Technology Co. Ltd, Marketing, Project Engineer.

ABSTRACTS

- Bie, W., Casper, M., Reiter, P., Vohland M. (2015): Sensitivity analysis of surface resistance in WaSiM-ETH with observations retrieved from remote sensing images, European Geosciences Union General Assembly 2015, Vienna, Austria, Vol. 17, EGU2015-11201.
- Bie, W., Casper, M., Reiter, P., Vohland M. (2014): Surface resistance calibration for a hydrological model using actual evapotranspiration retrieved from remote sensing data in Nahe catchment forest area, European Geosciences Union General Assembly 2014, Vienna, Austria, Vol. 16, EGU2014-11915.

PUBLICATIONS

- Bie, W., Casper, M. C., Reiter, P., and Vohland, M.: Surface resistance calibration for a hydrological model using evapotranspiration retrieved from remote sensing data in Nahe catchment forest area, Proc. IAHS, 368, 81-86, doi:10.5194/piahs-368-81-2015, 2015.
- Bie, W., Yu, Z., Tang, F.. The generating of a fine and detail texture to coal seams[C]. Guangzhou: International mining enterprise working committee, 2009: 79-83.
- Bie, W., Yu, Z., Wang Y.. Rock ore auxiliary classification & prediction system designing based on hyperspectral[C]. Beijing: Geological Press, 2010: 230-232.
- Wang Y., Yu, Z., Bie, W.. Rock ore hyperspectral characteristics identification & matching system[C]. Beijing: Geological press, 2010: 184-187.
- Tang, F., Yu, Z., Li L., Bie, W.. Satellite laser radar waveform data decomposition method to explore[C]. Beijing: Geological press, 2010: 233-236.

RESEARCH EXPERIENCES

- A national "863" scientific item of the "geological application system construction & typical application demonstration research" (2009).
  Main work: programmed with C# for the development of the spectrum library system.
- Dayang Coal Mine GIS Software Project.
  Main work: used software such as sufer8, T2 to produce a fine and detail texture of coal seams.
- Geological Modeling Mining System Project
  Main work: system designs concerning the framework and functions of a 3D geological modeling mining system.
- Xinxiang City Police Geographic Information System Project
  Main work: system designs concerning the framework and functions of the system devolepment.
- Hualien and AnShun City Mapping project
  Main work: mapped 1:2000 vector maps of the two cities by ArcMap based on the air photogragh.

AWARDS

- 2011 China Scholarship Council 48-month Full Scholarship for a Ph.D. degree
- 2009-2010 China University of Mining & Technology, College Excellent Student
- 2008-2011 China University of Mining & Technology Full Scholarship for a master degree
- 2004-2005 China University of Mining & Technology Third-class Scholarship
- 2003-2004 China University of Mining & Technology Third-class Scholarship
- 2002-2003 China University of Mining & Technology Third-class Scholarship